BIOPHYSICAL AND MECHANISTIC CHARACTERIZATION OF CARBAMOYL PHOSPHATE SYNTHETASE FROM *Escherichia coli*

A Dissertation

by

LILIYA LUND

Submitted to the Office of Graduate Studies of
Texas A&M University
in partial fulfillment of the requirements for the degree of

DOCTOR OF PHILOSOPHY

December 2010

Major Subject: Chemistry

Biophysical and Mechanistic Characterization of Carbamoyl Phosphate Synthetase from *Escherichia coli*

BIOPHYSICAL AND MECHANISTIC CHARACTERIZATION OF CARBAMOYL PHOSPHATE SYNTHETASE FROM *ESCHERICHIA COLI*

A Dissertation

by

LILIYA LUND

Submitted to the Office of Graduate Studies of
Texas A&M University
in partial fulfillment of the requirements for the degree of

DOCTOR OF PHILOSOPHY

Approved by:

Chair of Committee,	Frank M. Raushel
Committee Members,	Gregory D. Reinhart
	Marcetta Y. Darensbourg
	David P. Barondeau
Head of Department,	David H. Russell

December 2010

Major Subject: Chemistry

ABSTRACT

Biophysical and Mechanistic Characterization of Carbamoyl Phosphate Synthetase from *Escherichia coli.* (December 2010)

Liliya Lund, B.S., Loyola University, Chicago

Chair of Advisory Committee: Dr. Frank M. Raushel

Carbamoyl phosphate synthetase (CPS) from *E. coli* catalyzes the formation of carbamoyl phosphate, an intermediate in the biosynthesis of pyrimidine nucleotides and arginine, from glutamine, bicarbonate and two molecules of MgATP. This reaction is catalyzed by three separate active sites that are separated in space by ~100 Å. The transfer of ammonia and carbamate through the two intramolecular tunnels was investigated by molecular dynamics simulations and experimental characterization of mutations within. The presence of an unstable reaction intermediate, carboxyphosphate, was established. A method for studying the synchronization of the two active sites on the large subunit of CPS was developed.

The potential of mean force (PMF) calculations along the ammonia and carbamate transfer pathways indicate a low free-energy path for the translocation of ammonia. The highest barrier for ammonia is 7.2 kcal/mol which corresponds to a narrow *turning gate* surrounded by the side chains of Cys-232, Ala-251, and Ala-314 in the large subunit. A blockage in the passageway was introduced by the triple mutant C232V/A251V/A314V, which was unable to synthesize carbamoyl phosphate. The release of phosphate is necessary for the injection of carbamate into the carbamate

tunnel. Two mutants, A23F and G575F, were designed to block the migration of carbamate through carbamate tunnel. The mutants retained only 1.7% and 3.8% of the catalytic activity for the synthesis of carbamoyl phosphate relative to the wild-type CPS, respectively.

Formate can be utilized by CPS in the absence of bicarbonate to form formyl phosphate. This intermediate was observed by ^{31}P, ^{13}C, and ^{1}H NMR. For the three NMR methods a peak corresponding to formyl phosphate was observed at 2.15 ppm (^{31}P) , 162.4 ppm (^{13}C), and 8.39 and 7.94 ppm (^{1}H). The rate of formation of formyl phosphate is 0.025 ± 0.005 s^{-1}. Formamide was not detected in the presence of an ammonia source.

Fluorescence anisotropy measurements on the C551A/S171C and C551A/S717C mutants provided insight into a possible mechanism of synchronization between the two active sites on the large subunit. The biggest fluorescence anisotropy change was observed at the N-terminal domain in the presence of AMPPNP and ATP.

DEDICATION

To my daughter, Isabella, who is the sunshine of my life

ACKNOWLEDGEMENTS

I would like to thank my committee chair, Dr. F. M. Raushel, and my committee members, Dr. G. D. Reinhart, Dr. M. Y. Darensbourg, and Dr. D. P. Barondeau, for their guidance and support throughout the course of this research. I would also like to thank everyone at the Chemistry Department for their help, support, and useful discussions. Finally, many thanks go to my mother for her constant encouragement and to my daughter for giving me countless reasons to smile.

TABLE OF CONTENTS

LIST OF FIGURES

FIGURE Page

FIGURE Page

LIST OF TABLES

CHAPTER I

INTRODUCTION AND LITERATURE REVIEW

Carbamoyl phosphate synthetase (CPS) from *Escherichia coli* catalyzes one of the most complex reactions in biological chemistry. The product of this enzymatic transformation, carbamoyl phosphate, is utilized in the biosynthesis of arginine and pyrimidine nucleotides.[1-3] Carbamoyl phosphate is formed from glutamine, bicarbonate and two molecules of MgATP through a series of four separate reactions.[1] The biochemical evidence for the catalytic reaction mechanism of CPS has been obtained from extensive kinetic investigations, positional isotope effect studies, and partial reaction studies.[4-7]

In the initial step of the reaction, the first molecule of ATP is used to phosphorylate bicarbonate to generate the reactive intermediate, carboxyphosphate. This intermediate has a calculated half life of approximately 70 ms.[8] In a concurrent reaction, glutamine is hydrolyzed to glutamate and ammonia in the small subunit. The ammonia generated from this reaction travels ~45 Å through an intramolecular tunnel to reach the carboxyphosphate active site on the large subunit. In the following step, ammonia makes a nucleophilic attack on the carboxyphosphate intermediate to form the third intermediate, carbamate. Carbamate is the most unstable of the reaction intermediates formed, with a half life of 28 ms at neutral pH.[9] Finally, carbamate travels ~35 Å

This dissertation follows the style of the *Journal of the American Chemical Society.*

through a second intramolecular tunnel to attack the γ-phosphate of the second molecule of ATP at the carbamoyl phosphate active site in the large subunit. Ultimately, the final product, carbamoyl phosphate, is released from the protein. The generally accepted reaction mechanism is summarized in **Scheme 1.1**. There are four separate chemical reactions and three discrete, reactive, and unstable intermediates involved in this reaction mechanism: carboxyphosphate, ammonia, and carbamate.[5-6]

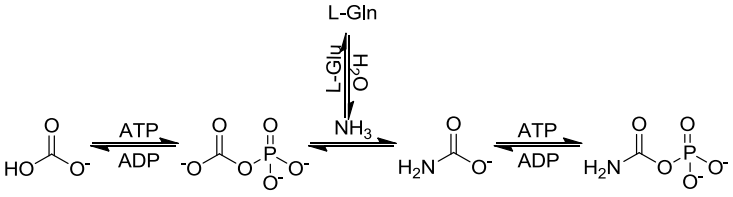

Scheme 1.1

Carbamoyl phosphate produced by CPS in prokaryotic and eukaryotic organisms is used in two biosynthetic pathways: pyrimidine and arginine biosynthesis. In terrestrial vertebrates carbamoyl phosphate is utilized in the urea cycle. In eukaryotic organisms CPS is present in two distinct forms denoted CPS I and CPS II. CPS I is only found in mitochondria and participates in arginine biosynthesis and the urea cycle. Free ammonia is necessary for the proper function of this enzyme. CPS II is a cytosolic enzyme involved in the synthesis of pyrimidine nucleotides. Glutamine acts as a source of ammonia for this enzyme. It is worth nothing that CPS II is part of a multienzyme complex which contains aspartate transcarbamoylase and dihydroorotase.[10-11] Prokaryotes only have one type of CPS that is used for both biosynthetic pathways; it employs glutamine as its ammonia source.

In the production of arginine, carbamoyl phosphate enters the urea cycle by condensing with ornithine to form citrulline through the action of ornithine transcarbamoylase (**Figure 1.1**). In the subsequent step citrulline reacts with aspartate to form argininosuccinate. Argininosuccinate is then cleaved to fumarate and arginine by argininosuccinase. Fumarate can enter the citric acid cycle, while arginine can go on to protein biosynthesis or participate in the urea cycle. If arginine goes on to finish the urea cycle, it is further cleaved to ornithine and urea by the last enzyme in the pathway, arginase (**Figure 1.1**)

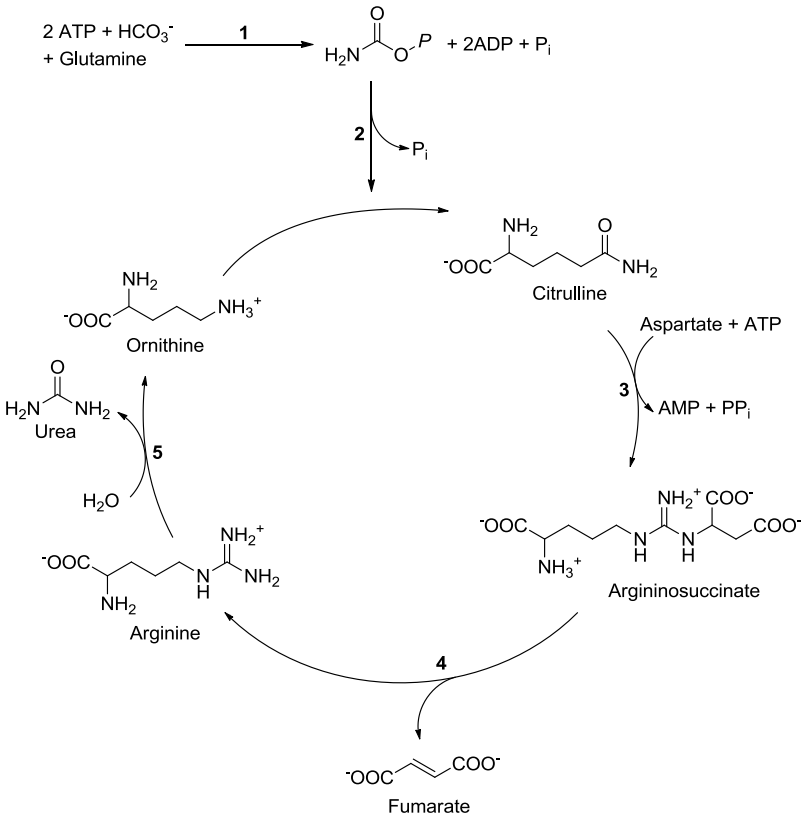

Figure 1.1. Urea cycle. **1**- Carbamoyl phosphate synthetase, **2**- Ornithine transcarbamoylase, **3**- Argininosuccinate synthetase, **4**- Argininosuccinase, **5**- Arginase.

When carbamoyl phosphate is utilized for the production of pyrimidine nucleotides it is first condensed with aspartate by aspartate transcarbamoylase to form *N*-carbamoyl aspartate (**Figure 1.2**). In subsequent steps dihydroorotase, dihydroorotate dehydrogenase, orotate phosphoribosyl transferase, and orotidine monophosphate decarboxylase convert *N*-carbamoyl aspartate to uridine monophosphate (UMP). The biosynthetic pathway is summarized in **Figure 1.2**. Ultimately, the C-2 and N-3 positions on the uridine ring are derived from carbamoyl phosphate produced by CPS.

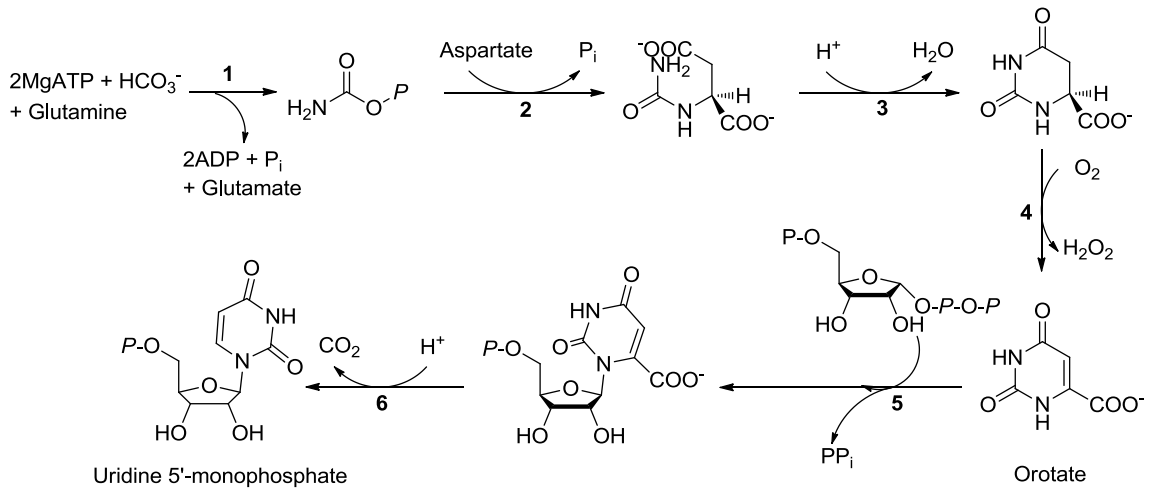

Figure 1.2. Pyrimidine biosynthesis pathway. **1**- Carbamoyl phosphate synthetase, **2**- Aspartate transcarbamoylase, **3**- Dihydrooratase, **4**- Dihydroorotate dehydrogenase, **5**- Orotate phosphoribosyl transferase, **6**- Orotodine monophosphate decarboxylase.

Structure of CPS

The isolated protein from *E. coli* is a heterodimer. It is composed of a small (42 kDa) and a large (118 kDa) subunit, thus forming an αβ-heterodimer (**Figure 1.3**).

Multiple heterodimers can readily oligomerize into an $(\alpha\beta)_4$-tetramer in the presence of the allosteric activator, ornithine (**Figure 1.4**). The smaller subunit of the heterodimer is composed of 382 residues and is responsible for the amidotransferase activity of the enzyme. [12-13] The large subunit is composed of 1073 amino acids and contains two binding sites for MgATP.[14] This subunit also contains binding sites for the allosteric effector molecules, UMP and ornithine.[15]

Based on gene sequencing and structural analysis two noteworthy things are apparent about CPS. The large subunit contains a homologous repeat sequence where residues 1-400 share 40% sequence identity with residues 557-933.[15] Residues 1-400 contain the site for the synthesis of carboxyphosphate, while residues 557-933 contain the active site for the synthesis of carbamoyl phosphate.[16-19] The high level of sequence identity between these two domains led to a hypothesis that the current form of the large subunit resulted from a gene duplication event from a more primitive enzyme with kinase activity.[15] The small subunit is homologous to the N-terminal domain of *trpG*-type amidotransferases. These enzymes belong to the class I amidotransferases, which are characterized by having a catalytic cysteine residue that participates in the nucleophilic attack of the carboxamide group of glutamine.[20]

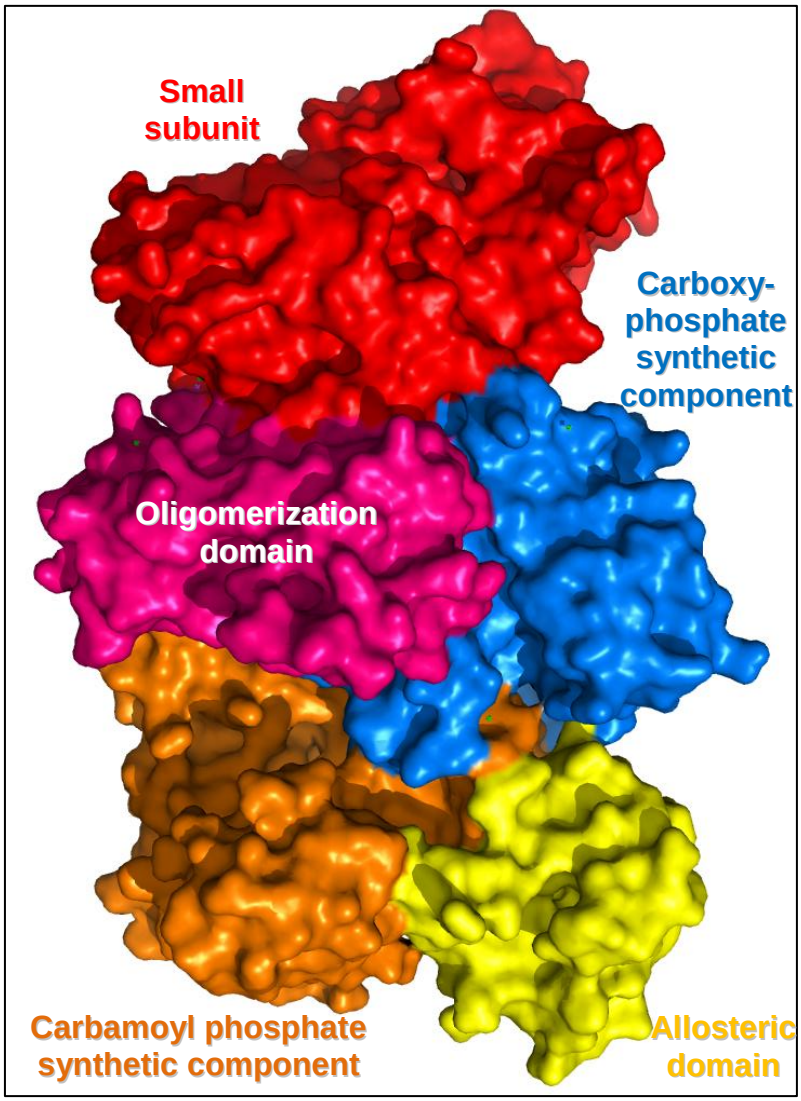

Figure 1.3. Surface representation of the carbamoyl phosphate synthetase (αβ)-heterodimer from *E. coli.* The small subunit is shown in red. The large subunit is broken up into four sections. In blue (residues 1-403) is the carboxyphosphate synthetic component. In purple (404-553) is the oligomerization domain. In orange (554-936) is the carbamoyl phosphate synthetic component. In yellow (937-1073) is the allosteric domain.[21] (PDB code 1bxr)

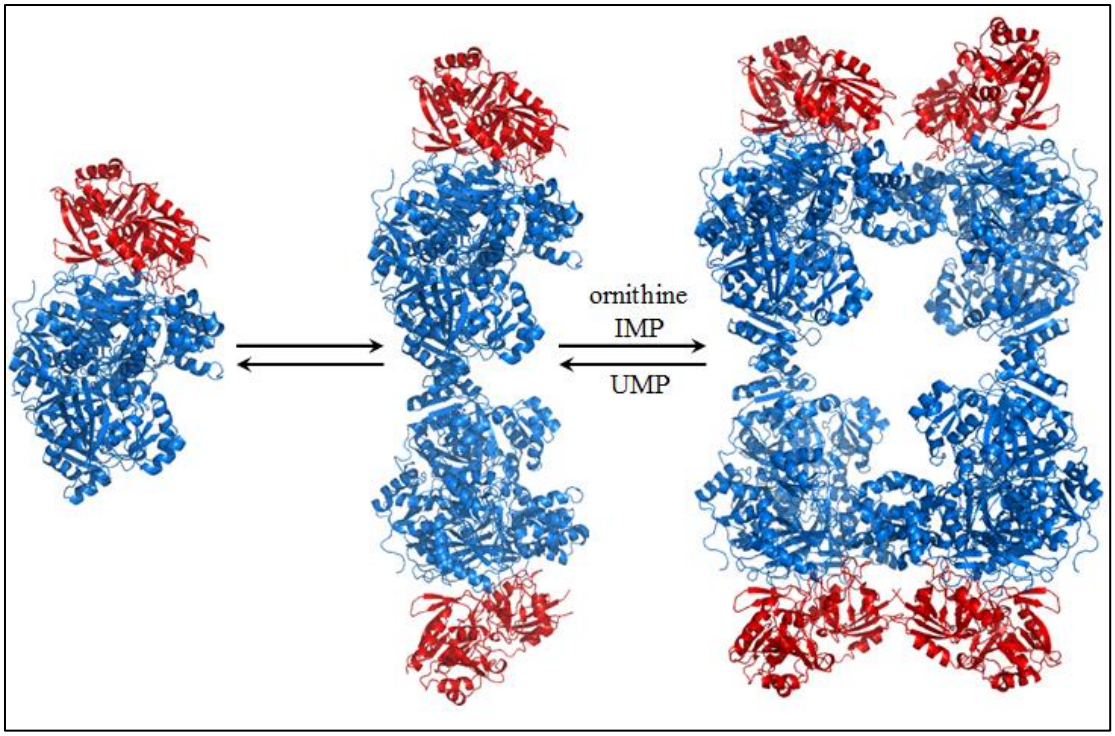

Figure1.4. Oligomeric states of carbamoyl phosphate synthetase.

The large subunit of CPS contains two sites for the binding of MgATP, and it also contains the allosteric and the oligomeric domains (**Figure 1.3**). Because carbamoyl phosphate is a product that is a substrate in other biosynthetic pathways, the activity of CPS is regulated. The *E. coli* CPS is regulated by a feedback inhibition mechanism. The primary regulators of CPS are ornithine and UMP; ornithine acts as an allosteric activator, while UMP acts as an allosteric inhibitor.[1-3] Both effector molecules modulate CPS by binding to two distinct binding sites on the large subunit, and thus influencing the binding of MgATP.[14,22] The binding of these effectors alters the K_M for ATP. It has been proposed that this change in K_M may be due to a structural

rearrangement of the ATP binding sites which makes it more favorable for ATP to bind, in the case of ornithine, or less favorable, in the case of UMP.

The binding of UMP or ornithine to CPS allows it to adopt a variety of oligomeric states.[21,23-25] It has been shown that CPS can form three distinct allosteric states. In the absence of all substrates, products, and allosteric effectors, CPS forms an αβ-monomer (**Figure 1.3**). However, when ornithine, and to a lesser extent, IMP, are added, CPS undergoes an association to a tetrameric state, $(\alpha\beta)_4$. This association is mediated by the interactions of the hydrophobic patches located on the surface of the oligomerization domains as well as interactions between residues on the surface of the allosteric domains. When UMP, an allosteric inhibitor, is added, the enzyme undergoes a change from a tetramer to an *end-to-end* dimer, $(\alpha\beta)_2$ (**Figure 1.4**).[23] Not only do these allosteric effectors change the physical shape of the protein, they also affect the apparent K_M for MgATP. Ornithine lowers the K_M for ATP twenty-fold, while UMP inhibits the reaction by increasing the K_M for ATP five-fold.[26] Previous experiments have shown that the different oligomeric states of CPS have no effect on the catalytic turnover rate of this enzyme. [23]

The Catalytic Mechanism of CPS

The kinetic mechanism of CPS was established by Raushel and Villafranca.[6] The catalytic mechanism follows an ordered Ter-Uni-Uni-Ter ping pong mechanism summarized in **Scheme 1.2**. The reaction sequence is initiated with the binding of the first molecule of MgATP and bicarbonate at the carboxyphosphate active site. This

triggers the activation of the glutaminase active site in the small subunit and the subsequent hydrolysis of glutamine to glutamate. Ammonia produced by this reaction migrates to the N-terminal active site on the large subunit and reacts with carboxyphosphate. The resultant carbamate translocates to the C-terminal active site on the large subunit where it is phosphorylated by the second molecule of MgATP to form the final product, carbamoyl phosphate.

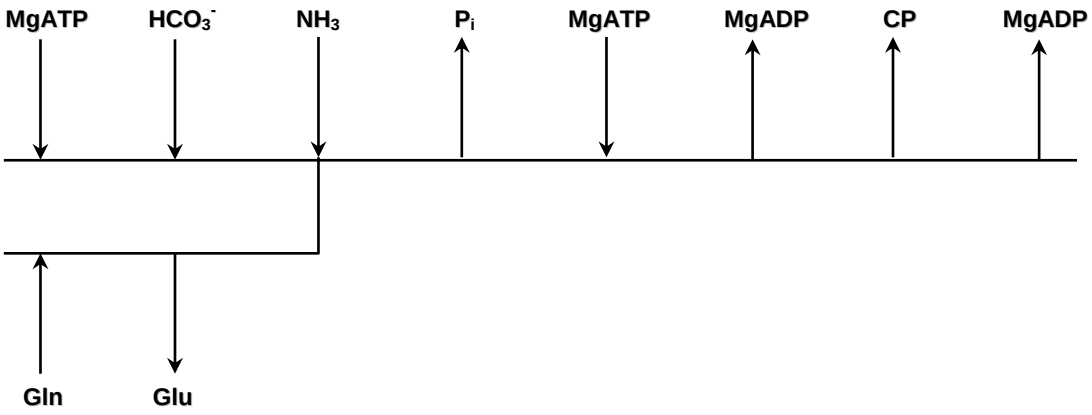

Scheme 1.2

From previous biochemical studies and crystallographic data, the mechanism for glutamine hydrolysis in the small subunit is summarized in **Figure 1.5**. The primary catalytic machinery of small subunit is composed of Cys-269, His-353, and Ser-47 (**Figure 1.6**). The reaction starts with a nucelophilic attack by the activated thiolate of Cys-269 on the carbonyl group of the glutamine substrate. The activation of this cysteine is accomplished by the two remaining members of the catalytic triad: His-353 and Ser-47.[27] Besides activating the catalytic cysteine residue, His-353 plays two more key roles in the reaction mechanism: it provides one of the protons for the amine leaving

group, and it abstracts a proton from the catalytic water molecule used to hydrolyze the thioester intermediate. The role of Ser-47 in the reaction mechanism is to orient the carbonyl carbon of the glutamine carboxamide group for the nucleophilic attack by Cys-269. It also serves to stabilize the tetrahedral intermediate in this reaction. Following the collapse of the tetrahedral intermediate ammonia is formed and injected into the first intramolecular tunnel. The thioester intermediate is then hydrolyzed and glutamate is released. The rate of the reaction in the small subunit is enhanced as much as 275-fold in the presence of ATP and bicarbonate.[28]

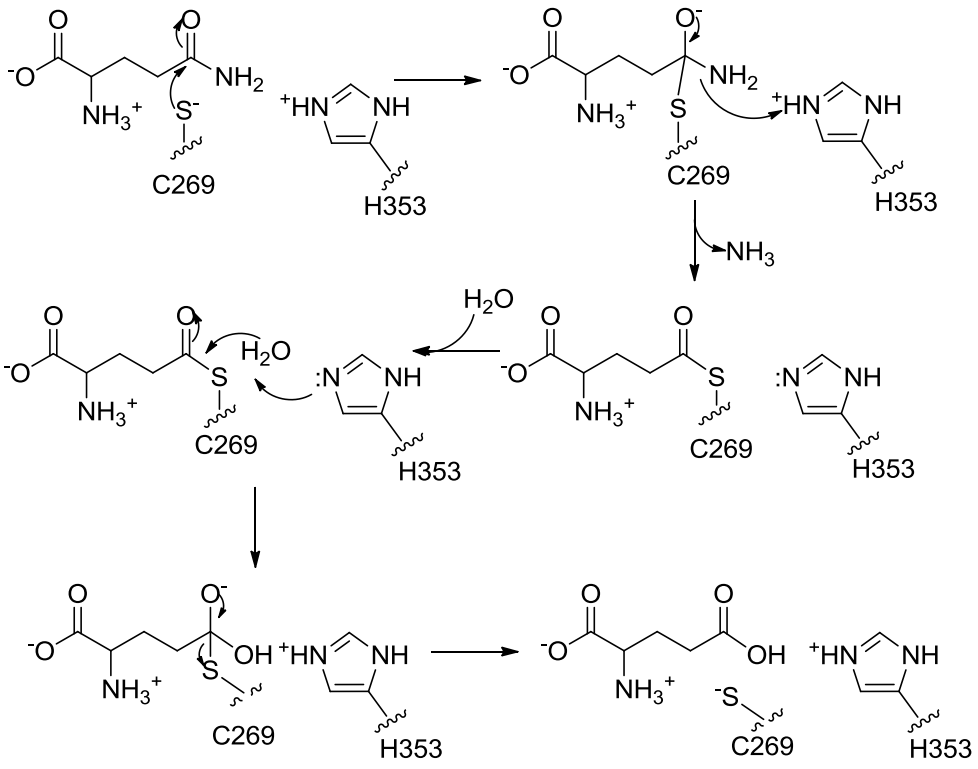

Figure 1.5. Catalytic mechanism in the small subunit of CPS.

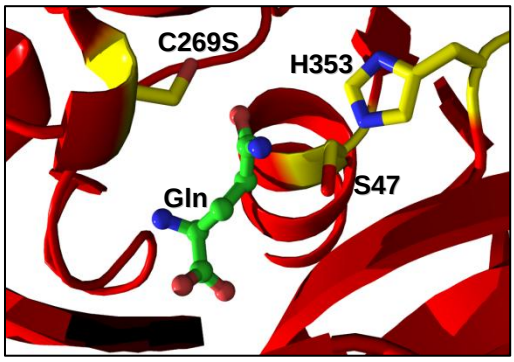

Figure 1.6. Close up view of the active site in the small subunit of the C269S mutant. Glutamine substrate is shown in green. The catalytic triad is shown in yellow. (PDB code 1c3o)

The ATP binding sites on the large subunit contain a subdomain, known as the B-domain (**Figure 1.7**). These domains adopt a fold that is known as the ATP-grasp fold. The B-domains are thought to undergo conformational changes that allow substrates to enter, and products to exit the active sites. Structural characterization of the enzyme provided direct evidence for the conformational change that occurs at the C-terminal B-domain: this domain clamps down over the active site to isolate the reactants from bulk water.[29-31] In the presence of the nonhydrolysable ATP analog, β,γ-imidoadenosine 5′-triphosphate (AMPPNP), this domain is observed in the closed conformation, while in the presence of ADP the domain appears to be in a more open conformation.[21,29] These data suggest that the opening and closing of the B-domain allows substrates and products to enter and exit the carbamoyl phosphate active site.[29] In

the crystal structures with ADP and P_i or AMPPNP bound in the carboxyphosphate active site, the N-terminal B-domain remains in the closed conformation.

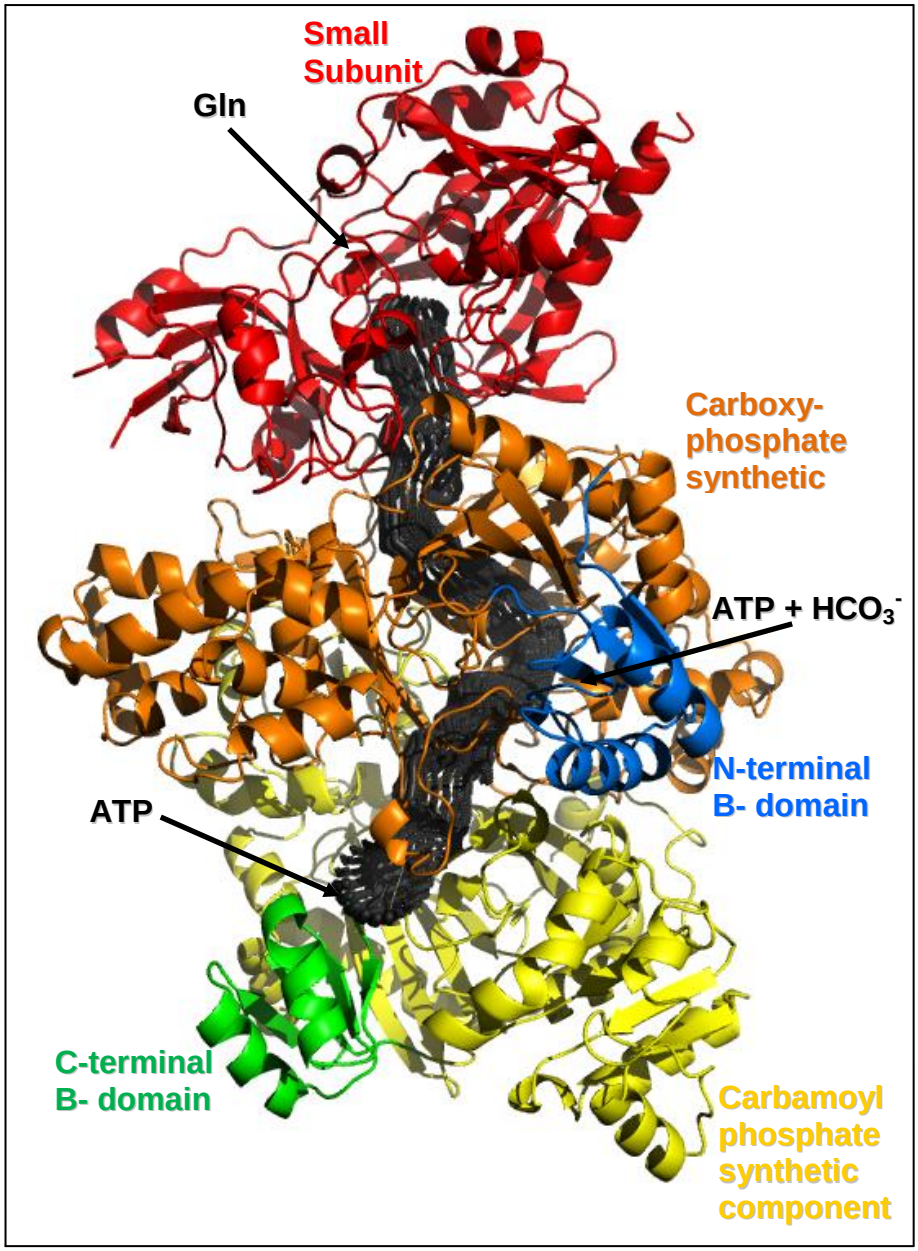

Figure 1.7. Crystallographic structure of *E. coli* CPS. Location of different domains within the protein is shown in different colors. The intramolecular tunnel is shown in dark grey spheres. (PDB code 1bxr)

Less information is available about the residues involved in catalysis at the carboxyphosphate and the carbamoyl phosphate active sites. The residues that participate in interactions with the substrate, MgATP, and the products, ADP and P_i, have been identified through crystal structures and confirmed by both computational and experimental methods. His-243 has been shown to be important in the synthesis of carbamate (**Figure 1.8A**).[17] This was accomplished by kinetically characterizing the H243N mutant which revealed that all of the partial reactions proceeded at rates close to that of the wild-type enzyme. However, the mutant was unable to synthesize carbamoyl phosphate because the imidazole side chain of His-243 may serve as a proton acceptor from ammonia during the nucleophilic attack on the carboxyphosphate intermediate.[17] Another critical residue in the carboxyphosphate active site is Arg-306 (**Figure 1.8A**). It plays an important role in interacting with the bound ATP. The importance of this residue was demonstrated by characterizing the R306A mutant. The mutant was unable to carry out the synthesis of carbamoyl phosphate and showed no activation of the bicarbonate-dependent ATPase activity in the presence of glutamine.[32] Arg-306 is also responsible for the opening of the second intramolecular tunnel and allowing carbamate to pass through to the carbamoyl phosphate active site.[33] An analogous residue, Arg-848, located at the carbamoyl phosphate active site plays a key role in stabilizing ATP and ADP at that site (**Figure 1.8B**).[32]

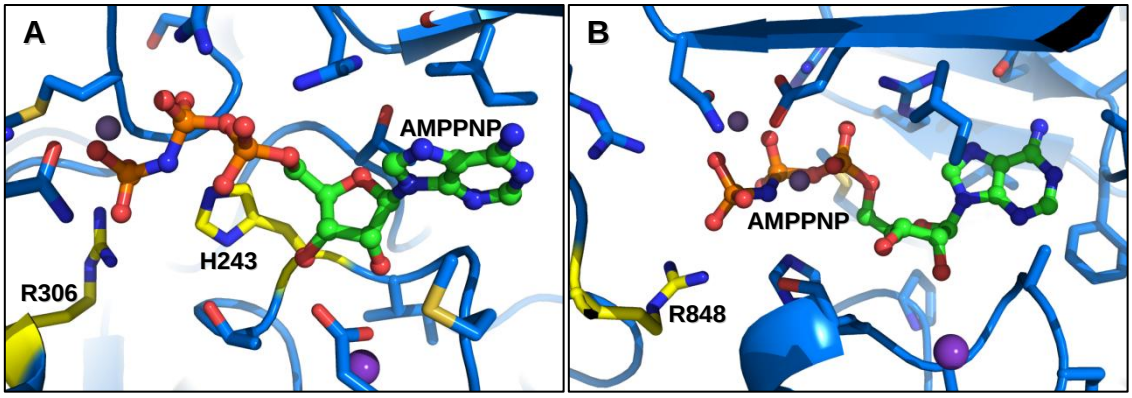

Figure 1.8. Close up view of the **A**) carboxyphosphate and **B**) carbamoyl phosphate active sites with the nonhydrolysable ATP analog, AMPPNP, bound. Key residues involved in substrate interactions are highlighted in yellow. Mn^{2+} ions are shown in grey, K^{+} ions are shown in bright purple. All other active sites residues are shown in blue. (PDB code 1bxr)

Molecular Tunnel

One of the most intriguing properties of CPS is the fact that it has an intramolecular tunnel that spans nearly 100 Å and two non-covalently bound subunits (**Figure 1.7**). The presence of the tunnel has been identified though X-ray crystal structures.[21,34-35] The tunnel can be divided into two parts: one for the transport of ammonia and the other for the transport of carbamate. The ammonia tunnel serves as a means for delivering ammonia derived from glutamine hydrolysis, in the small subunit, to the site of carboxyphosphate synthesis in the large subunit. This tunnel is composed of highly conserved residues and contains several water molecules. The carbamate tunnel transports carbamate from the site of its formation to the site of its utilization in the C-terminal active site in the large subunit. It is composed of highly conserved and

mostly hydrophobic residues, it also contains water molecules. The validity of both tunnels was tested with a series of mutants in both the large and the small subunits.[32,36-39]

The most significant of these mutations was G359F in the small subunit.[35] The intent of this mutant was to create a blockage within the tunnel, however, instead of creating a blockage, this mutation opened a hole in the tunnel wall though which ammonia was able to diffuse into bulk solvent. Rapid quench investigations also revealed that there is a coupling between the two sites that are served by this tunnel.[28] Hydrolysis of glutamine in the small subunit occurs approximately 275 times faster when bicarbonate is phosphorylated by ATP. The perforation in the tunnel created by the G359F mutant caused an uncoupling between the carboxyphosphate and glutaminase active sites. These studies imply that the phosphorylation of bicarbonate is the trigger for the release of ammonia into the tunnel.

Mutational analysis of the residues lining the carbamate tunnel showed that it was possible to engineer a blockage in the tunnel, but it was not possible to create a "hole". Several mutants, such as G575L, A23L/G575S, and A23L/G575L, exhibited diminished rates of synthesis of carbamoyl phosphate, but the individual activities of the N- and C-terminal active sites on the large subunit remained largely unperturbed.[39] No evidence for any coupling or uncoupling of the activities of these two active sites was observed.

Molecular tunnels have also been found in all members of the amidotransferase superfamily for which crystal structures are available.[40] Such enzymes include: glutamine phosphoribosylpyrophosphate amidotransferase[41], asparagine synthase[42],

glutamate synthase[43], imidazole glycerol phosphate synthase[44], glucosamine 6-phosphate synthase[45], tRNA-dependent amidtoransferase[46], and cytidine triphosphate synthetase.[47] All of these enzymes utilize ammonia that is derived from hydrolysis of glutamine. Besides ammonia, other intermediates have also been found to migrate through intramolecular tunnels. Tryptophan synthase has a tunnel for the transport of indole.[48] Acetyl-CoA synthase/carbon monoxide dehydrogenase transports carbon monoxide, and a 4-hydroxy-2-ketovalerate aldolase/acylating acetaldehyde dehydrogenase contains a tunnel for the transport of acetaldehyde.[49-50] The common thread between all of these enzymes is that they contain multiple active sites and have unstable reaction intermediates that need to be protected from solvent.

Glutamine phosphoribosylpyrophosphate amidotransferase (GPATase) plays a critical role in the biosynthesis of purines, pyrimidines, amino acids, and amino sugars.[51] Crystallographic studies of GPATase revealed an interesting new twist to the intramolecular channeling of substrates. The ammonia tunnel forms by a large-scale loop reorganization after the binding of phosphoribosylpyrophosphate (PRPP) at the acceptor domain.[52] GPATase catalyzes the first step in the *de novo* pathway for the biosynthesis of purine nucleotides by converting phosphoribosylpyrophosphate to phosphoribosylamine (**Scheme 1.3**). The enzyme is a dimer composed of two identical units. Each monomer contains two domains, the glutaminase domain and the acceptor domain (**Figure 1.9**). Each domain contains an active site. When the crystal structure of GPATase was solved in the presence of diazo-5-oxonorleucine and a stable carboxylic

analog of PRPP, a ~20 Å long hydrophobic tunnel was observed connecting the two active sites (**Figure 1.9**)[52].

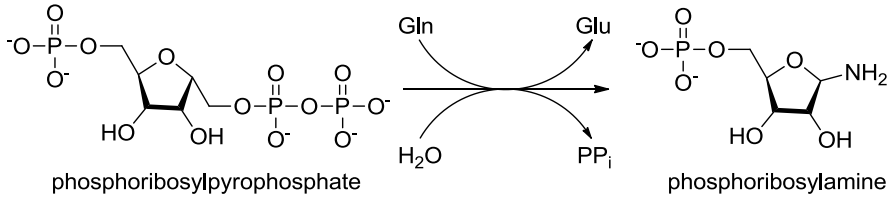

Scheme 1.3. Reaction catalyzed by glutamine phosphoribosylpyrophosphate amidotransferase.

Recent computational studies on GPATase using locally enhanced sampling (LES) and potential of mean force (PMF) calculations revealed that the largely hydrophobic tunnel found in the activated form of the enzyme is reminiscent of a "pipe" through which ammonia travels without application of external forces.[51] Furthermore, these studies showed that ammonia was guided through the tunnel by local motions of the residues lining the interior of the tunnel. NH_3 migrates through the tunnel by forming and breaking hydrogen bonds with the backbone carbonyl groups and side chains of the residues in the tunnel. The largest energy barrier in the passage of NH_3 to the second active site is 11 kcal/mol which corresponds to the energy required to break the hydrogen bonds with the active site residues before gaining entry into the tunnel. The transport of an ammonium ion through the tunnel was not energetically favorable.

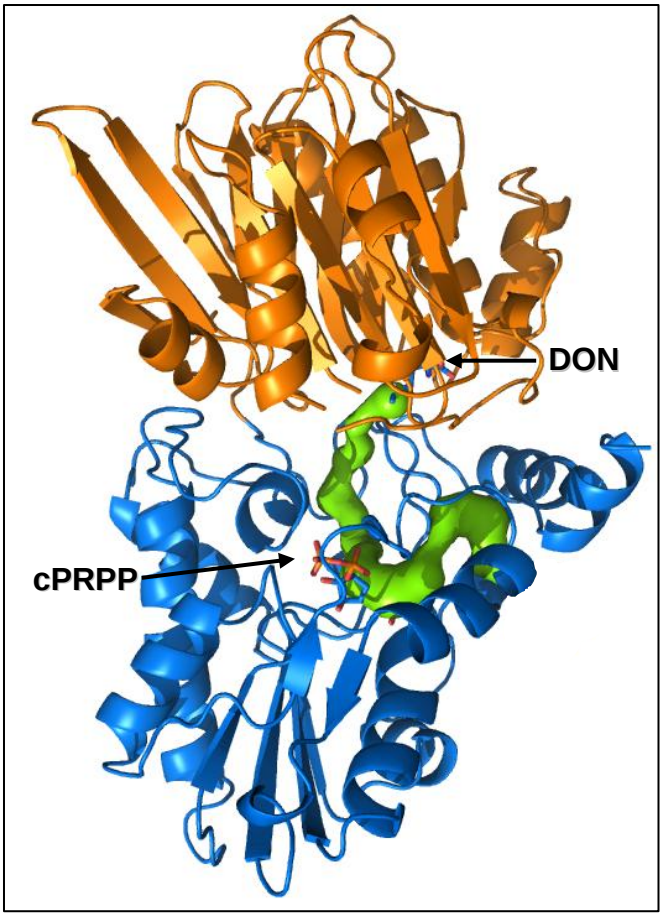

Figure 1.9. Crystal structure of glutamine phosphoribosylpyrophosphate amidotransferase.[52] The glutaminase domain is shown in orange, the acceptor domain is shown in blue. The intramolecular tunnel was calculated using the Caver2.0v0.003 program and is depicted in green.[53] DON – 6-diazo-5-oxonorleucine, cPRPP – carboxylic acid analog. (PDB code 1ecc)

Another example of an enzyme with an intramolecular ammonia tunnel is imidazole glycerol phosphate synthase (IGP synthase). This enzyme catalyzes the fifth step in the biosynthesis of histidine, which is also the branching point for the purine biosynthetic pathway.[54] IGP synthase is responsible for the formation of imidazole glycerol phosphate (IGP) and 5'-5-aminoimidazole-4-carboxamide ribonucleotide

(AICAR) from N^1-(5'-phosphoribulosyl)-formimino-5-aminoimidazole-4-carboxamide ribonucleotide (PRFAR) and glutamine (**Scheme 1.4**).[55] From X-ray crystallographic data the structure of the enzyme, isolated from *S. cerevisiae*, revealed that it is a monomer with two active sites (**Figure 1.10**).[44] The first active site catalyzes the hydrolysis of glutamine, while the second site is required for the cyclization part of the reaction. The glutaminase domain of the enzyme is mostly composed of β-sheets, while the cyclase domain adopts a classical $(\beta/\alpha)_8$ TIM barrel fold.[44] The cyclase active site of the enzyme is located on the farthest end of the β-barrel from the glutaminase active site. Thus, both sites are linked by a tunnel for the transport of ammonia.

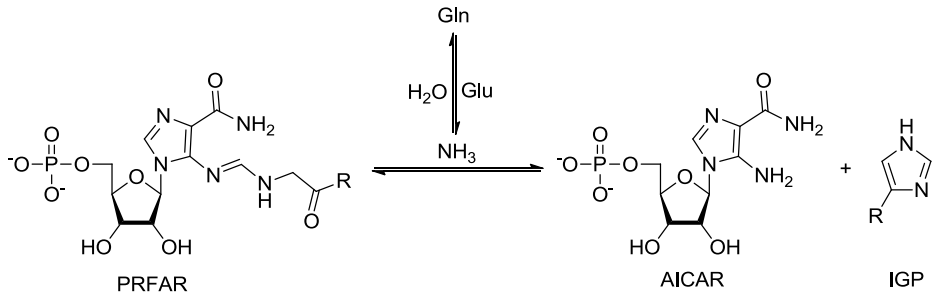

Scheme 1.4. Reaction catalyzed by imidazole glycerol phosphate synthase. PRFAR – N^1-(5'-phosphoribulosyl)-formimino-5-aminoimidazole-4-carboxamide ribonucleotide, AICAR – 5'-5-aminoimidazole-4-carboxamide ribonucleotide, IGP – imidazole glycerol phosphate.

Figure 1.10. Crystal structure of imidazole glycerol phosphate synthase.[44] The glutaminase domain is shown in orange and the cyclase domain is shown in blue. The intramolecular tunnel was calculated using the Caver2.0v0.003 program and is depicted in green.[53] Water molecules are shown as red spheres. (PDB code 1ox5)

The crystal structure of IGP synthase revealed the presence of a possible gate, formed by highly conserved residues Arg-239, Glu-293, Lys-99, and Glu-465, located at the interface between the glutaminase and cyclase domains. Computational studies using extended equilibrium MD simulations as well as steered molecular dynamics (SMD) provided a possible mechanism for the transport of ammonia.[54] They also showed an unusual way in which ammonia gets around the proposed charged gate inside the tunnel.[54] Similar to the ammonia tunnel in CPS, the entire molecular tunnel in IGP

synthase is filled with water molecules. While several water molecules populate the tunnel, SMD calculations showed that the transport of water alone through the tunnel was energetically unfavorable. Ammonia is able to move through the tunnel by forming and breaking hydrogen bonds with both water molecules and residues inside the tunnel. An interesting feature of NH_3 migration through this tunnel is that it bypasses the previously mentioned charged gate located between the two domains. A small opening between Lys-99 and Glu-46 provides a pocket big enough for ammonia to squeeze through without having to traverse the energetically unfavorable space in the middle of the gate.[54] By contrast, the ammonia tunnel in CPS does not have a charged gate that NH_3 must pass through, however, it does contain a very narrow gate with a relatively high energy barrier.

Carbamoyl phosphate synthetase catalyzes one of the most intriguing reactions in biochemistry. Separate reactions performed by CPS are simple when looked at by themselves, but when combined together form a complex and elegant reaction mechanism. CPS has evolved and perfected a method for synchronizing these reactions and timing conformational changes in a way that maximizes enzymatic efficiency. Over the last fifty years the enzyme has been characterized kinetically, chemically, crystallographically, and computationally. With each investigation new ground is gained, but new questions arise. Are the N- and C-terminal active sites on the large subunit synchronized? What is the rate limiting step in the reaction mechanism? Can direct proof be found for the presence of the carboxyphosphate intermediate? The work presented in this dissertation makes an attempt to address these questions.

CHAPTER II

TOWARD DETERMINATION OF SYNCHRONIZATION BETWEEN THE ACTIVE SITES IN THE LARGE SUBUNIT OF CARBAMOYL PHOSPHATE SYNTHETASE

Introduction

Carbamoyl phosphate synthetase (CPS) from *E. coli* catalyzes the formation of carbamoyl phosphate. The carbamoyl phosphate synthesized by CPS is directly involved in pyrimidine and arginine biosynthesis.[3] CPS is able to produce carbamoyl phosphate from two molecules of MgATP, one molecule of bicarbonate, and one molecule of glutamine.[1] The generally accepted reaction mechanism is summarized in **Scheme 2.1**. In the initial reaction, the first molecule of ATP is used to phosphorylate bicarbonate to generate the reactive intermediate, carboxyphosphate. Glutamine is hydrolyzed to glutamate and ammonia, followed by the reaction of ammonia with the carboxyphosphate intermediate to form carbamate. Finally, a second molecule of ATP is used to phosphorylate carbamate to form the ultimate product, carbamoyl phosphate. There are thus four separate reactions and three discrete, reactive, and unstable intermediates involved in this reaction mechanism: carboxyphosphate, ammonia, and carbamate.[5-6]

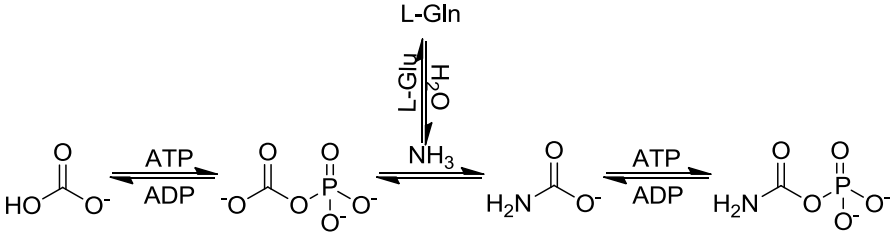

Scheme 2.1

The isolated protein from *E. coli* is a heterodimer that is composed of a small (42 kDa) and a large (118 kDa) subunit, thus forming an αβ-heterodimer (**Figure 2.1**). It is also possible for multiple heterodimers to oligomerize and form an $(\alpha\beta)_4$-tetramer in the presence of the allosteric activator, ornithine. The smaller subunit of the heterodimer is responsible for the amidotransferase activity of the enzyme.[13,56] Here glutamine is hydrolyzed to glutamate and ammonia via a thioester intermediate.[57] The ammonia derived from the small subunit travels approximately 45 Å to react with the carboxyphosphate waiting at the first catalytic site on the large subunit. The carbamate formed at this site, is channeled ~ 35 Å to the second catalytic site on the large subunit.[34] At this active site, carbamate is phosphorylated by a second molecule of MgATP to form the ultimate product, carbamoyl phosphate.[21]

One of the very interesting aspects about CPS is that the large subunit contains a homologous repeat sequence where residues 1-400 share 40% sequence identity with residues 557-933.[15] This has been postulated to be a result of a gene duplication event from a more primitive protein with kinase activity. The N-terminal domain of the large subunit catalyzes the formation of carboxyphosphate (carboxyphosphate synthetic component). The C-terminal domain of the subunit catalyzes the formation of carbamoyl phosphate (carbamoyl phosphate synthetic component) (**Figure 2.1**).[16-19] Each of these domains contains an ATP binding site.[16]

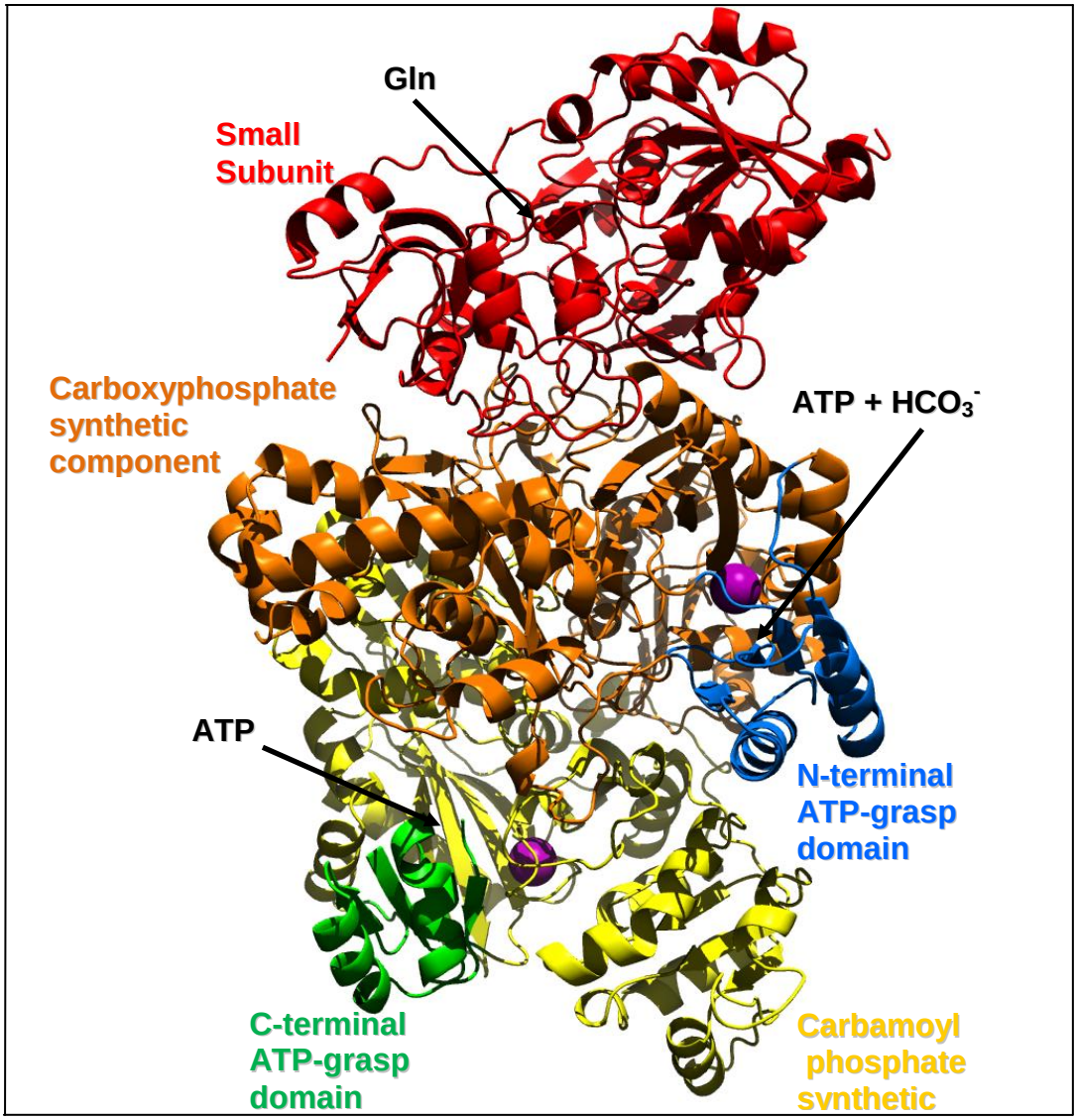

Figure 2.1. X-Ray crystal structure of *E. coli* CPS. Location of different domains within the protein is shown in different colors. The intramolecular tunnel is shown in dark grey spheres. Potassium ions are shown as purple spheres. (PDB code 1bxr)

The ATP binding sites on the large subunit contain subdomains, termed as B-domains (**Figure 2.1**). The B-domains are thought to undergo conformational changes that allow substrates to enter, and products to exit the active sites. Structural characterization of the enzyme provided direct evidence for the conformational change that occurs at the C-terminal B-domain: this domain clamps down over the active site to isolate the reactants from bulk water.[29,31,58] In the presence of the nonhydrolysable ATP analog, β,γ-imidoadenosine 5′-triphosphate (AMPPNP), this domain is observed in the closed conformation, while in the presence of ADP the domain appears to be in a more open conformation.[21,29] These data suggest that the opening and closing of the B-domain allows substrates and products to enter and exit the carbamoyl phosphate active site.[29] In the crystal structures with ADP and P_i or AMPPNP bound in the carboxyphosphate active site, the N-terminal B-domain remains in the closed conformation (**Figure 2.2**). Since there is approximately 37% sequence identity between the N- and C-terminal B-domains, it is expected that a conformational change similar to the one observed for the C-terminal B-domain will occur within the N-terminal B-domain.

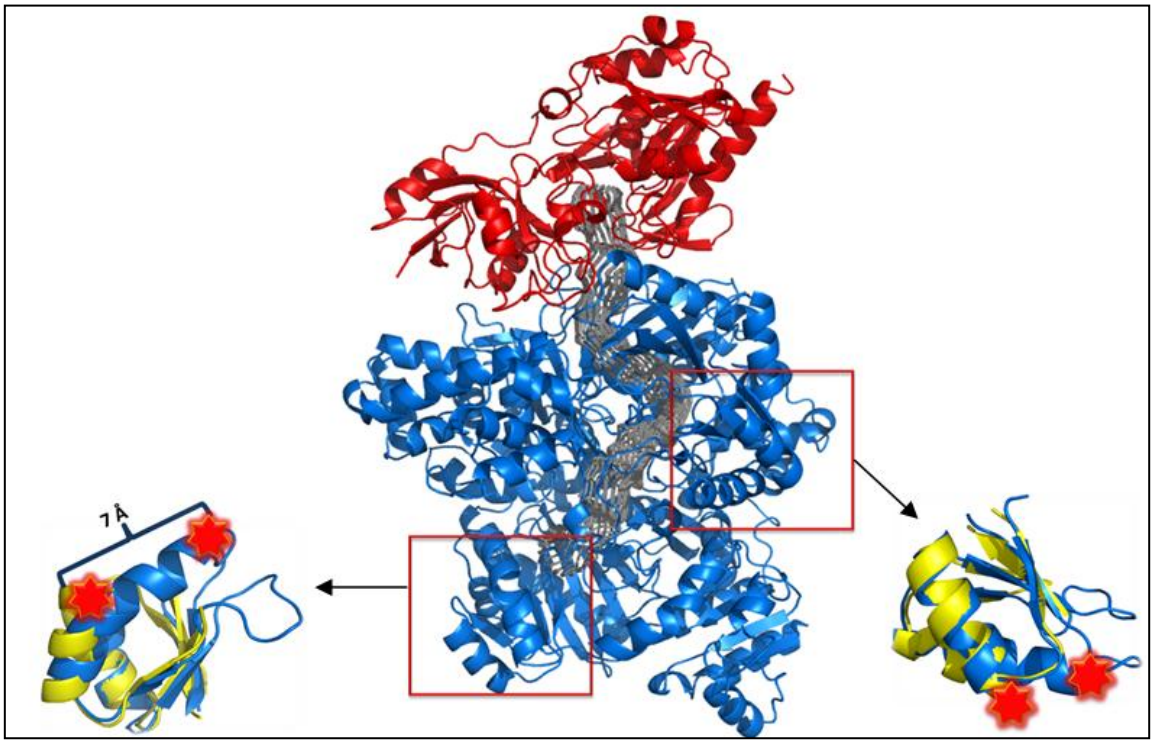

Figure 2.2. Conformational changes of CPS in the presence of substrates. The large subunit of CPS is depicted in blue, with the small subunit shown in red. The intermolecular tunnel is shown in grey. The N- and C- terminal B-subdomains are highlighted with red boxes. In the close-up view of the B-domains the blue represents the closed conformation, while the yellow shows the open state. Engineered Cys residues, 171 and 717, are shown in red.

The kinetic mechanism of CPS suggests that the two MgATP molecules utilized by CPS bind to the enzyme in an ordered manner. The reaction is initiated with the binding of the first molecule of MgATP. This is followed by the binding of bicarbonate and the formation of the carboxyphosphate intermediate. Ammonia is formed as a result of glutamine hydrolysis in the small subunit and is channeled to the carboxyphosphate active site to react with carboxyphosphate to form carbamate. Following formation of

carbamate, P_i is released and a second molecule of MgATP binds at the carbamoyl phosphate active site.[5-6] The reaction mechanism is summarized in **Scheme 2.2**.

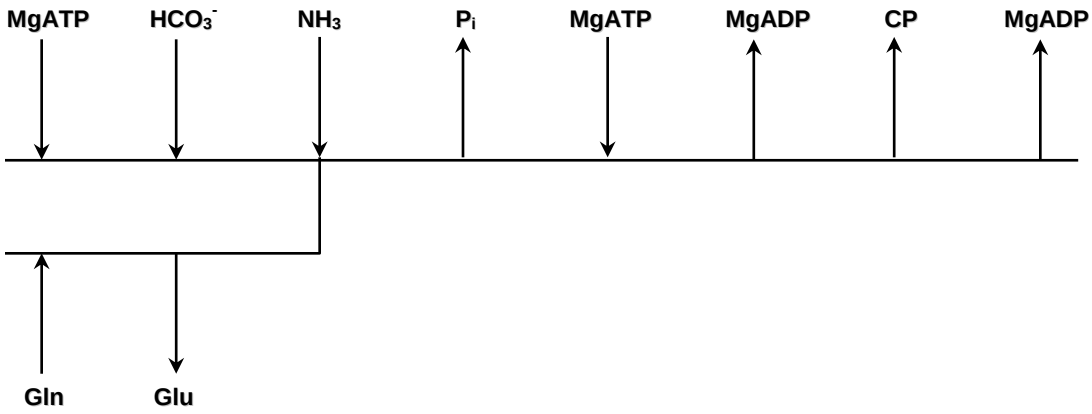

Scheme 2.2

It has yet to be determined what coupling, if any, occurs between these two sites on the large subunit. It has been proposed by Rubio *et al*. through pulse/chase experiments that both ATP molecules bind to the large subunit randomly. This observation is supported by the fact that there were two molecules of the nonhydrolysable ATP analog, AMPPNP, bound at both active sites on the large subunit when CPS was crystallized in its presence.[29] It was also observed by Rubio *et al*. that the second molecule of ATP, which phosphorylates carbamate, exchanges with ATP in solution at a much slower rate when bicarbonate is present. This exchange rate increases when HCO_3^- and K^+ are excluded from the reaction mixture.[58] Based on this information one can propose that the second ATP binds to CPS at approximately the same time as the one that participates in the phosphorylation of bicarbonate. However, as the reaction proceeds at the carboxyphosphate active site, a signal may be propagated to the carbamoyl phosphate active site that closes the corresponding B-domain, thus

sequestering the second ATP in that active site. The formation of carbamoyl phosphate, is proposed to trigger the opening of the carbamoyl-phosphate B-domain, thereby releasing the products, ADP and carbamoyl phosphate. Since the two ATP binding sites are so far apart, a signaling mechanism must exist to synchronize their activities. It is not clear how the two domains accomplish this. The primary goal of this work was to develop an approach toward understanding how the communication mechanism functions between the carbamoyl phosphate and the carboxyphosphate active sites.

Materials and Methods

Bacterial Strains and Plasmids. Site-directed mutagenesis of CPS was performed as described previously.[28,59] The RC50 strain used for protein expression was a generous gift from Dr. Carol J. Lusty. All plasmids used in this project were derived from pMS03 and 6WY.[38,60] In the 6WY plasmid, a generous gift from Jason L. Johnson, all of the intrinsic tryptophans in wild-type CPS were mutated to tyrosines. Oligonucleotide synthesis and DNA sequencing reactions were performed by the Gene Technology Laboratory, Texas A&M University.

Construction and Purification of Mutant Proteins. Site-directed mutagenesis was performed using the QuikChange® protocol from Stratagene. All of the site-directed changes made to wild-type CPS were confirmed by DNA sequencing of the modified plasmids. The plasmids containing the *car*AB genes were transformed in the RC50 cell line of *E. coli* for expression of the wild-type and mutant forms of CPS. The wild-type and mutant variants of CPS were purified as previously described.[38] Mutation sites were

determined based on solvent exposure calculations done using CCP4MG molecular graphics program.[61-62] The following mutants were made in the large subunit using the tryptophan-less construct (6WY): F172W and F718W. Mutants C551S, C551A, S717C, C551S/S717C, C551A/S717C, C551A/C248A, C551A/S171C, and S171C in the large subunit were made using the pMS03 plasmid. All mutants were expressed and purified to greater than 95% homogeneity, as judged by SDS-polyacrylamide gel electrophoresis.

In-trans CPS Construction. The pMS03 plasmid was used as the starting point for the *in-trans* CPS construct. A modified version of a previously reported procedure was used to express the large subunit in two halves.[63] In summary, a DNA sequence encoding a stop codon and a ribosomal binding site, 5'-TAATCAGGAGTAAAAGA-3', was inserted into the pMS03 plasmid between Tyr-542 and Met-543 in the large subunit using the QuikChange® protocol from Stratagene. This site was chosen as the point of division between the N- and C-terminal halves of the large subunit based on its location on the surface of the protein. The placement of this break would cause the least amount of structural perturbation.

Solvent-Exposed Sulfhydryl Determination. 5,5'-Dithio-bis(2-nitrobenzoic acid) (DTNB) was used to determine the number of solvent-exposed sulfhydryl groups present on wild-type CPS as well as C551S, C551A, C551A/C248A, C551A/S171C, C551A/S717C, and C551S/S717C mutants. The reaction mixture contained 50 mM HEPES, pH 7.6, 10 mM ornithine, 1 mg of protein, and a 10-fold excess of DTNB. Each reaction was incubated for 30 minutes at 30 ºC before measuring the absorbance at 412 nm. In the case of the wild-type and C551S enzymes, 1 mM ATP and 20 mM

$MgCl_2$ were added after the first 30 minutes incubation phase. Absorbance at 412 nm was measured after an additional 30 minute incubation phase.

Fluorophore Labeling. Cysteine-containing mutants, C551A/S171C and C551A/S717C, were labeled with a thiol-specific reagent N-ethylmaleimide (NEM) fluorescein in DMSO. Each reaction mixture contained 20 μM enzyme, 200 μM fluorescein, 13 mM ornithine, and 25 mM HEPES, pH 7.5. All components were mixed in the dark and incubated at 4 ºC overnight. Unreacted fluorophore was removed using a Sephadex G-50 column. The Cys-fluorescein content of each enzyme was calculated using an extinction coefficient of 73,000 $M^{-1}cm^{-1}$ at 492 nm, and compared to the protein concentration determined by the absorbance at 280 nm. Labeling efficiencies were in the range of 50-90% for each enzyme.

Kinetic Measurements. The reaction mixtures for the glutamine-dependent ATPase assay contained 50 mM Hepes, pH 7.6, 20 mM $MgCl_2$, 100 mM KCl, 40 mM $KHCO_3$, 10 mM glutamine, 10 mM ornithine, 1.0 mM phosphoenolpyruvate, 0.2 mM NADH, 2 units of pyruvate kinase, 3 units of lactate dehydrogenase, and varying amounts of ATP. Glutamine was excluded from the bicarbonate-dependent ATPase assays. Both of these assays were followed by monitoring the decrease in absorbance at 340 nm using a Molecular Devices SpectraMax Plus 96-well plate reader. The synthesis of carbamoyl phosphate was determined by measuring the rate of citrulline formation in a coupled assay containing ornithine transcarbamoylase (OTCase) and ornithine.[19] The assay mixtures contained 50 mM Hepes, pH 7.6, 20 mM $MgCl_2$, 100 mM KCl, 40 mM $KHCO_3$, 5.0 mM ATP, 10 mM ornithine, 12 units of OTCase, and 10 mM glutamine.

Fluorescence Anisotropy Measurements. Ligand-induced changes in fluorescence anisotropy of C551A/S171C and C551A/S717C mutants were measured on a PTI QM-4 Quantmaster fluorometer equipped with a 75W xenon arc lamp and a Schott OD515 polarizer. Emission was monitored at 521 nm following excitation at 492 nm. All fluorescence experiments contained 100 nM fluorescently labeled CPS and combinations of the following: 10 mM ornithine, 100 mM KCl, 20 mM $MgCl_2$, 1 mM ADP, 1 mM P_i, 1 mM AMPPNP, 10 mM glutamine, 40 mM HCO_3^-, 1 mM ATP, and 1 mM carbamoyl phosphate. Reactant combinations are summarized in the figure on page 36**.** Corrections were made for signal contributions from the blank.

Results

Tryptophan-less Mutants. The most straight forward way of studying protein motions through fluorescence or fluorescence anisotropy is by introducing tryptophans at locations of interest on the protein. CPS has six intrinsic tryptophans that all contribute in some way to the fluorescence response of the protein.[60] By removing these tryptophans it was possible to start with a "clean slate" and introduce reporter tryptophans at the N- and C-terminal B-domains on the large subunit of CPS. F172W and Y718W mutants were made in the Trp-less construct. These sites were chosen based on their locations at the most mobile portions of the B-domains. While it was possible to engineer the constructs for these mutants, it was impossible to purify these proteins. Poor expression and insolubility were major obstacles that rendered this method impractical.

Free Sulfhydryl Group Determination. Another approach to studying enzymatic motions by fluorescence techniques is by engineering cysteines at key locations and modifying them with a fluorescent probe. It has been shown by Foley R. *et al*., through labeling experiments with ^{14}C-NEM and titration with DTNB, that there are three reactive cysteine residues located on CPS. One cysteine reacts with thiol-modifying reagents solely in the presence of ornithine, while the other two require additional substrates and allosteric effectors in order to react.[64] The second –SH group becomes exposed to solvent in the presence of MgATP, while the third thiol group requires addition of UMP. It was important to determine the identity of the most reactive cysteine in order to be able to avoid background labeling by thiol-reactive fluorophores.

From the solvent exposure calculations performed for each of the 18 cysteine residues present in CPS, it was apparent that Cys-551 was the most solvent-exposed thiol (**Figure 2.3**). Therefore, it was the most likely to react with a thiol-modifying agent and produce background signal. This residue was mutated to a serine and an alanine in order to determine which substitution was tolerated the best. The kinetic constants for both mutants for the glutamine-dependent ATPase reaction were comparable to those measured for wild-type CPS (**Table 2.1**).

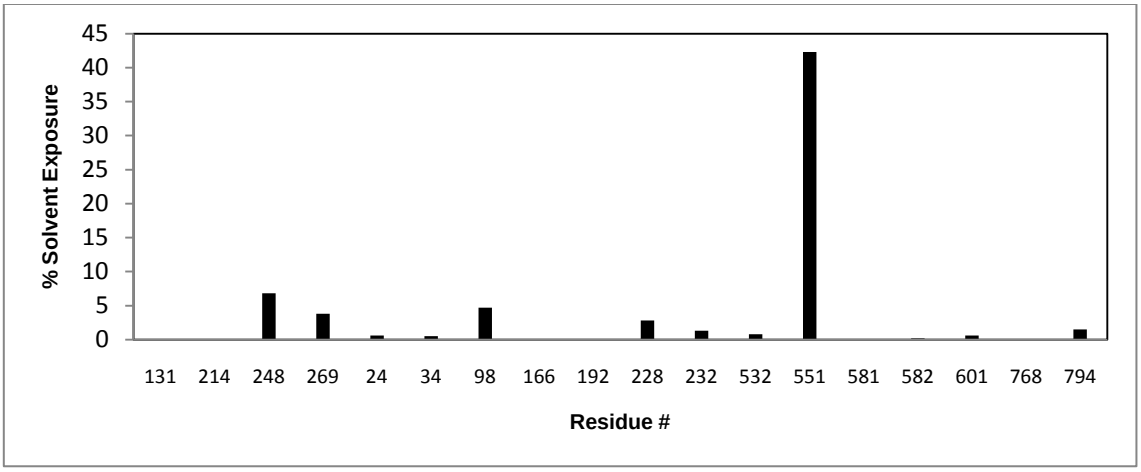

Figure 2.3. Solvent exposure of cysteine residues calculated from the closed conformation of wild-type CPS. PDB code: 1bxr. Residues 131, 214, 248 and 269 are located in the small subunit.

Table 2.1. Kinetic Characterization of the Wild-Type and Mutant Forms of CPS

Enzyme	Gln-Dependent ATPase		HCO_3^-- Dependent ATPase[a]	
	k_{cat} (s^{-1})	K_M (mM ATP)	k_{cat} (s^{-1})	K_M (mM ATP)
WT CPS	3.60 ± 0.11	0.24 ± 0.04	0.170 ± 0.003	0.051 ± 0.008
Trp-less CPS	2.40 ± 0.10	0.051 ± 0.01		
Trans-CPS	0.68 ± 0.02	0.075 ± 0.018	0.22 ± 0.013	0.24 ± 0.067
WT-Fluorescein	1.56 ± 0.09	0.67 ± 0.11		
C551S	6.8 ± 0.50	0.086 ± 0.02		
C551S-DTNB	12.2 ± 1.0	0.07 ± 0.02	1.2 ± 0.14	0.01 ± 0.006
S717C	9.5 ± 0.36	0.92 ± 0.06	1.3 ± 0.06	0.11 ± 0.01
S171C	1.8 ± 0.10	0.38 ±0.06		
C551A	2.7 ± 0.04	0.12 ± 0.007		
C551A/C248A	16.16 ± 1.3	0.27 ± 0.08		
C551A/S717C	2.35 ± 0.14	0.38 ± 0.08		
C551A/S171C	9.2 ± 0.70	0.26 ± 0.07		
C551A/S171C-Fluorescein	0.86 ± 0.08	1.09 ± 0.25		
C551A/S717C-Fluorescein	0.12 ± 0.01	0.014 ± 0.007		

[a] HCO_3^--dependent ATPase activity was measured in the absence of glutamine.

The amount of free thiol present on these mutants was determined by titrations with DTNB (**Table 2.2)**. Wild-type CPS had one free thiol that reacted with DTNB immediately after mixing the reagents together (**Table 2.2**), and a second thiol that only became accessible to solvent in the presence of ATP and Mg^{2+}. Based on solvent exposure analysis shown in **Figure 2.3** Cys-551 was most likely residue to be involved in this process. To test for this, wild-type CPS was incubated with N-ethylmaleimide (NEM) and digested by chymotrypsin. The fragments were then analyzed by MALDI mass spectroscopy. While only about 30% of sequence coverage was obtained, it was possible to identify peaks in each spectrum that corresponded to labeled and unlabeled peptide fragments that contained Cys-551 (**Figure 2.4**).

The C551S and C551A mutations were designed to eliminate the most reactive cysteine, however after the introduction of these point mutations to CPS, there was still one equivalent of free -SH present per enzyme after 30 minutes of incubation (**Table 2.2**). Cys-248 was identified as a possible residue responsible for this labeling pattern. While it was largely buried inside the small subunit in the structure used for calculating the solvent exposure of each cysteine, it is possible that its proximity to the site for glutamine hydrolysis caused it to become more exposed during the course of natural protein motions. This residue was mutated to an alanine in the C551A mutant in order to see if the same labeling pattern would be observed. The labeling data for the double mutant appeared to be identical to the C551A single mutant, which meant that C248A was not the -SH group exposed during the labeling experiment (**Table 2.2**).

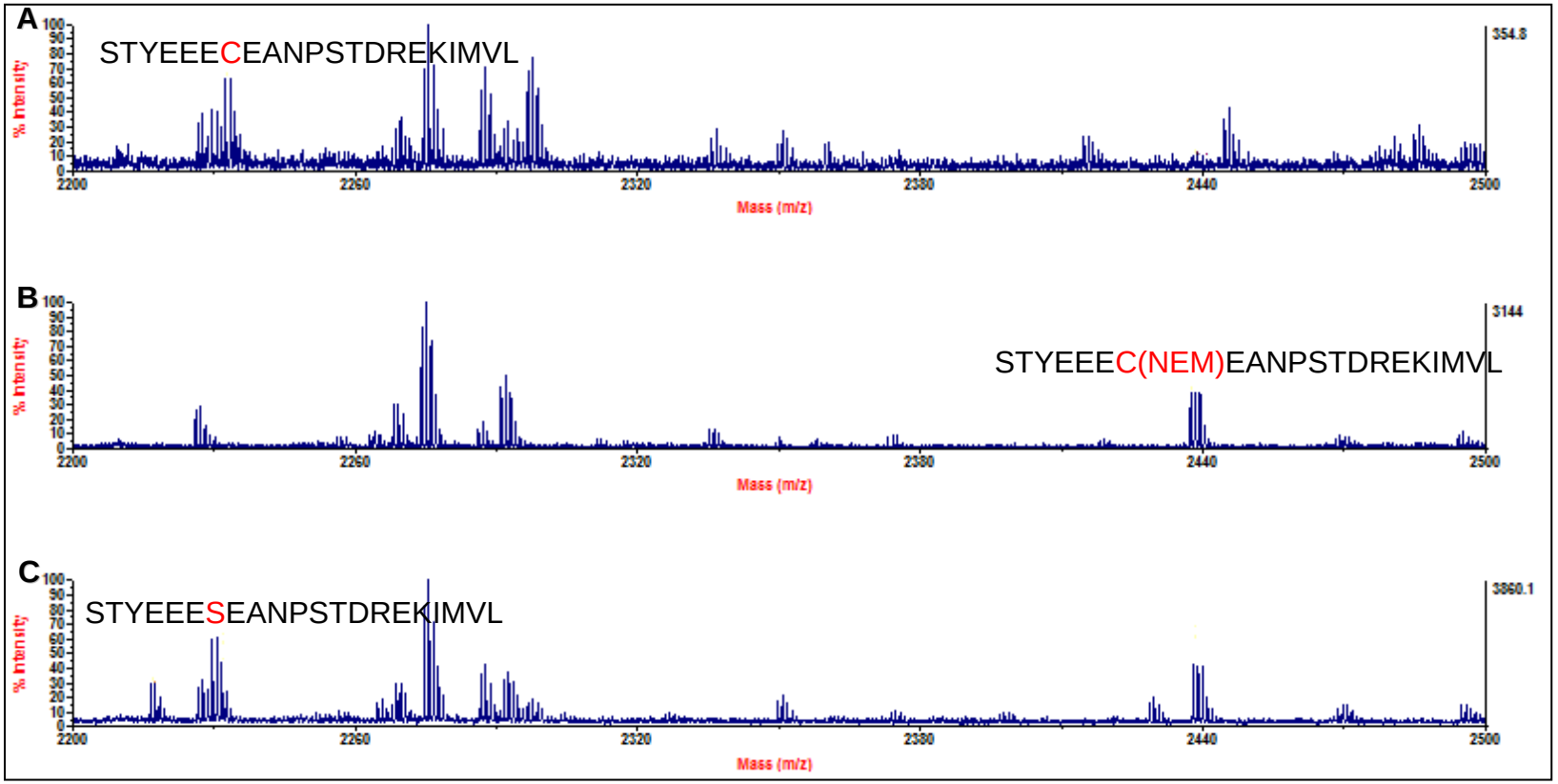

Figure 2.4. MALDI spectrum of A) wild-type CPS, B) wild-type CPS incubated with N-ethylmaleimide (NEM), C) C551A mutant incubated with NEM. Peptide fragments containing residues of interest are shown above their corresponding peaks. C551, C551+NEM, and C551S are highlighted in red.

Table 2.2. Titrations with DTNB.

Enzyme	SH groups at t = 0 min	SH groups at t = 30 min	SH groups +ATP, Mg^{2+}
WT	0.9	1.1	2.0
C551S	0.5	1.2	2.4
C551A	0.2	1.1	ND
C248A/C551A	0.3	0.9	ND
C551A/S171C	0.4	0.8	ND
C551A/S717C	0.2	1.0	ND

ND - not determined

The C551A mutant was used to generate cysteine insertion mutants necessary for fluorophore labeling studies. This mutant was chosen because the unknown thiol that reacted with DTNB did so in a slower manner than Cys-551 in the wild-type enzyme. Immediately after mixing C551A with DTNB only 0.2 equivalents of free -SH groups were present per enzyme rather than 0.9 observed when wild-type CPS was subjected to the same conditions (**Table 2.2**). Thus the underlying assumption for engineering the C551A/S171C and C551A/S717C mutants was that the newly introduced cysteine residues would be more solvent exposed and would react with the label faster than the unknown thiol. These two mutants were engineered to contain a cysteine residue at the most mobile portion of each of the B-domains associated with the carboxyphosphate and carbamoyl phosphate active sites, respectively (**Figure 2.2**). DTNB titration experiments were used to assess the amount of free sulfhydryl groups on various CPS mutants immediately after mixing the reagents together and after a 30 minute incubation time. Only one labeled cysteine equivalent was observed for both C551A/S171C and

C551A/S717C mutants after 30 min. This labeling pattern may be indicative of the engineered cysteine residues outcompeting the unknown thiol for DTNB. It was not possible to confirm the location of DTNB on the mutant enzymes by mass spectrometry analysis due to the large size of CPS and the nonspecific cleavage of the protein by trypsin and pepsin. However, despite the inconclusive labeling data C551A/S171C and C551A/S717C mutants were selected for further analysis by fluorescence anisotropy techniques.

Anisotropy. The degree of rotation of the fluorophore while it is in the excited state can be monitored in terms of the depolarization of the fluorescence emission, or anisotropy. Here the changes in the steady-state anisotropy of the two double mutants, C551A/S171C and C551A/S717C are reported. The overall rotational motion of a large protein like CPS is slow relative to the fluorescence lifetime of fluorescein so that differences in anisotropy will be dominated by changes in local motion experienced by fluorescein bound at the B-domains. The following steady-state anisotropy values were measured for each protein in the absence of all ligands: wild-type CPS, 0.209 ± 0.0008, C551A/S171C, 0.195 ± 0.0007, and C551A/S717C, 0.174 ± 0.0008. Wild-type CPS was labeled with fluorescein at Cys-551, while the two mutants were labeled with fluorescein at S171C and S717C, respectively. The slight variations in anisotropy values measured for these three different proteins are indicative of the somewhat different environments that each fluorophore experiences. Higher anisotropy values usually represent a more rigid environment, while lower values represent a more flexible one. From the initial anisotropy readings, it is possible to say at the local environment around

S717C is more flexible than that of fluorescein at S171C or C551. All anisotropy readings in the presence of various ligands showed a decrease in the rotational response of the fluorophore from the unliganded form of the protein.

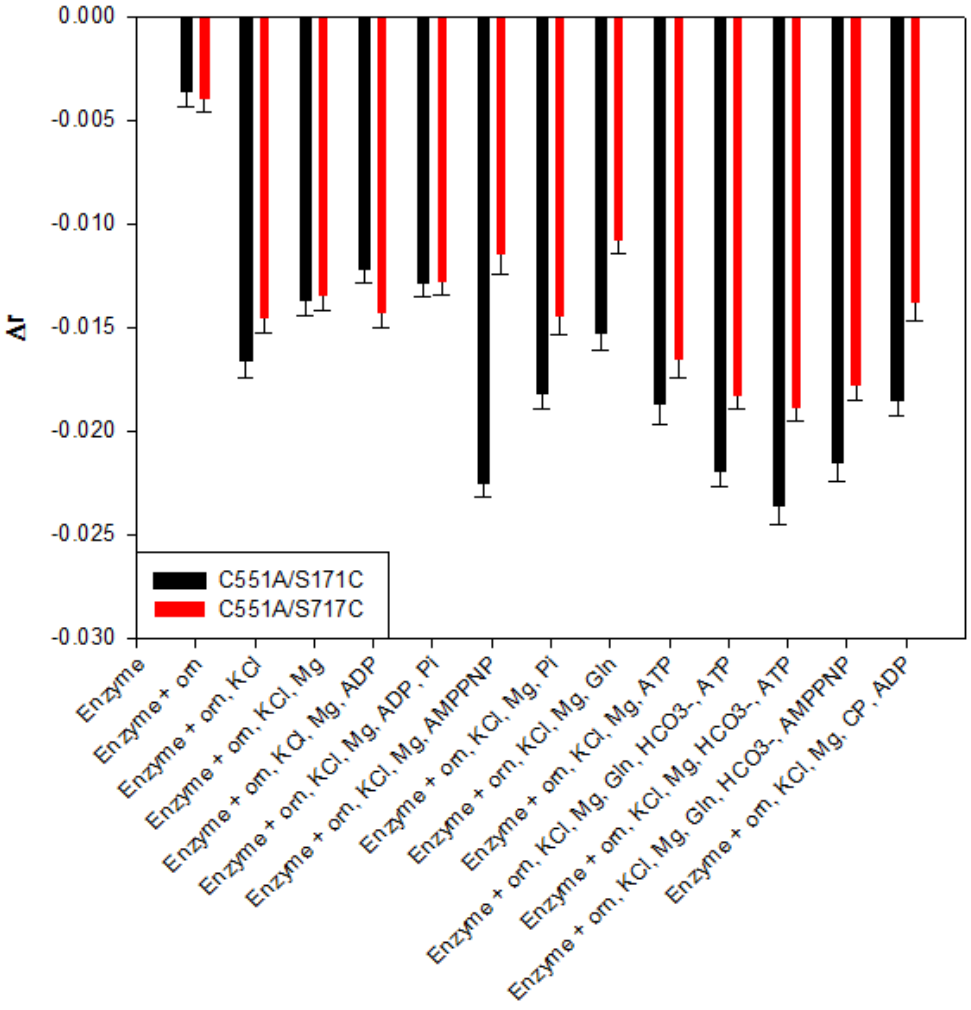

Figure 2.5. Absolute changes in anisotropy of fluorescein tagged to Cys-171 and Cys-717 in the C551A/S171C and C551A/S717C mutants in the presence of various ligands. Experimental setup and concentrations of reactants are described in *Materials and Methods*.

Figure 2.5 summarizes all of the ligand-induced changes in the anisotropy values of the fluorescein-labeled double mutants, C551A/S171C and C551A/S717C. These changes in anisotropy are quite small, but statistically relevant.[60,65] When ornithine was added to either mutant, a slight change in the rotational response of both the N- and C-terminally positioned fluorophores was observed. When K^+ was added to this mixture the anisotropy decreased even further, by about 0.01, for both mutants. CPS is the most active in the presence of ornithine, and K^+ is required for activity, therefore this combination of ligands, was taken as the physiologically relevant base for comparing all other ligand combinations.

From previously reported X-ray crystal structure, both B-domains are observed in the closed conformation when the non-hydrolysable ATP analog, AMPPNP is bound.[29] The anisotropy response of both B-domains was tested in the presence of this analog. When AMPPNP and Mg^{2+} were added to CPS, in the presence of ornithine and K^+, an additional decrease in anisotropy of about 0.01 was observed for the N-terminal B-domain. Under these same conditions the C-terminal B-domain remained unaffected. Further addition of glutamine and bicarbonate to these solutions did not have effect on the rotational response of the fluorophores.

The effect of ATP in combination of bicarbonate and glutamine was also tested for both B-domains. When ATP and Mg^{2+} were added to CPS in the presence of ornithine and K^+, the anisotropy response of both active sites was close to that of the response in the presence of AMPPNP and Mg^{2+}. Addition of either HCO_3^- or glutamine, or both, did not show any further effect on the anisotropy signal of either fluorophore.

The effect of ADP on the conformation of that B-domains was tested in the presence and absence of P_i and the final reaction product, carbamoyl phosphate. For either B-domain, there was no change observed in the anisotropy signal when ADP was added to CPS in the presence of ornithine and K^+. In addition, when P_i or carbamoyl phosphate were included in the assay, no change in the signal was seen for either B-domain. Finally, no change in the rotational response of both fluorescent probes was observed when P_i or glutamine were added to the reaction mixture in the presence of ornithine and K^+. Neither molecule had any effect on the signal arising from both B-domains (**Figure 2.5**).

In-trans CPS. A different way to resolve the ambiguity of the anisotropy results as well as to directly address the coupling between carboxyphosphate and carbamoyl phosphate active sites would be to create an in *trans* protein. This modified CPS contains a stop codon and an additional ribosomal binding site in its *carB* gene. Based on gene sequencing and structural analysis it has been determined that the large subunit contains a homologous repeat sequence where residues 1-400 share 40% sequence identity with residues 557-933.[15] The high level of sequence identity between these two domains led to a hypothesis that the current form of the large subunit resulted from a gene duplication event from a more primitive enzyme with kinase activity.[15] Given this information, it should be possible to divide the large subunit into two functional halves. In a similar experiment it has been shown that the small subunit of CPS can be expressed in *trans*.[63]

The large subunit has been cut into two halves between Tyr-542 and Met-543. This site was chosen because both residues represent the designated boundary between

the oligomerization domain and the carbamoyl phosphate synthetic component.[34] Tyr-542 and Met-543 are also located in a relatively mobile loop on the surface of the protein, thus making any conformations adopted by the newly created N- and C-termini better tolerated.

The insertion of additional DNA and the expression of the in *trans* CPS were a success. The two halves of the large subunit as well as the small subunit were able to associate together after purification to form an intact enzyme (**Figure 2.6**). This was evidenced by the ability of this mutant to catalyze the synthesis of carbamoyl phosphate at a rate of $0.042 \pm 0.002\ s^{-1}$. Although this rate is almost 50 times slower than that of wild-type CPS, it is remarkable that the two halves of the large subunit are able to associate correctly with each other, and the small subunit, in solution and reform a tunnel that is critical for the transport of carbamate to the site of its phosphorylation. It was possible to observe a three-fold level of activation of the ATPase reaction in the presence of glutamine (**Table 2.1**). While all of the kinetic constants determined for this construct are slower than those of wild-type CPS, the fact that this enzyme is able to exhibit a detectable level of activity is quite remarkable.

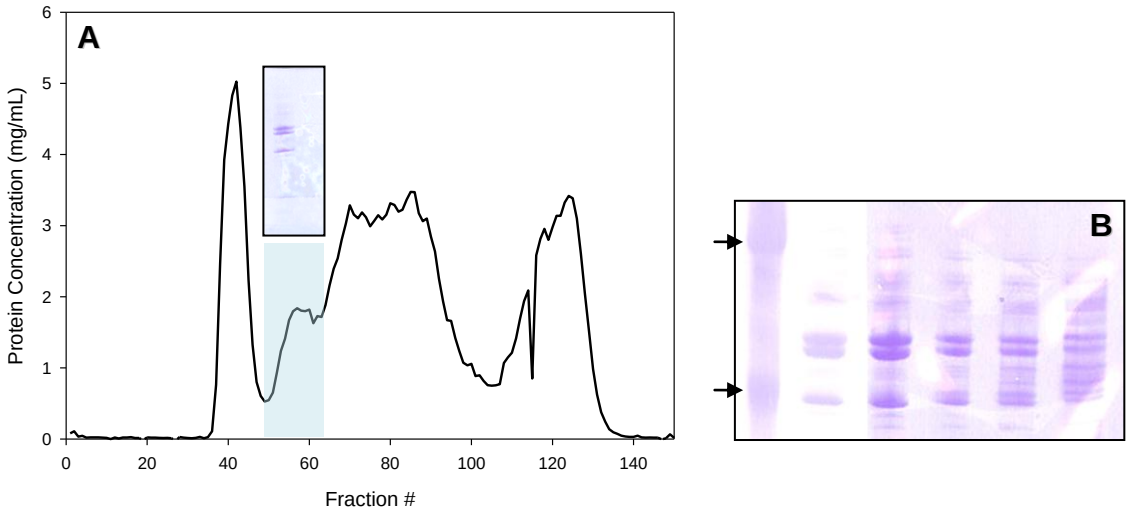

Figure 2.6. **A**) Chromatogram of the gel filtration purification step for in *trans* CPS. Final product of the purification of in *trans* CPS is shown in a box above the highlighted region. **B**) SDS PAGE gel of the highlighted region. The arrows point to the large (top) and small (bottom) subunits of wild-type CPS. Lane 1: purified wild-type CPS marker, lane 2-6: fractions 54-62 (every 2nd fraction shown).

Discussion

Since the first crystal structure of CPS was solved in 1997, the conformation of the two B-domains located on the carboxyphosphate and the carbamoyl phosphate active sites has been of interest. The mechanism by which these domains close and open has not been completely elucidated, but great strides have been made in being able to develop a model for this. In a crystal structure solved by Thoden in the presence of the nonhydrolysable ATP analog AMPPNP both of the B-subdomains were found in the closed conformation. These findings are in line with the fact that both active sites must remain closed to bulk solvent in order to protect unstable intermediates. A different crystal structure solved in the presence of ADP and P_i revealed an open conformation at

the carbamoyl phosphate active site and a bound molecule of ADP. However, the N-terminal active site remained closed with both ADP and P_i bound. In all of the crystal structures of CPS solved to date, the N-terminal B-domain remains in the closed conformation.

In this investigation we explored possible ways of studying the motions of both the N- and C-terminal B-domains. Fluorescence anisotropy is a sensitive technique that is able to report on the changes in the immediate environment of the fluorescent probe by measuring depolarization of its fluorescence emission. In order to employ this technique it was necessary to introduce fluorescent reporters to CPS at appropriate sites on the mobile B-domains. The use of engineered tryptophans in a tryptophan-less CPS construct was not possible in our hands due to low expression levels and very poor solubility of the mutants. After a thorough examination of the solvent accessible cysteine residues, the most solvent exposed Cys-551 was mutated to an alanine, and two cysteines were engineered at positions 171 and 717 in the large subunit.

The anisotropy measurements made on the C551A/S171C and C551A/S717C mutants provided some insight into a possible mechanism of synchronization of the opening and closing of the N- and C-terminal B-domains. It was found that in the absence of all ligands the protein environment around both fluorophores was more rigid than in their presence. Upon addition of ornithine and K^+ to the reaction mixture the anisotropy of both mutants decreased a noteworthy amount. Based on crystallographic data, K^+ binds to regions of the protein near the carboxyphosphate and carbamoyl phosphate active sites termed the "K-loops" (**Figure 2.1**). Potassium ions do not have a

role in catalysis, but rather help support the structure of the active sites. It has been previously reported that there is a requirement for potassium ions for the proper function of CPS. [66] The anisotropy data suggests that once potassium ions are bound that they somehow alter the active site environment. It may be possible that the binding of K^+ makes the active site environment more conducive to ATP binding.

The biggest anisotropy change observed at the N-terminal domain was in the presence of AMPPNP and ATP. Even though these ligands were added at the same time as various other molecules, it was these two substrates that were responsible for the change in the rotational response of the fluorophore at S171C. This is evident from no change in anisotropy being observed when P_i, Mg^{2+}, and glutamine were individually tested in the reaction mixture with CPS in the presence of ornithine and K^+ (**Figure 2.5**). From the X-ray crystallography data these domain adopts a closed conformation in the presence of AMPPNP. The change in anisotropy in the presence of this compound can be indicative of a conformational change that brings the domain from the open conformation to the closed. The presence and absence of ADP, in the presence of ornithine and K^+, had no effect on either active site. The C-terminal B-domain remained unaffected in the presence of all ligands tested in this study.

While the anisotropy experiments were not conclusive, they provide a better insight into a possible connection between the N- and C-terminal active sites on the large subunit. Further experimentation is necessary to provide a clear picture of this relationship. A possible way of understanding these events is by using an in *trans*

construct of CPS. It has been shown to be a kinetically competent species that presents many possibilities for manipulation.

One such possibility is to label the in *trans* expressed protein with fluorescent probes at the previously mentioned S171C and S717C. Cys-551 will need to be eliminated to prevent labeling at undesirable sites. Since CPS (αβ) monomers, not dimers or tetramers, would be studied in this experiment it would also be necessary to mutate Asn-987, at the oligomerization domain, to aspartate. This mutation will ensure that the protein remains an (αβ) monomer throughout the course of the experiment, even in the presence of allosteric effector molecules.[23]

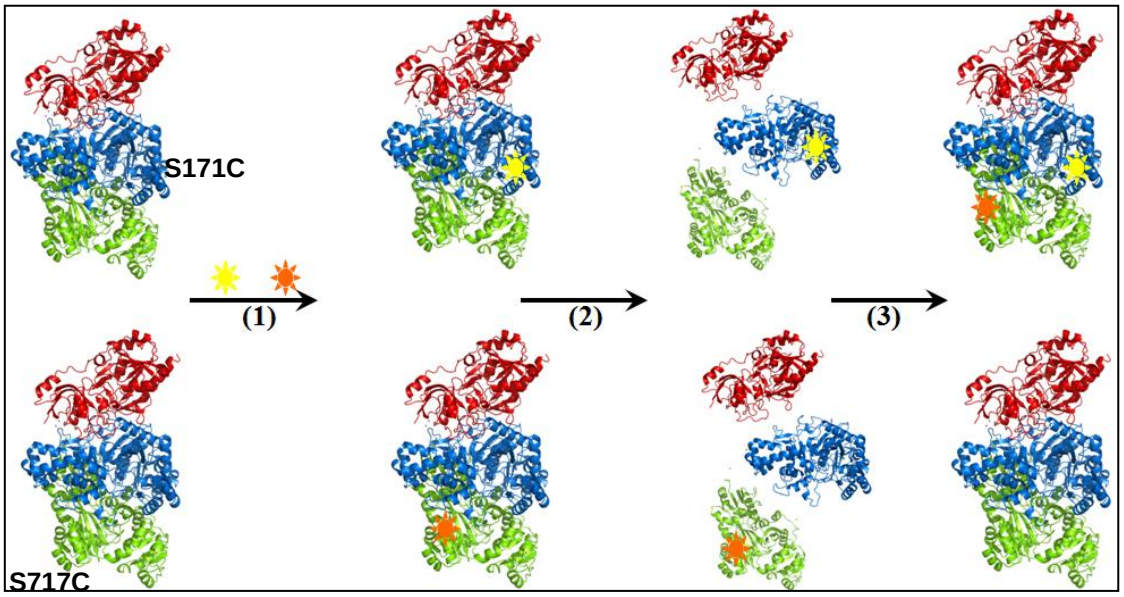

Figure 2.7. In *trans* CPS labeling scheme. The small subunit (red), N-terminal half of the large subunit (blue), C-terminal half of the large subunit (green), and fluorescent probes (orange and yellow) are shown. (**1**) S171C and S717C in *trans* CPS mutants are modified with fluorescent probes. (**2**) The labeled proteins are dialyzed in KSCN in order to facilitate subunit exchange. (**3**) The chaotropic agent is removed and the subunits reassociate to form labeled hybrid proteins.

The labeled hybrid proteins will be formed when the fluorescently labeled proteins are incubated with a chaotropic agent, such as KSCN or guanidinium chloride, and then dialyzed against the usual buffer. This will promote exchange between the two halves of the large subunit (**Figure 2.7**).[67] This technique has been used before to study protein-ligand associations of phosphofructokinase.[67] This methodology, combined with addition of charge tags, made it possible to label identical subunits in a tetramer with two different fluorescent probes in a very controlled manner.[67-68] Further work is needed to fully evaluate the possible combinations of mutants, subunits, and fluorophores that will finally illuminate the intricacies of the subtle communication networks present in CPS.

CHAPTER III

A THEORETICAL AND EXPERIMENTAL INVESTIGATION OF AMMONIA TRANSPORT WITHIN THE SMALL AND LARGE SUBUNIT OF CARBAMOYL PHOSPHATE SYNTHETASE FROM *E. coli**

Introduction

Carbamoyl phosphate synthetase (CPS) from *Escherichia coli* catalyzes one of the most complex reactions in biological chemistry. The product of this enzymatic transformation, carbamoyl phosphate, is utilized in the biosynthesis of arginine and pyrimidine nucleotides.[1-3] Carbamoyl phosphate is formed from glutamine, bicarbonate and two molecules of MgATP through a series of four separate reactions.[1] The generally accepted reaction mechanism is summarized in **Scheme 3.1**. In the initial reaction, the first molecule of ATP is used to phosphorylate bicarbonate to generate the reactive intermediate, carboxyphosphate. Glutamine is hydrolyzed to glutamate and ammonia, followed by the reaction of ammonia with the carboxyphosphate intermediate to form carbamate.

Finally, a second molecule of ATP is used to phosphorylate carbamate to form the ultimate product, carbamoyl phosphate. There are thus four separate reactions and three discrete, reactive, and unstable intermediates involved in this reaction mechanism: carboxyphosphate, ammonia, and carbamate.[5-6]

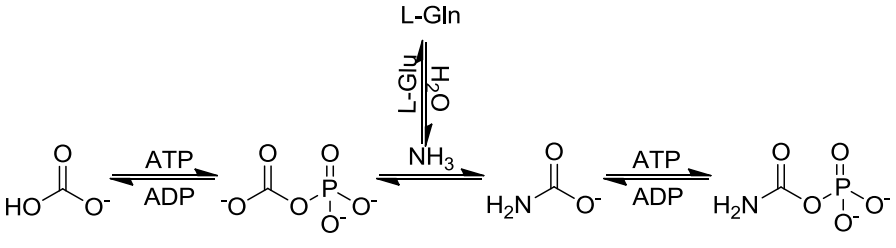

Scheme 3.1

The protein isolated from *E. coli* is a heterodimer composed of a small (42 kDa) and a large (118 kDa) subunit. Structural data have confirmed the presence of three spatially distinct active sites that are linked by two long molecular tunnels that extend approximately 100 Å from one end of the protein to the other (**Figure 3.1**). The small subunit contains the active site for the hydrolysis of glutamine, which is hydrolyzed to glutamate and ammonia via a thioester intermediate.[1,56-57,69] The ammonia derived from this reaction travels ~45 Å to the active site for the synthesis of the carboxy phosphate intermediate, located in the N-terminal half of the large subunit. The carbamate intermediate, formed by the reaction of ammonia with carboxy phosphate, is subsequently channeled ~35 Å to the active site for the synthesis of carbamoyl phosphate. This active site is located within the C-terminal half of the large subunit where carbamate is phosphorylated by the second molecule of MgATP to form the

ultimate product, carbamoyl phosphate.[3, 21] CPS thus contains two long molecular tunnels for the transport of ammonia and carbamate.

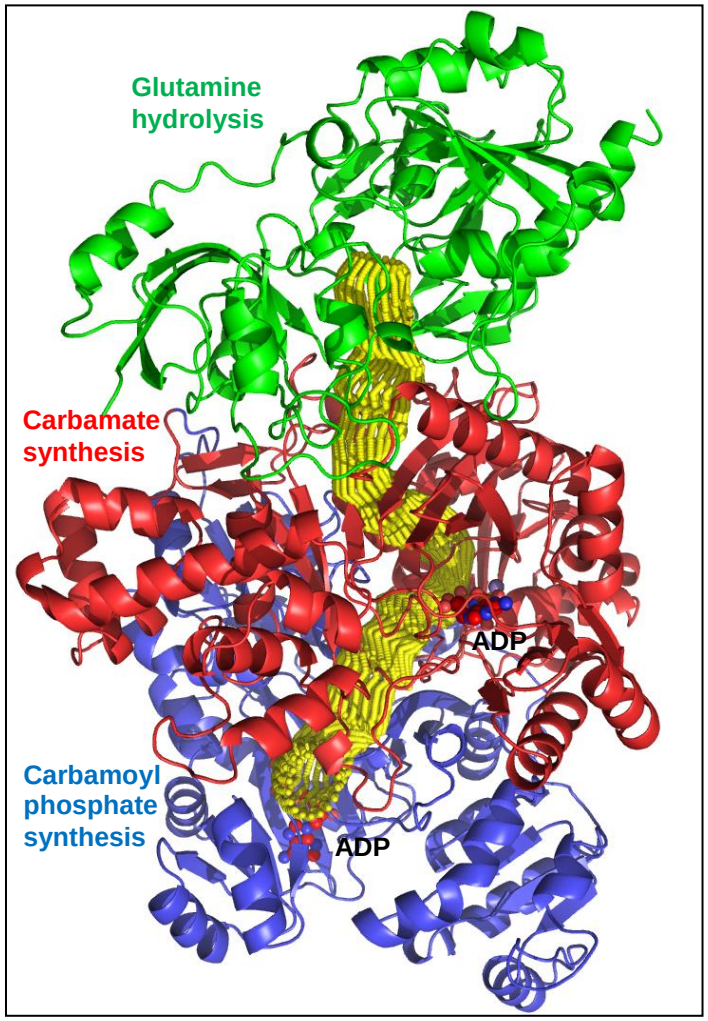

Figure 3.1. The crystal structure of carbamoyl phosphate synthetase. The small subunit containing the site for glutamine hydrolysis is shown in green. The large subunit is shown in red and blue. In red is the N-terminal domain which is responsible for the synthesis of carboxyphosphate and carbamate. In blue is the C-terminal domain which is responsible for the synthesis of carbamoyl phosphate. The two intramolecular tunnels for the transport of ammonia and carbamate are shown in yellow. The image was constructed using the PDB file: 1BXR.

Intramolecular protein tunnels have been found in a number of enzymes where it is necessary to shelter unstable and reactive intermediates from bulk solution. Tunnels for the translocation of ammonia have been found in all members of the amidotransferase superfamily for which structural data are available.[34-21] All of these enzymes utilize ammonia derived from the hydrolysis of glutamine.[40,70] Isotopic labeling studies have demonstrated that the ammonia derived from the hydrolysis of glutamine in CPS does not exchange with added ammonia present in the bulk solution.[71] These data demonstrate that the wild-type enzyme is not leaky and that there is a strong coupling between the reactions at the separate active sites. The functional significance of the ammonia tunnel has also been demonstrated by constructing a "hole" in the tunnel with the use of the G359F mutant.[35,38] As a result, ammonia was observed leaking directly into the bulk solution.

The ~45 Å journey of ammonia starts at the site of its formation in the small subunit. Here, glutamine is hydrolyzed to glutamate via a thioester intermediate that is formed by the nucloephilic attack of Cys-269 on the carboxamide moiety (**Scheme 3.2)**.[72] The activation of this cysteine is accomplished by the two remaining members of the catalytic triad: His-353 and Ser-47.[27] His-353 plays two key roles in the reaction mechanism: one by providing one of the protons for the amine leaving group, two by abstracting a proton from the catalytic water molecule used to hydrolyze the thioester intermediate. The role of Ser-47 in the reaction mechanism is to orient the carbonyl carbon of the glutamine carboxamide group for the nucleophilic attack by Cys-269. It also serves to stabilize the tetrahedral intermediate in this reaction. Following the

collapse of the tetrahedral intermediate ammonia is formed and injected into the tunnel. The resulting thioester intermediate is then hydrolyzed and glutamine and released. This reaction mechanism is summarized in **Scheme 3.2**. The tetrahedral intermediate analog glutamate γ-semialdehyde, a potent inhibitor of hydrolotic properties of the amidotransferase domain, was observed crystallographically in the C269S mutant.[72] The glutamylthioester intermediate was also experimentally shown by X-ray crystallography with the use of the H353N mutant.[72]

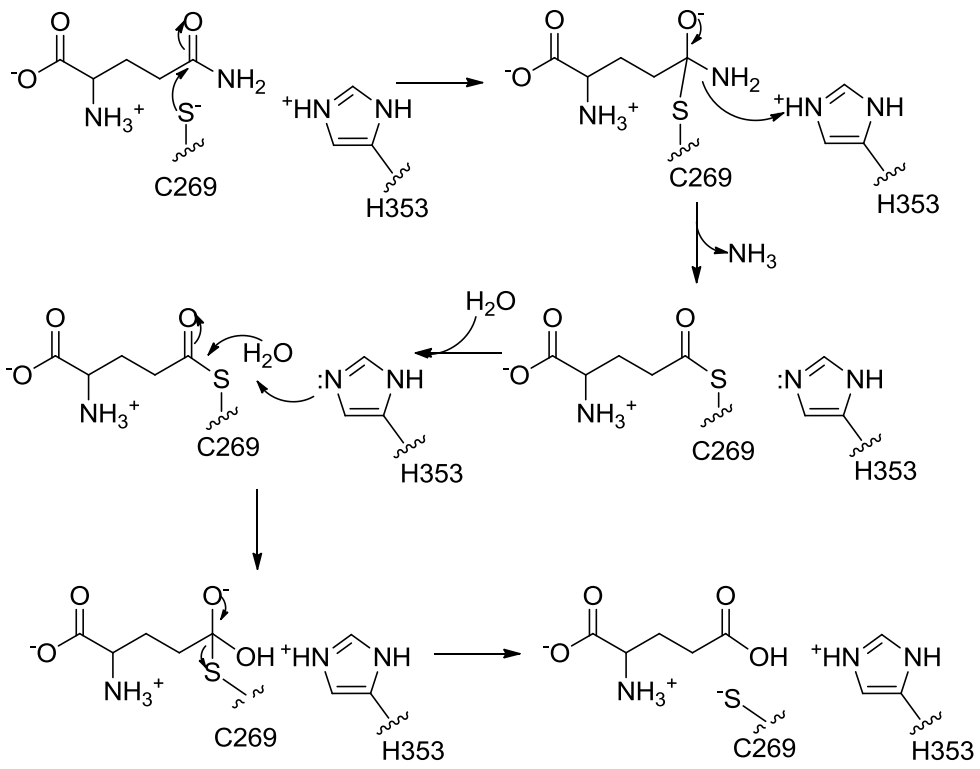

Scheme 3.2

While the chemistry of ammonia formation and the presence of the ammonia tunnel are known, the mechanism and dynamics of NH_3 transport are unclear. There are significant difficulties in experimentally tracking the migration of ammonia from one active site to the next. Therefore, molecular dynamics (MD) simulations were coupled with mutagenesis in order to bring to light the interactions between the substrate and the inner protein environment. Previously, MD simulations have been used to investigate ammonia transport in systems such imidazole glycerol phosphate synthase (IGPS), the membrane protein AmtB, and glutamine 5'-phosphoribosyl pyrophosphate amidotransferase.[51,54,73] In all of these investigations artificial forces were introduced to speed the transport of substrates through the enzyme.

Here the focus was placed upon observing the spontaneous transport of ammonia though the small and the large subunit of CPS at room temperature in the absence of artificial driving forces using MD simulations coupled with experimental techniques. A free energy profile for the migration of ammonia was calculated. Based on this information, various mutants along the path for the migration of ammonia were constructed to perturb and examine the interaction of ammonia with the internal protein environment. It was found that ammonia traverses the ~45 Å tunnel in three steps. First, ammonia is injected into the tunnel by hydrogen bonding with the side chain of His-353. Second, NH_3 travels through a narrow passage in the small subunit, defined by Ser-35 and Thr-37, to enter a large water pocket located at the interface between the small and large subunits. Finally, ammonia passes through a narrow turning gate comprised of residues Cys-232, Ala-251, and Ala-314 in the large subunit. This is the most

energetically unfavorable step in the entire migration process. Based on the experimental evidence obtained from mutants and the computational data, it has been determined that the migration of ammonia from the glutaminase active site to the carboxyphosphate active site is not the rate limiting step in the reaction mechanism of CPS.

Materials and Methods

Construction of Models for the Thioester Intermediate. All of the models for the transport of ammonia were constructed by Dr. Yubo Fan from the Chemistry Department at Texas A&M University. The starting point for simulations was taken from the X-ray crystal structure of CPS (PDB code: 1cs0).[72] The residues Met-1, Ala-381, Lys-382, and two loops in the large subunit, 717-723 and 742-749, were missing from the crystal structure and were incorporated into the structure with SWISS-MODEL.[74-76] The two loops are a part of the ATP-binding site located in the C-terminal half of the large subunit.

In the simulations reported here, the covalently bound inhibitor, glutamate γ-semialdehyde, bonded with Cys-269 was replaced with a γ-glutamyl cysteine residue (Cyg). The geometry of the Cyg group was optimized to a local minimum and the conformation of the side chain was kept the same as the substituted Cys-269 in the crystal structure (**Figure 3.2**). The charge distribution on all atoms in Cyg, NH_3, and NH_4^+ was obtained using the RESP-fit method[77-78] based on B3LYP/cc-pVTZ calculations[79-82] with solvent effect ($\varepsilon = 4$) taken into account using the polarizable

continuum model (PCM).[83-85] The geometries of NH_3 and NH_4^+ were fully optimized in the gas phase at the same level as that for the charge distribution calculations. The charge on the nitrogen of NH_3 was -0.9822 and -0.8022 for the nitrogen atom of NH_4^+. All crystalline waters within the enzyme or on the protein exterior, including Mn^{2+}, K^+, and Cl^-, were utilized for the simulations. All operations were processed using AMBER Leap module, which led to models containing ~120,000 atoms, including ~39,000 waters.[86-87]

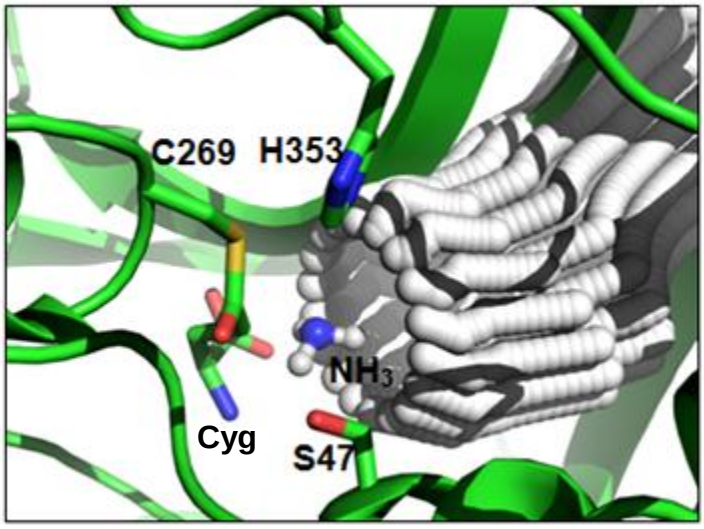

Figure 3.2. Active site for the hydrolysis of glutamine in the small subunit of CPS and the proposed tunnel for ammonia transport. Cys-269 was modified as a γ-glutamyl thioester intermediate (Cyg). The resulting Cyg group was optimized to a local minimum and the conformation was kept consistent with the wild-type enzyme. Nitrogen, oxygen, hydrogen, and carbon atoms are shown in blue, red, white, and green, respectively. The white spheres represent the approximate boundaries of the ammonia tunnel. [30] The image was constructed using PDB file: 1C3O.

The force field for ADP[88], P_i[88], and Mn^{2+}[89] are contributed by Richard Bryce at the University of Manchester. MD simulations were conducted in the isothermal-isobaric (NPT) ensemble at 300 K and 1 atm. The SHAKE algorithm was used to constrain all bonds involving hydrogens.[90] A 10.0 Å cutoff was applied for nonbonding interactions. The Particle Mesh Ewald method was employed to treat the long-range electrostatic interactions.[91-92]

Free-Energy Calculations. All of the MD simulations and PMF calculations in this study were performed by Dr. Yubo Fan from the Chemistry Department at Texas A&M University. The reaction coordinate was divided into two parts. The first part of the free energy calculations was defined as the distance between the nitrogen atom of ammonia and the carbonyl atom of the thioester intermediate in Cyg-269. In the second part, the reaction coordinate was defined as the distance between the ammonia nitrogen and one of the Mn^{2+} ions in the carboxyphosphate active site. The division of the tunnel is summarized in **Figure 3.3.** The free energy profiles or potentials of mean force (PMF) along the tunnel were computed using the umbrella sampling technique with a biasing harmonic potential involving a force constant of 40 kcal/(mol/$Å^2$).[93-96]

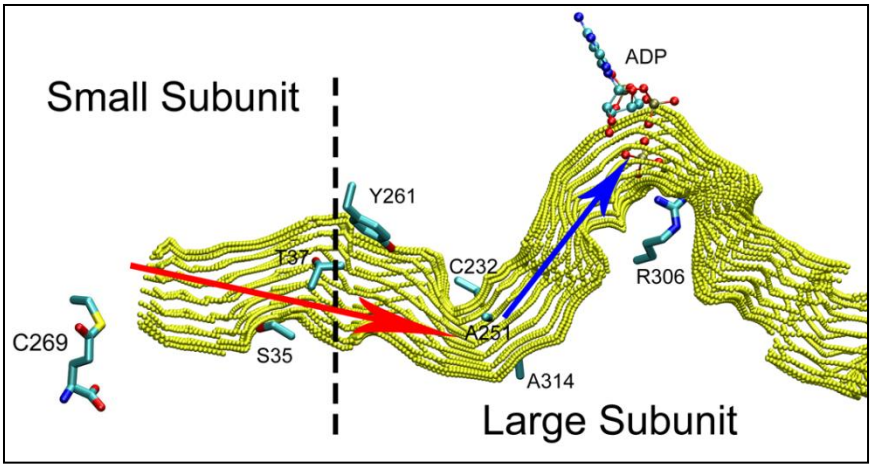

Figure 3.3. The molecular tunnel for the transport of ammonia from the site of glutamine hydrolysis to the site of carbamate formation. The red and blue arrows show the separation of the two calculations.

Bacterial Strains and Plasmids. Site-directed mutagenesis of CPS was performed as described previously.[28,59] The RC50 strain used for protein expression was a generous gift from Dr. Carol J. Lusty. All plasmids used in this project were derived from pMS03.[38] Oligonucleotide synthesis and DNA sequencing reactions were performed by the Gene Technology Laboratory, Texas A&M University.

Construction and Purification of Mutant Proteins. Site-directed mutagenesis was performed using the QuikChange® protocol from Stratagene. All of the site-directed changes made to wild-type CPS were confirmed by DNA sequencing of the modified plasmids. The plasmids containing the *car*AB genes were transformed in the RC50 cell line of *E. coli* for expression of the wild-type and mutant forms of CPS. The wild-type and mutant variants of CPS were purified as previously described.[38] The mutants S35A, S35Y, T37A, C232D/A251T/A314T, C232V/A251V/A314V, C232G/A251G/A314G,

A251C, A314C, A311L, I352F and T249V in the ammonia tunnel were expressed and purified to greater than 95% homogeneity, as judged by SDS-polyacrylamide gel electrophoresis.

Circular Dichroism Measurements. The secondary structure of all mutant proteins was determined using circular dichroism measurements. All measurements were taken on an Aviv 62DS spectropolarimeter. Each protein sample contained 450 nM protein in 5.0 mM phosphate buffer, pH 7.6. Measurements were made using quartz cuvettes with a 1.0 cm path length.

Kinetic Measurements. The rate of glutamine hydrolysis was determined by coupling the formation of glutamate to the production of α-ketoglutarate with L-glutamate dehydrogenase and 3-acetylpyridine adenine dinucleotide (APAD).[97] The reaction mixtures contained 50 mM Hepes (pH 7.6), 20 mM $MgCl_2$, 100 mM KCl, 40 mM $KHCO_3$, 5.0 mM ATP, 10 mM ornithine, 1.0 mM APAD, 30 U L-glutamate dehydrogenase, and varying amounts of glutamine. The rate of ADP formation was measured using a pyruvate kinase/lactate dehydrogenase coupling system.[38] The reaction mixtures for the glutamine-dependent assay contained 50 mM Hepes, pH 7.6, 20 mM $MgCl_2$, 100 mM KCl, 40 mM $KHCO_3$, 10 mM glutamine, 10 mM ornithine, 1.0 mM phosphoenolpyruvate, 0.2 mM NADH, 2 units of pyruvate kinase, 3 units of lactate dehydrogenase, and varying amounts of ATP. Glutamine was excluded from the bicarbonate-dependent and NH_4^+-dependent ATPase assays. Varying amounts of NH_4Cl and 5 mM ATP were used for the NH_4^+-dependent ATPase assay. Both of these assays were followed by monitoring the decrease in absorbance at 340 nm using a Molecular

Devices SpectraMax Plus 96-well plate reader. The synthesis of carbamoyl phosphate was determined by measuring the rate of citrulline formation in a coupled assay containing ornithine transcarbamoylase (OTCase) and ornithine.[19] The assay mixtures contained 50 mM Hepes, pH 7.6, 20 mM $MgCl_2$, 100 mM KCl, 40 mM $KHCO_3$, 5.0 mM ATP, 10 mM ornithine, 12 units of OTCase, and 10 mM glutamine. The rate of ATP synthesis was measured with a hexokinase/glucose-6-phosphate dehydrogenase (G6PDH) coupling system.[97] The assay mixture for the ADP-dependent assay included 50 mM Hepes, pH 7.6, 20 mM $MgCl_2$, 100 mM KCl, 10 mM ornithine, 0.75 mM NAD, 2 units of hexokinase, 1.0 mM glucose, 1 unit of G6PDH, 1.0 mM carbamoyl phosphate, and varying amounts of ADP.

Results

Translocation of NH_3 in the Small Subunit. In the MD simulation there was a movement of 13 Å observed in two successful trajectories, lasting 14 and 9.5 ns, respectively. This is the first time that a spontaneous transfer of ammonia through a molecular tunnel has been observed in an enzyme. The tunnel that was observed in the X-ray crystal structure was apparently the lowest free-energy path for this process.

The translocation of ammonia through the small subunit occurs in three stages. In the first stage NH_3 is directed away from the thioester intermediate. This is accomplished by oscillation and hydrogen bond exchange between the thioester intermediate, His-353, Ser-47, as well as several water molecules. The hydrogen bond between the imidazole ring of His-353 and NH_3 is what directs ammonia into the tunnel

(**Figure 3.4A**). A new hydrogen bond between NH_3 and Lys-202 is formed while the hydrogen bond to Ser-47 remains intact (**Figure 3.4B**). As ammonia moves deeper into the tunnel it begins to interact with a cluster of water molecules, causing hydrogen-bonding interactions between it and the side chain of Ser-47 to weaken and eventually break (**Figure 3.4C**). As the ammonia is delivered deeper into the tunnel by the long and flexible side chain of Lys-202 it begins to interact with a cluster of water molecules inside the tunnel (**Figure 3.4D**). When the interaction between NH_3 and Lys-202 is broken, ammonia travels further into the tunnel by exchanging hydrogen bonds with water molecules. Once close to the interface between the large and small subunits, ammonia hydrogen bonds with the side chain of Ser-35 and the backbone carbonyl groups of Gly-292 and Pro-358 (**Figure 3.4E**). The side chain of Ser-35 rotates and ammonia forms a hydrogen bond with the side chain of Thr-37 (**Figure 3.4F**). This final set of hydrogen bonding interactions is thought to be the driving force needed to push ammonia through the hydrophilic exit of the small subunit. It is worth noting that during the simulation there was very little conformational changes observed in the small subunit.

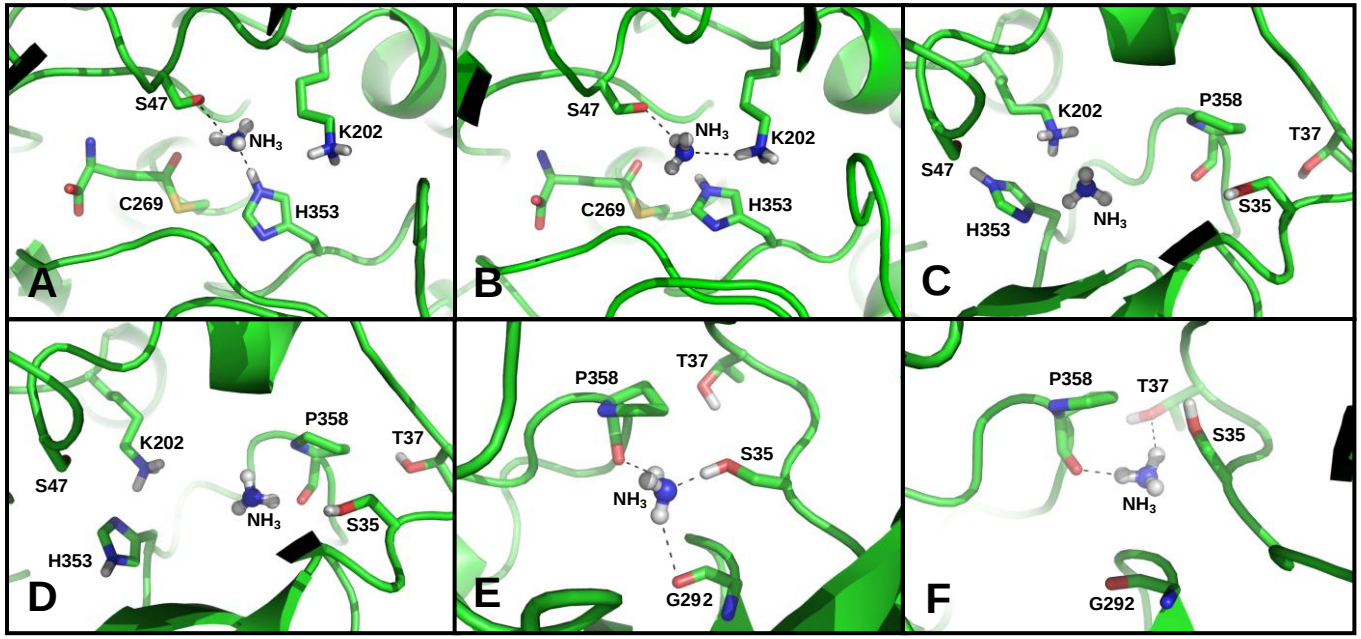

Figure 3.4. Snapshots of the migration of ammonia through the tunnel in the small subunit. The dashed lines represent hydrogen bonds. *R*=4.58 Å (A), *R*=4.55 Å (B), *R*=7.88 Å (C), *R*=10.64 Å (D), *R*=12.75 Å (E), and *R*=15.71 Å (F). *R* represents the distance between the nitrogen atom of NH_3 and the carbonyl carbon of the thioester intermediate in Cyg-269.

Free Energy Profiles for the Migration of Ammonia in the Small Subunit. An umbrella sampling technique was used to calculate the free energy profiles for the translocation of ammonia through the small subunit. The PMF profiles show that there are two small energetic barriers that NH_3 must overcome before exiting the small subunit, at 6.0 and 14.3 Å from Cyg-269 (**Figure 3.5A**). A PMF profile was also calculated for the migration of NH_4^+. These data showed that the ammonium ion has a high energy barrier to overcome in order to make it through the small subunit (**Figure 3.5B**). NH_4^+ has a much higher solvation energy than NH_3, which makes it more difficult for it to desolvate in order to pass through the narrow hydrophilic passage immediately after Ser-35. The highest energy barriers for ammonium ion transport are observed between 14 and 18 Å. These are too high for $NH_4^+$to traverse, so it becomes trapped in the tunnel.

Ammonia has two relatively small barriers to cross along its path to the subunit interface. The first barrier being 6.8 kcal/mol at 6.0 Å away from Cyg-269, and the second one being 5.5 kcal/mol at 14.3 Å away from Cyg-269. The first energy barrier corresponds to the breakage of a hydrogen bond between the imidazole side-chain of His-353 and ammonia. The second energy barrier is due to the desolvation of NH_3 as it exits the water pocket and interacts with Ser-35. The lowest energy in the PMF for ammonia is around 10 Å. This distance corresponds to the center of the water pocket inside the small subunit portion of the tunnel. Here ammonia is solvated and is freely exchanging hydrogen bonds with water molecules.

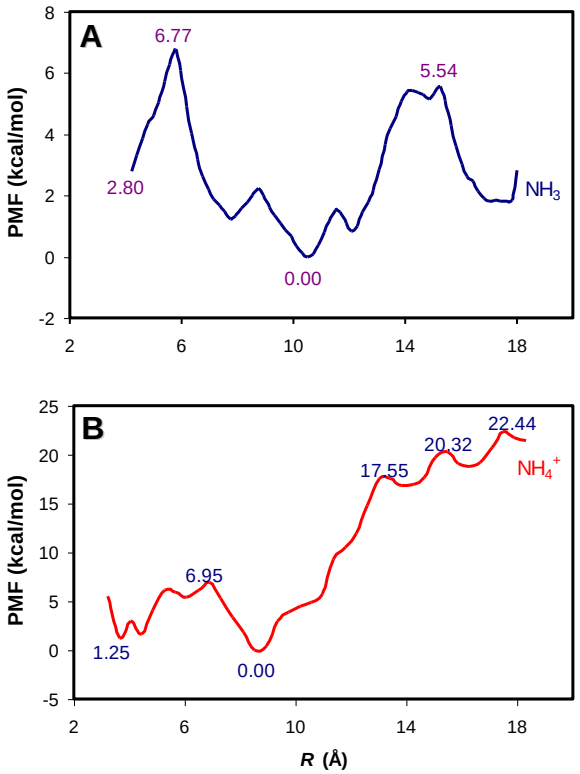

Figure 3.5. Potential of mean force (PMF) profiles for the translocation of **A)** NH_3 and **B**) NH_4^+ along the tunnel in the small subunit of CPS. The lowest point in each profile is defined as zero energy. The reaction coordinate *R*, is the distance between the nitrogen in NH_3/NH_4^+ and the carbonyl carbon bonding to the sulfur in Cyg-269.

Translocation of NH_3 into the Large Subunit. The calculations on the ammonia tunnel located in the small subunit showed that NH_3 must be largely desolvated as it passes by Ser-35 and Thr-37. As ammonia leaves the small subunit it enters the first water pocket which is positioned between Thr-37 in the small subunit and Tyr-261 in the large subunit. The first energy barrier of 3.0 kcal/mol is located at Tyr-261 which protrudes in the water pocket, thus dividing it in two (**Figure 3.6**). The second water pocket is located between Tyr-261 and a narrow turning gate composed of Cys-232, Ala-251, and Ala-314. This water pocket represents a deep energy minimum located at

approximately 24 Å in the trajectory. This water pocket is big enough to accommodate a large water cluster which is capable of efficiently solvating ammonia.

The next energy barrier of 7.2 kcal/mol occurs when ammonia has to traverse a narrow turning gate in the tunnel formed by Cys-232, Ala-251, and Ala-314. This energy barrier occurs at about 30 Å in the trajectory (**Figure 3.6**). The reason for this barrier is that the diameter of the gate is barely large enough to let ammonia pass through. Because the size of the gate is so narrow, ammonia must be completely dehydrated in order to be able to pass through it (**Figure 3.7**). The size of the energy barrier in this region of the trajectory is also increased by the fact that none of the residues comprising the gate are able to hydrogen bond with ammonia.

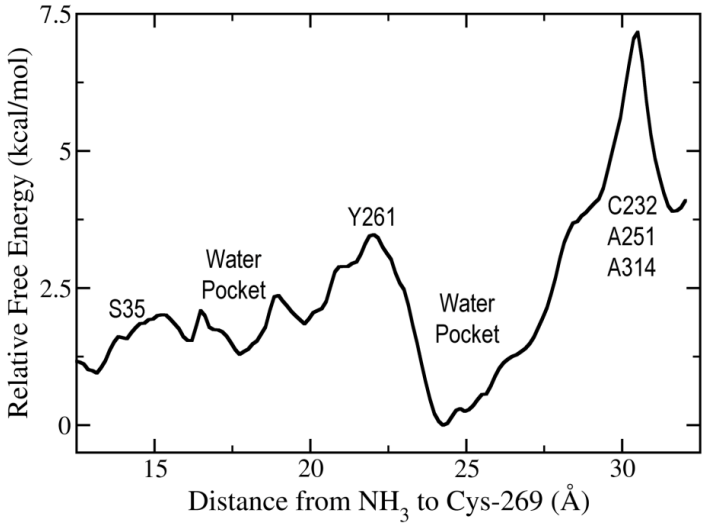

Figure 3.6. Potentials of mean force from Thr-37 in the small subunit to the narrow turn comprised of Cys-232, Ala-251 and Ala-314. The reaction coordinate is defined as the distance from the nitrogen atom in the ammonia to the carbonyl carbon of the thioester intermediate in Cys-269.

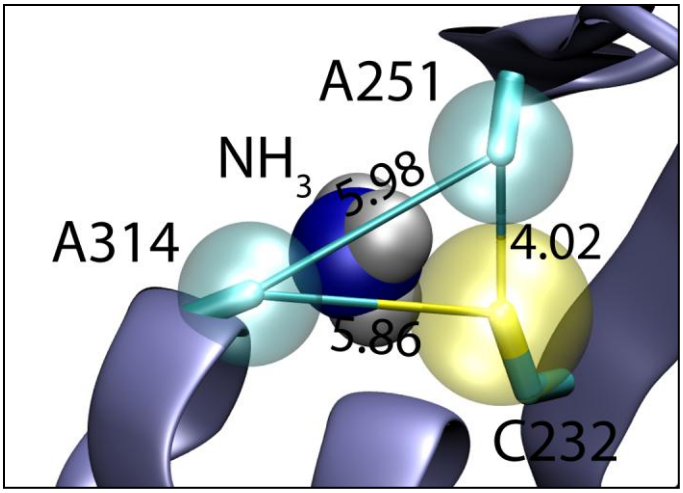

Figure 3.7. The triangular gate surrounded by Cys-232, Ala-251 and Ala-314 leading to the site of carbamate formation. The van der Waals spheres for the sulfur atom of Cys-232 and C_α atoms of Ala-251 and Ala-314 are shown in transparency. The distances are in Å.

Influence of Carboxyphosphate Formation on the Turning Gate. According to crystallographic information available, Arg-306, which is located on the same α-helix as Ala-314 of the turning gate, directly interacts with either the γ-phosphoryl group of the ATP or P_i (**Figure 3.8**). Therefore, formation of carboxyphosphate in the active site would be expected to alter the conformation of Arg-306, and that of the turning gate. The change in conformation of Arg-306 in the presence of either phosphate or carboxyphosphate closes or opens the narrow turning gate. This hypothesis was tested by calculating two separate trajectories of ammonia transport: P_i bound and carboxyphosphate bound (**Figure 3.9A**).

The calculations showed that in the trajectory with carboxyphosphate bound the energy barrier at the turning gate was 1.8 kcal/mol lower than with P_i bound. The decrease in the energy barrier is due to a conformational change that is induced by

carboxyphosphate. Once formed in the active site, this intermediate pushes on the α-helix, thus widening the gate and allowing ammonia to pass through more easily (**Figure 3.9B,C**). The qualitative data obtained from this calculation is in good agreement with the experimental observations that glutamine hydrolysis occurs 30 times faster in the presence of bicarbonate and ATP.

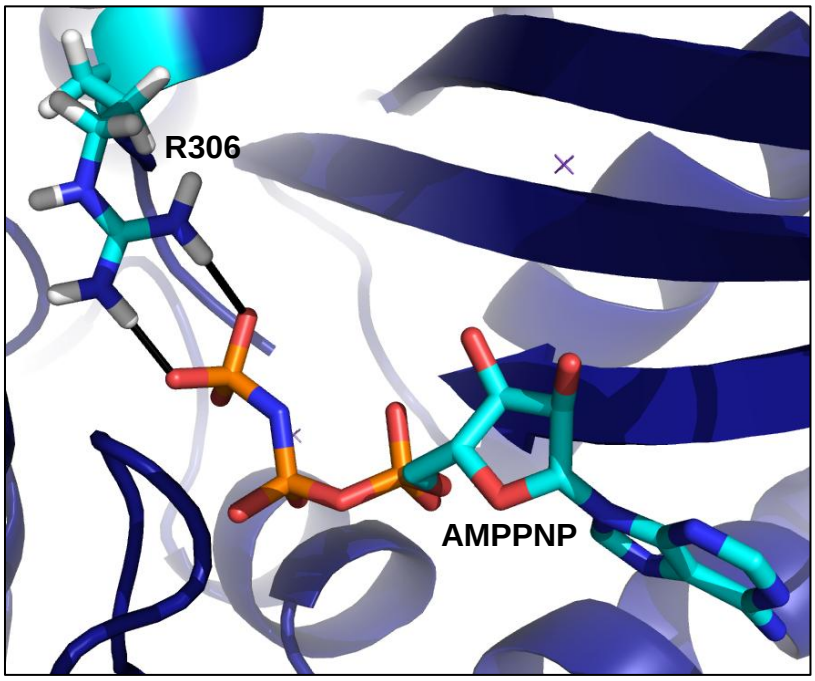

Figure 3.8. Close up view of the carboxyphosphate active site. Arg-306 and AMPPNP are shown. The interactions between the guanidino group of Arg-306 and the γ-phosphate of AMPPNP are shown in black.

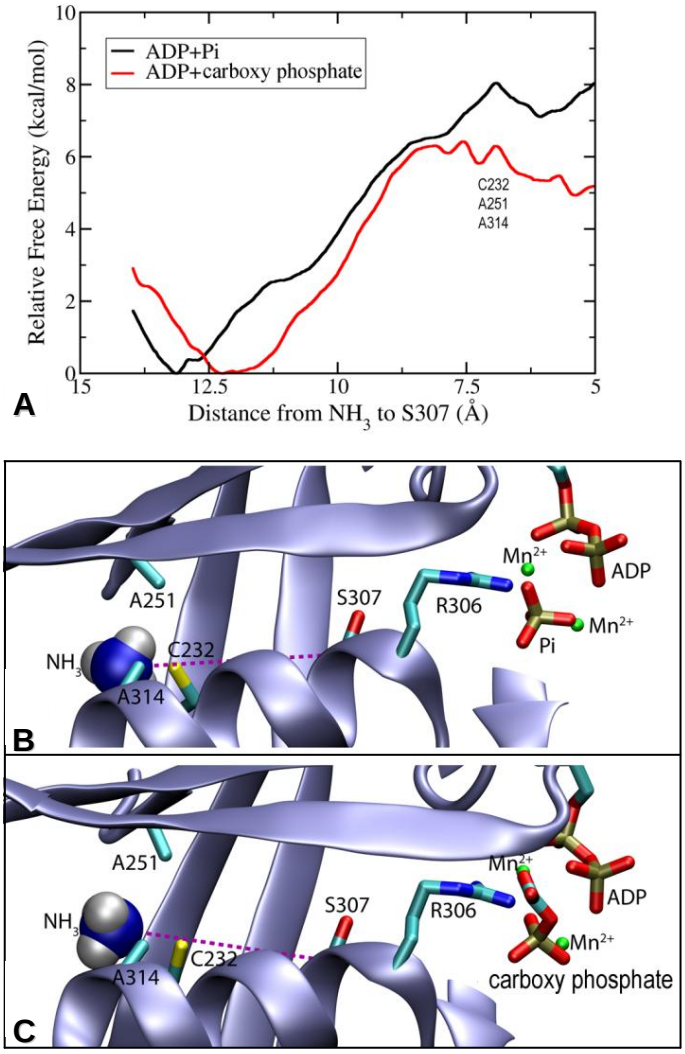

Figure 3.9. **A**) Potentials of mean force (PMF) *vs* the distance from the nitrogen atom in ammonia to the C_α of Ser-307 in the large subunit; **B**) the reaction coordinate (dotted line in magenta) for the umbrella sampling and the structure with bound P_i; **C**) the reaction coordinate (dotted line in magenta) for the umbrella sampling and the structure with the bound carboxyphosphate intermediate.

Mutation of Tunnel Residues. Amino acid residues within the ammonia tunnel, both in the large and small subunits, were mutated in an attempt to better evaluate their role in the transport of NH_3. All of the mutants, with the exception of C232G/A251G/A314G were meant to engineer blockages along the path for the migration of ammonia to the second active site in CPS. These residues are fully conserved in CPS from other organisms. The residues for mutagenesis were selected based on their participation in the shuttling of ammonia to the active site for carboxy phosphate formation as determined by the MD simulations. Ser-35 was mutated to a tyrosine in an attempt to position the phenolic side chain across the ammonia tunnel and potentially form hydrogen bonds with Gln-262 and Asp-258. In the MD simulations this mutation nearly blocked the tunnel by forming hydrogen bonds with Gln-262 and Asp-258 across the ammonia tunnel, while the relative distances between the C_α atoms of the residues involved were not significantly changed (shifts < 0.5Å).

Ser-35 and Thr-37, in the small subunit, were mutated to alanine. Ser-35 is conserved in about half of bacterial carbamoyl phosphate synthetases. In the other half there is an alanine present in that position. Thr-37 is conserved, but there are a few instances where there is a cysteine found in that position. Both residues are thought to facilitate the transport of ammonia through the tunnel by providing additional hydrogen bonding interactions. By removing those hydroxyl groups it may be possible to determine what role, if any, these residues play in ammonia transport.

The C232D/A251T/A314T mutant in the large subunit was designed to block the ammonia tunnel by introducing a hydrogen bond network across it. Asp-232, Thr-251

and Thr-314 can potentially form hydrogen bonds with one another in the center of the tunnel while the methyl groups from the two threonine residues may further impede the movement of ammonia. A similar approach was taken with the C232V/A251V/A314V mutant. The valine residues were predicted to come together in the middle of the tunnel through a hydrophobic collapse. This "greasy" plug inside the tunnel would diminish the size of the tunnel diameter. These residues were also mutated to glycine in an effort to remove any steric hindrance that may have been the cause of the relatively large energy barrier (**Figure 3.6**).

Thr-249, which is the residue responsible for forming a hydrogen bond with ammonia after it passes through the turning gate, was mutated to a valine in order to remove this hydrogen bond. Without this interaction in place it may be more difficult for ammonia to enter the water pocket immediately after exiting the turning gate composed of Cys-232, Ala-251, and Ala-314. It was anticipated that this mutant would exhibit a low rate of carbamoyl phosphate synthesis as well as a lower rate for the glutamine-dependent ATPase reaction.

Several other approaches were used to assess the energy barrier created by the C232/A251/A314 triad. Ala-251 and Ala-314 were mutated to cysteine to initiate the formation of an internal disulfide bond with Cys-232. In addition, the A311L and I352F mutations in the ammonia tunnel took advantage of the inward pointing side chains of the alanine and isoleucine residues directly following the triad. The alanine side chain was mutated to a larger leucine side chain to create a barrier that would be directly behind the narrowest part of the tunnel, thus potentially inhibiting the passage of

ammonia to the active site for carboxy phosphate formation. The isoleucine side chain was mutated to a phenylalanine in a similar attempt to create a larger hydrophobic barrier.

Characterization of Mutants. All of the mutant proteins were analyzed by circular dichroism. The single and triple mutations did not have any effect on the overall structure of the protein (**Figure 3.10**). Kinetic data in **Table 3.1** show that the S35Y mutation did not have a significant effect in blocking the ammonia tunnel. This was most evident from the wild-type-like kinetic constants for the glutamine-dependent ATPase reaction. However, this mutation did cause a 10-fold drop in k_{cat} and a 10-fold increase in the K_m for ATP in the bicarbonate-dependent ATPase reaction. The ATP-dependent glutaminase reaction catalyzed by the small subunit remained unaffected by this mutation. Since tyrosine also has a hydroxyl group, but on a larger side chain, it may be that this group can still participate in hydrogen bonding with NH_3 or is unable to slow down the hydrogen bond exchange between ammonia and water clusters in the tunnel.

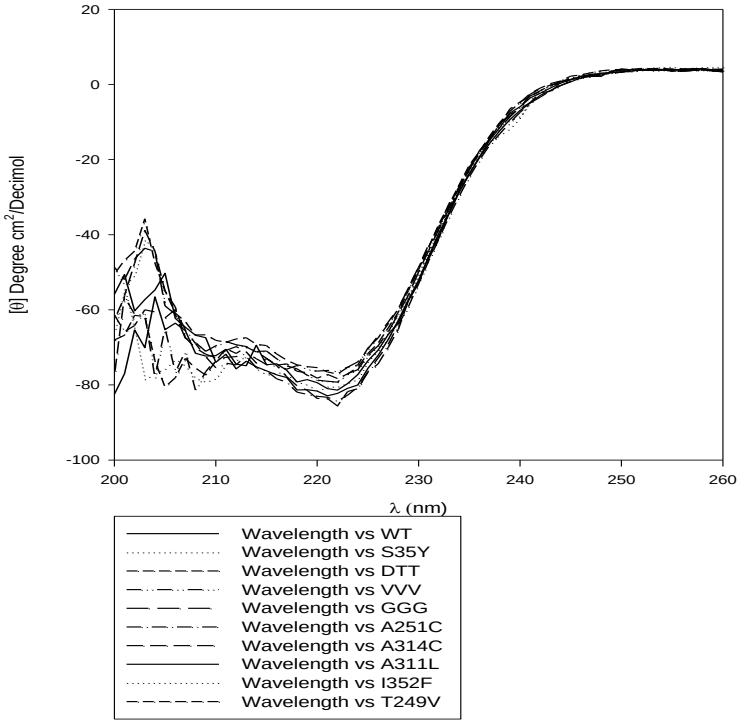

Figure 3.10. CD spectra of the ammonia tunnel mutants.

Table 3.1. Kinetic Characterization of the Wild-Type and Various Mutants of CPS.

Enzyme	Gln-dependent ATPase		HCO_3^--dependent ATPase[a]		ATP-dependent Glutaminase	
	k_{cat} (s^{-1})	K_m (mM ATP)	k_{cat} (s^{-1})	K_m (mM ATP)	k_{cat} (s^{-1})	K_m (mM Gln)
Wild-type	3.60 ± 0.11	0.24 ± 0.04	0.170 ± 0.003	0.051 ± 0.008	2.20 ± 0.04	0.15 ± 0.01
S35Y	3.7 ± 0.09	0.43 ± 0.04	0.079 ± 0.002	0.18 ± 0.03	2.7 ± 0.15	0.27 ± 0.05
C232D/A251T/A314T	0.33 ± 0.02	0.33 ± 0.07	0.010 ± 0.0003	0.054 ± 0.01	5.0 ± 0.40	0.59 ± 0.12
C232V/A251V/A314V	0.02 ± 0.001	1.6 ± 0.3	0.011 ± 0.002	2.9 ± 0.9	4.5 ± 0.18	0.19 ± 0.03
C232G/A251G/A314G	2.00 ± 0.06	0.057 ± 0.01	0.26 ± 0.005	0.13 ± 0.01	1.5 ± 0.04	0.15 ± 0.01
A251C	2.4 ± 0.04	0.067 ± 0.008	0.30 ± 0.006	0.036 ± 0.007	1.6 ± 0.1	0.25 ± 0.05
A314C	2.3 ± 0.04	0.084 ± 0.01	0.35 ± 0.003	0.014 ± 0.002	0.93 ± 0.03	0.18 ± 0.02
A311L	0.78 ± 0.002	0.15 ± 0.02	0.18 ± 0.004	0.13 ± 0.002	1.6 ± 0.08	0.45 ± 0.06
I352F	3.4 ± 0.22	0.32 ± 0.09	0.15 ± 0.004	0.075 ± 0.014	1.1 ± 0.03	0.19 ± 0.02
T249V	1.8 ± 0.04	0.07 ± 0.008	0.45 ± 0.01	0.035 ± 0.004	1.4 ± 0.06	0.06 ± 0.01

[a] HCO_3^--dependent ATPase activity was measured in the absence of glutamine.

The kinetic constants for S35A and T37A in the glutamine-dependent ATPase reaction did not show much deviation from those of the wild-type enzyme. The k_{cat} for the T37A mutant was 7.5 ± 0.19 s^{-1} and 3.8 ± 0.1 s^{-1} for the S35A mutant, with both Michaelis constants being 0.52 ± 0.04 and 0.57 ± 0.06 mM ATP, respectively. It is possible that these hydroxyl groups participate in ammonia transport, but when removed they can be easily replaced by a water molecule. Therefore, these residues do not play an essential role in translocation of ammonia through the small subunit portion of the tunnel.

The C232D/A251T/A314T mutant exhibited a 10-fold decrease in the values of k_{cat} for all of the partial reactions and a 100-fold decrease in k_{cat} for the production of carbamoyl phosphate (**Table 3.2**). These results suggest that the combination of these three substitutions has successfully blocked the passage of ammonia, but it is unclear whether the drop in kinetic constants is partially due to a conformational change that disrupts the activity of the enzyme. This concern arises from the decrease in the rate of ATP synthesis (from ADP and carbamoyl phosphate), which occurs 40 Å away from the site of these mutations. Conversely, the rate of glutamine hydrolysis in the presence of ATP is slightly enhanced relative to the wild-type enzyme and significantly increased in the absence of ATP, relative to the wild-type enzyme, with the C232D/A251T/A314T mutant (**Table 3.3**).

This increase in activity may be due to the larger residues mimicking the movement of the α-helix that expands the gate in the presence of carboxyphosphate. This movement may be part of the signal transduction network between the active sites

for carboxy phosphate and glutamine. This issue was clarified with the introduction of three valine residues as substitutes for C232, A251, and A314 that took advantage of a potential hydrophobic collapse in the middle of the ammonia tunnel. With this mutation there was little enhancement of the ATPase reaction in the presence of glutamine and but these mutations caused a >20-fold increase in the rate of the glutamine hydrolysis in the absence of ATP. The formation of carboxyphosphate was decoupled from the hydrolysis of glutamine.[28]

Table 3.2. Kinetic Characterization of ATP and Carbamoyl Phosphate (CP) Synthesis Activities.

Enzyme	ATP-Synthesis[a]		CP Synthesis	ATP:CP
	k_{cat} (s^{-1})	K_m (mM ADP)	k_{cat} (s^{-1})	
Wild-type	0.13 ± 0.005	0.13 ± 0.03	1.90 ± 0.01	1.9
S35Y[b]	0.17 ± 0.004	0.14 ± 0.02	1.0 ± 0.01	3.7
C232D/A251T/A314T	0.032 ± 0.0002	0.017 ± 0.002	0.088 ± 0.008	3.8
C232V/A251V/A314V	0.28 ± 0.009	0.12 ± 0.02		
C232G/A251G/A314G	0.086 ± 0.001	0.054 ± 0.006	0.89 ± 0.009	2.2
A251C	0.10 ± 0.002	0.044 ± 0.009	0.81 ± 0.006	3.0
A314C	0.10 ± 0.05	0.045 ± 0.006	0.73 ± 0.02	3.1
A311L	0.10 ± 0.002	0.15 ± 0.02	0.29 ± 0.009	2.7
I352F	0.24 ± 0.006	0.15 ± 0.02	1.08 ± 0.01	3.1
T249V	0.22 ± 0.006	0.056 ± 0.005	0.90 ± 0.01	2.0

[a] From ADP and carbamoyl phosphate.
[b] Small subunit.

Table 3.3. ATP-free Glutaminase Activity

Enzyme	k_{cat} (s^{-1})	K_m (mM Gln)
Wild-type	0.072 ± 0.006	0.32 ± 0.08
C232D/A251T/A314T	1.1 ± 0.1	0.62 ± 0.14
C232V/A251V/A314V	1.5 ± 0.19	0.50 ± 0.16

Even though the rate of glutamine hydrolysis was increased, no carbamoyl phosphate was synthesized by this mutant. The ability of the triple mutant to utilize ammonia from solvent was comparable to its ability to utilize glutamine. The rate constant for the NH_4^+-dependent ATPase reaction with this mutant was 0.072 ± 0.002 s^{-1} and the K_M for a ammonium was 5.0 ± 0.8 mM. These values are significantly different from the wild-type values for the NH_4^+-dependent ATPase reaction (k_{cat} = 3.9 ± 0.1 s^{-1}, K_M = 130 ± 13 mM (NH_4^+)[38]), but similar to those measured with this mutant for the Gln-dependent ATPase reaction (**Table 3.1).** The only partial reaction not affected by this mutation was the ATP synthesis reaction. This result is consistent with a physical blockage created in the tunnel that only affects the transport of ammonia.

The triple glycine mutant was constructed with the intent to lower the energy barrier observed at the C232/A251/A314 triad. However, the kinetic constants for this mutant were not kinetically different from the wild-type enzyme. No enhancements in the rate constants for any of the reactions were observed. The mutation itself may have created a larger opening for ammonia to pass through the tunnel, but it was not possible to observe this experimentally, since the transport of ammonia is apparently not rate-limiting.

The single mutants used to study the narrow portion of the tunnel: C251A, A314C, I352F, T249V, and A311L (with the exception of A311L) only slightly interfere with the passage of ammonia through the tunnel. The two cysteine mutants exhibited wild-type-like kinetic constants in all of the reactions tested. These data suggest that an internal disulfide bond was not formed. Likewise, the mutant enzymes I352F and T249V possessed wild-type-like kinetic constants that suggest that the phenylalanine was not large enough to "plug" the tunnel and that the removal of the hydrogen bond interaction between NH_3 and Thr-249 is insufficient to prevent ammonia from translocating through the tunnel. There was an uncoupling of reactions observed between the glutaminase and carboxy phosphate active sites in the A311L mutant. This is exemplified by the 10-fold decrease in the rate of the glutamine-dependent ATPase reaction. The effectiveness of this single mutation can also be seen in the lowered rate for the carbamoyl phosphate synthesis reaction. These data suggest that A311L may interfere with the passage of ammonia.

Discussion

The MD simulations demonstrate the functional existence of a molecular tunnel that traverses two non-covalently joined subunits in CPS. This tunnel serves as a means to transport ammonia from the site of its formation in the small subunit to the site of its utilization in the large subunit. The transfer of ammonia between the two active sites is spontaneous. The highest energy barrier in the small subunit is 6.7 kcal/mol, which is due to the loss of the hydrogen-bonding interaction with the imidazole side chain of His-

353. The highest energy barrier in the large subunit is 7.2 kcal/mol and is caused by the need for ammonia to desolvate before passing through the narrow turning gate C232-A251-A314.

In the small subunit His-353, Ser-47, and Lys-202 function cooperatively by forming and breaking hydrogen bonds with ammonia in order to efficiently deliver it into the tunnel. Once inside the tunnel ammonia moves stepwise by forming and breaking hydrogen bonds with the backbone carbonyl groups of Gly-292, Pro-358and Gly-293, and the side chains of Ser-35 and Thr-37. There is also a functional requirement for His-353 and Ser-35. The conformation of these side chains is what enables the delivery of NH_3 into the large water pocket between the small and large subunit. In this part of the trajectory the solvation energy is what drives the ammonia forward though the tunnel.

Most of the residues identified in the MD simulations as being important for function in the translocation of ammonia have been mutated and the effects on the kinetic constants for CPS have been determined. The most important of these residues appear to be Cys-269, His-353, and Ser-47. The mutation of Cys-269 to either serine or alanine results in a protein that is unable to hydrolyze glutamine.[20] However, the C269S mutant is able to bind glutamine and stimulate the hydrolysis of ATP in the large subunit.[20] The mutation of His-353 also results in a protein that is unable to hydrolyze glutamine.[57] However, an X-ray structure of the H353N mutant in the presence of glutamine showed that the thioester intermediate could form but not be hydrolyzed.[31] Thus, this residue seems to be more important for the hydrolysis of the thioester

intermediate than for its formation. The hydroxyl group of Ser-47 functions as part of the oxyanion hole during the formation and hydrolysis of the thioester intermediate. Mutation of this residue to alanine results in a protein that is unable to hydrolyze glutamine in the absence of ATP and HCO_3^-.[27] However, in the presence of ATP and HCO_3^-, the Michaelis constant for the glutamine is elevated by a factor of >10 but k_{cat} is largely unaffected.[27]

Perturbations to the kinetic constants have also been observed for mutations to Lys-202 and Glu-355.[27] When Lys-202 is mutated to methionine the k_{cat} values are unchanged but the K_M value for glutamine is elevated by a factor of ~10. When Glu-355 is mutated to alanine there is no change in k_{cat} but a significant increase in the K_M for glutamine.[27] However, when this residue is mutated to glutamine there is no detectable hydrolysis of glutamine and no carbamoyl phosphate formation.[27]

Once in the large subunit, ammonia has only one energy barrier to overcome. The magnitude of the energy barrier is 7.2 kcal/mol at the narrow turning gate formed by Cys-232, Ala-251, and Ala-314. Migration of ammonia in this part of the tunnel starts with a large drop in free energy once ammonia is injected into a large water pocket between Thr-37 and Tyr-291. From there ammonia travels through another water pocket and squeezes through the narrow turning gate by shedding all of its accompanying water molecules. The interaction between ammonia and Thr-249 is responsible for the delivery of NH_3 through this narrow gate.

The computational data point to the migration of ammonia through the C232-A251-A314 gate as the rate-limiting step in the transport process. A triple mutant

C232V/A251V/A314V was designed to block the passage of ammonia through this portion of the tunnel. The rate of ATP hydrolysis was decreased by a factor of 180 and there was no carbamoyl phosphate synthesis detected. However, the active site responsible for the final step in the synthesis of carbamoyl phosphate was fully functional as was observed by the wild-type like kinetics of the ATP-synthesis reaction. Also, the activity of the glutaminase active site was completely unaffected by this mutation.

The diffusion through the tunnel is fast, with an estimated rate constant on the order of 9.9 ms^{-1}. This rate is approximately 200 times faster than the rate constant for the overall synthesis of carbamoyl phosphate. Even though there are three energy barriers involved with the transport of ammonia to the carboxyphosphate active site, the transport of ammonia is not the rate limiting step in the reaction mechanism.

CHAPTER IV

A THEORETICAL AND EXPERIMENTAL INVESTIGATION OF CARBAMATE TRANSPORT WITHIN THE LARGE SUBUNIT OF CARBAMOYL PHOSPHATE SYNTHETASE FROM *E. coli**

Introduction

Carbamoyl phosphate synthetase (CPS) from *Escherichia coli* catalyzes the formation of carbamoyl phosphate, an intermediate in the biosynthesis of pyrimidine nucleotides and arginine, from glutamine, bicarbonate and two molecules of MgATP.[1,3] In the proposed reaction mechanism, ATP phosphorylates bicarbonate to form carboxyphosphate, and glutamine is hydrolyzed to glutamate and ammonia. The ammonia then reacts with the carboxyphosphate intermediate to form carbamate. In the final step, a second molecule of ATP phosphorylates carbamate to produce the ultimate product, carbamoyl phosphate. Overall, three unstable intermediates (ammonia, carboxyphosphate and carbamate) and carbamoyl phosphate are formed in a series of four separate reactions. The reaction mechanism is summarized in **Scheme 4.1**.

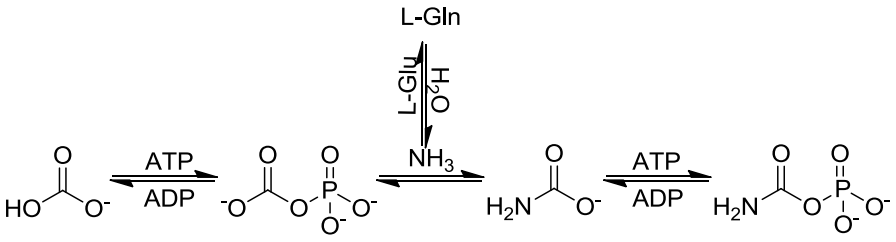

Scheme 4.1

CPS from *E. coli* is a heterodimeric protein that is composed of two subunits of molecular weight ~40 kD and ~118 kD.[98] The hydrolysis of glutamine occurs within the small subunit whereas carbamoyl phosphate is produced in the large subunit.[14] The catalytic properties of site-directed mutants and the X-ray structure of CPS have identified the N-terminal half of the large subunit as containing the active site for the formation of carboxy phosphate and carbamate, whereas the C-terminal half harbors the active site for the synthesis of carbamoyl phosphate. The three active sites are connected by two molecular tunnels that extend nearly 100 Å from one end of the protein to the other as illustrated in **Figure 4.1**.[34] Ammonia migrates from the site of synthesis in the small subunit to the site of utilization in the N-terminal domain of the large subunit through a passageway designated as the "ammonia tunnel". After carbamate is formed from the reaction of ammonia with carboxyphosphate, this intermediate migrates through the "carbamate tunnel" to the third active site where it is phosphorylated by the second ATP to carbamoyl phosphate. Of the thirty residues that come together to form the carbamate tunnel, half come from the N-terminal domain, with the remaining half coming from the C-terminal domain. The tunnel is capped at both ends by arginine residues; Arg-306 from the N-terminal domain and Arg-848 from the C-terminal

domain. While the tunnel itself is comprised primarily of nonionic amino acids, five glutamate residues, Glu-25, Glu-383, Glu-604, Glu-577, and Glu-916 are positioned with their side chains pointing to the interior of the carbamate tunnel. These residues are highly conserved in CPS from both eukaryotic and prokaryotic species.

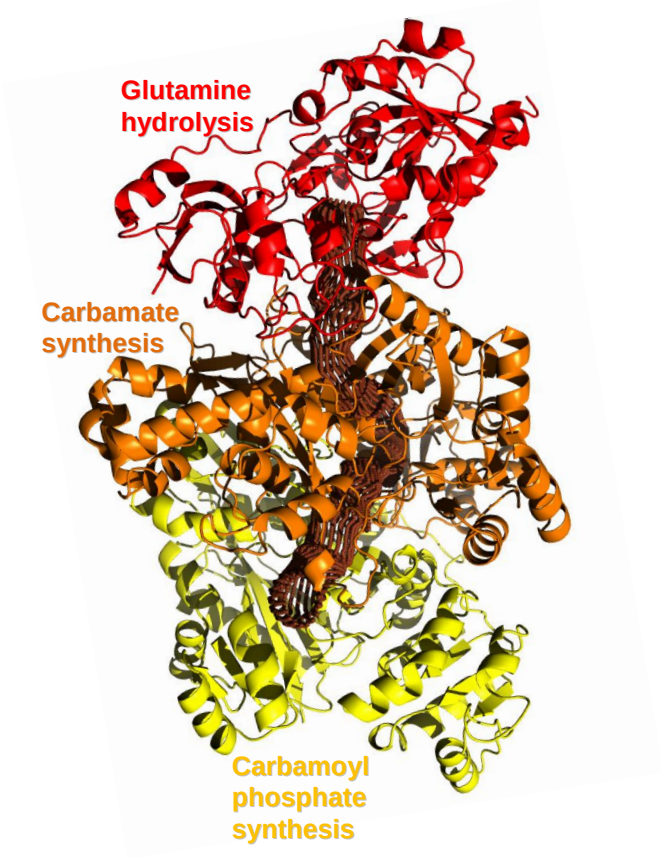

Figure 4.1. The crystal structure of carbamoyl phosphate synthetase from *E. coli*. The small subunit containing the site for glutamine hydrolysis is shown in red. The large subunit is shown in orange and yellow. In orange is the N-terminal domain which is responsible for the synthesis of carboxyphosphate and carbamate. In yellow is the C-terminal domain which is responsible for the synthesis of carbamoyl phosphate. The two intramolecular tunnels for the transport of ammonia and carbamate are shown in brown. The image was constructed using the PDB file: 1BXR.

Enzymes have evolved molecular tunnels to protect unstable and reactive intermediates from bulk solvent. Protein tunnels for the migration of ammonia have been found in all members of the glutamine amidotransferase family of enzymes.[34,45-46,52,70,99-104] In addition to the transport of ammonia, tunnels have been identified for the translocation of other reactive species. For example, tryptophan synthase,[105-107] acetyl-coenzyme A synthase/carbon monoxide dehydrogenase,[50,108-109] 4-hydroxy-2-ketovalerate aldolase/acylating acetaldehyde dehydrogenase,[49] and CPS use molecular tunnels to transport indole, carbon monoxide, acetaldehyde, and carbamate, respectively.

In this study, we have calculated the free energy profile for the migration of carbamate along the carbamate tunnel using the umbrella sampling technique. The transport of carbamate through the entire carbamate tunnel is composed of three steps. The sequence of events is initiated by the reaction of ammonia with carboxy phosphate to form carbamate and phosphate. Phosphate is released into solution and the side chain of Arg-306 rotates towards the interior of the carbamate tunnel and is locked in place by electrostatic interactions with Glu-25, Glu-383 and Glu-604 before carbamate is injected into the tunnel. After passing through a relatively narrow region surrounded by Ile-18, Ile-20, Ala-23 and Val-381 with a free energy barrier of 6.7 kcal/mol, carbamate enters a large water pocket in the middle of the tunnel with a free energy drop of 12 kcal/mol. Carbamate approaches the site of phosphorylation in the C-terminal domain of the large subunit by overcoming a free energy barrier of 8.4 kcal/mol near the juxtaposition of Glu-577, Glu-916 and Arg-848. All of the residues critical for migration of carbamate have been studied experimentally through mutagenesis and kinetic characterization. In

this simulation, carbamate travels nearly 30 Å through the internal water-tight tunnel from the site of formation in the N-terminal domain to the site of utilization in the C-terminal domain of CPS.

Materials and Methods

Construction of Models for the Transport of Carbamate. All of the models for the transport of carbamate were constructed by Dr. Yubo Fan from the Chemistry Department at Texas A&M University. The starting point for the simulations of carbamate transfer was the crystal structure of the large subunit (PDB codes: 1c30 and 1bxr). Two missing loops, residues 717-723 and 742-749, in the large subunit of CPS (PDB code: 1c30) were inserted using SWISS-MODEL.[74-76] These two loops were part of the ATP binding domain in the C-terminal half of the large subunit. In the crystal structure, 1bxr, the bound AMPPNP was replaced with ATP in the C-terminal active site. Conversely, in the carboxyphosphate active site, AMPPNP was replaced with either ADP and P_i or ADP alone. The charge distributions on all atoms of carbamate were calculated using the RESP-fit method[77-78] based on B3LYP/cc-pVTZ calculations[79-82] with the solvent effect ($\varepsilon = 4$) taken into account using the polarizable continuum model (PCM).[83-85] The charges on the carbon, hydrogen, oxygen, and nitrogen atoms in carbamate are +0.883517, +0.325533, -0.824983, -0.884618, respectively. Mn^{2+} and all of the crystalline waters within the enzyme and on the protein exterior were used in the simulations. The protonation states of all histadine residues were adjusted based on local environments. The net negative charge of the protein was

neutralized by added Na^+ ions. Explicit TIP3P waters were added as a truncated octahedral water box with a 10 Å buffer.[110] All operations were processed using the AMBER Leap module, which led to models containing ~70,000 atoms, including ~19,000 waters.[86-87] These models were further extended using the periodic boundary condition. The AMBER force field 99,[111] with the parameters for the peptide backbone re-optimized, was utilized for all standard amino acid residues while the general AMBER force field was used for carbamate.[112] The force fields for ADP[88], P_i[88] and Mn^{2+} [89] were previously developed for the Amber program. MD simulations were conducted in an isothermal–isobaric (NPT) ensemble at 300 K and 1 atm. The SHAKE algorithm was used to constrain all bonds involving hydrogens.[90] A 10 Å cutoff was applied for nonbonding interactions. The Particle Mesh Ewald method was employed to treat long-range electrostatic interactions.[91-92] MD trajectories were obtained with these structures using the AMBER suite of programs.[86-87]

Free Energy Calculations. All of the MD simulations and PMF calculations in this study were performed by Dr. Yubo Fan from the Chemistry Department at Texas A&M University. The reaction coordinate for the free-energy simulations was defined as the distance from the carbon atom of carbamate to the β-phosphoryl group of ADP in the active site for carbamate formation as shown in the figure on page 88. The free-energy profiles or potentials of mean force (PMF) were computed along the translocation trajectories using the umbrella sampling technique with a biasing harmonic potential involving a force constant of 40 $kcal \cdot mol^{-1} \cdot Å^{-2}$.[93-96,113] Because of the repulsion between carbamate and phosphate in complexes **B** and **C**, in the table on page

89, when the reaction coordinate is shorter than 10 Å, the PMFs for these two systems were calculated from 10 to 33 Å.

Expression and Purification of Mutant Proteins. The plasmids containing the *car*AB genes were transformed in the RC50 cell line of *E. coli* for expression of the wild-type and mutant forms of CPS, and the proteins were purified as previously described.[97] The mutants A23F, A23K, M174M, M378E, M174E/M378E, L648E, L720E, M911E, I18W/A23F/C24F, G575F and G575K were expressed and purified to greater than 95% homogeneity, as judged by SDS-polyacrylamide gel electrophoresis.

Kinetic Measurements. The rate of glutamine hydrolysis was determined by coupling the formation of glutamate to the production of α-ketoglutarate with L-glutamate dehydrogenase (GDH) and 3-acetylpyridine adenine dinucleotide (APAD).[19] The reaction mixtures contained 50 mM HEPES, pH 7.6, 20 mM $MgCl_2$, 100 mM KCl, 40 mM $KHCO_3$, 5.0 mM ATP, 10 mM ornithine, 1.0 mM APAD, 30 units of GDH, and varying amounts of glutamine. The rate of ADP formation was measured using a pyruvate kinase (PK)/lactate dehydrogenase (LDH) coupling system.[19] The reaction mixtures for the glutamine-dependent assay contained 50 mM HEPES, pH 7.6, 20 mM $MgCl_2$, 100 mM KCl, 40 mM $KHCO_3$, 10 mM glutamine, 10 mM ornithine, 1.0 mM phosphoenolpyruvate, 0.2 mM NADH, 2 units of PK, 3 units of LDH, and varying amounts of ATP. Glutamine was excluded from the HCO_3^--dependent ATPase assays. This assay was followed by monitoring the decrease in absorbance at 340 nm using a SpectraMax Plus 96-well plate reader from Molecular Devices. The synthesis of carbamoyl phosphate was determined by measuring the rate of citrulline formation in a

coupled assay containing ornithine transcarbamoylase (OTC) and ornithine.[114] The assay mixture contained 50 mM HEPES, pH 7.6, 20 mM $MgCl_2$, 100 mM KCl, 40 mM $KHCO_3$, 5.0 mM ATP, 10 mM ornithine, 12 units of OTC, and 10 mM glutamine. The rate of ATP synthesis was measured with a hexokinase (HK)/glucose-6-phosphate dehydrogenase (G6PDH) coupling system.[19] The assay mixture for the ADP-dependent assay included 50 mM HEPES, pH 7.6, 20 mM $MgCl_2$, 100 mM KCl, 10 mM ornithine, 0.75 mM NAD, 2.0 units HK, 1.0 mM glucose, 1.0 unit G6PDH, 1.0 mM carbamoyl phosphate, and varying amounts of ADP.

Results

Physical Properties of the Carbamate Tunnel. The tunnel used for the transport of carbamate connects the site for the synthesis of carboxyphosphate to the site of carbamoyl phosphate synthesis. Based on X-ray crystallography data and MD simulations the tunnel can be divided into three sections, each one containing a water pocket. The first water pocket occurs between Ala-23 and the ADP bound at the carboxyphosphate active site (**Figure 4.2**). Because this pocket directly connects to the active site, the water molecules in it are able to freely exchange with bulk solvent. The second water pocket is located between Ala-23 and Gly-575. It is tightly sealed and no exchange of water with solvent was observed. The third pocket extends from Gly-575 all the way to the ATP bound at the carbamoyl phosphate active site. Like the middle water pocket, this one is also tightly sealed and no exchange with bulk solvent is possible. Since the third water pocket connects directly to the carbamoyl phosphate

active site, the only way it can remain water tight is when the active site is closed in the presence of ATP.

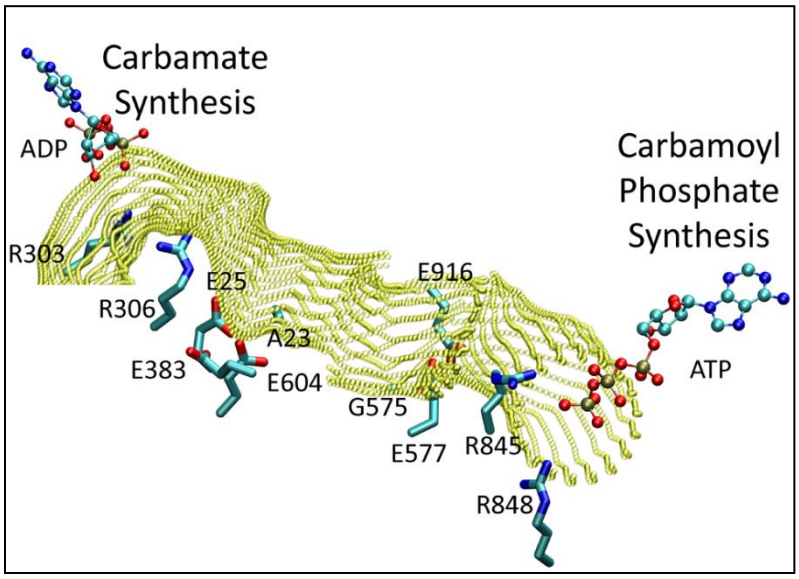

Figure 4.2. The molecular tunnel for the transport of carbamate from the site of its formation to the site of the carbamoyl phosphate synthesis. ADP and ATP are bound to the sites for carbamate formation and utilization, respectively. The transport of carbamate starts in the area near Arg-303 and Arg-306, and ends near Arg-845. There are two narrow regions of the tunnel near Ala-23 and Gly-575.

Transport of Carbamate through the Tunnel. Mechanistic studies on CPS have shown that carbamoyl phosphate is not synthesized until phosphate is released and a second molecule of ATP binds at the carbamoyl phosphate active site.[5] Phosphate is a highly charged species and its presence and absence can have substantial consequences for the environment and conformation of the active site. It interacts with the side chain of Arg-306 keeping this reside in the closed conformation. Once it is released, Arg-306 is able to rotate to participate in electrostatic interactions with the triad of glutamates at

the entrance to the carbamate tunnel, Glu-25, Glu-383, and Glu-604. In order to better understand the role of phosphate in carbamate transport, three different scenarios, described in **Table 4.1**, were constructed for the MD calculations.

Table 4.1. Definition of the Complexes with Different Ligands Bound.

Name	PDB code	Substrate(s)		
		Site 1[a]	Site 2[b]	Arg-306[c]
A	1BXR	ADP	ATP	Open
B	1BXR	ADP + P_i	ATP	Closed
C	1C30	ADP + P_i	ADP	Open

[a] Site for carbamate synthesis.
[b] Site for carbamoyl phosphate synthesis.
[c] When Arg-306 is hydrogen bonded to the phosphate Site 1 the tunnel is *closed* and it is *open* when this residue is hydrogen bonded to Glu-25, Glu-383 and Glu-604.

In Case **A**, where phosphate is released and only ADP is bound, two energy barriers are observed in the calculation (red curve, **Figure 4.3**). These two barriers have magnitudes of 8.4 and 6.7 kcal/mol. They likely correspond to the translocation of carbamate from the first to the second water pocket and from the second to the third, respectively. When carbamate was positioned in the middle of the tunnel for the calculation, Arg-306 rotated toward glutamates 25, 383, and 604. This conformational change resulted in an *open* configuration for the entrance to the carbamate tunnel. These results indicate that the release of phosphate is critical for the delivery of carbamate to the carbamoyl phosphate active site.

In Case **B**, where phosphate and ADP are bound in the carboxyphosphate active site with ATP bound at the carbamoyl phosphate active site, the energy profile for the transport of carbamate looks similar to that of Case **A** for the last two thirds of the trajectory (blue curve, **Figure 4.3**). The relative free energy at the beginning of the tunnel is very high due to the strong repulsion between carbamate and the Arg-306-P_i interaction. The interaction between phosphate and the side chain of Arg-306 results in a *closed* confirmation of the tunnel opening, thus trapping carbamate in the active site. In order to move into the tunnel, carbamate must break at least one of the hydrogen bonds between Arg-306 and P_i. When carbamate is placed 10 Å away from the carboxyphosphate active site inside the tunnel, a slight barrier at 17 Å is observed. This increase in relative free energy is a result of carbamate being repulsed by the exposed negative charges on Glu-25, Glu-383 and Glu-604. It is worth mentioning again that in the *open* conformation, these negative charges are shielded by the side chain of Arg-306.

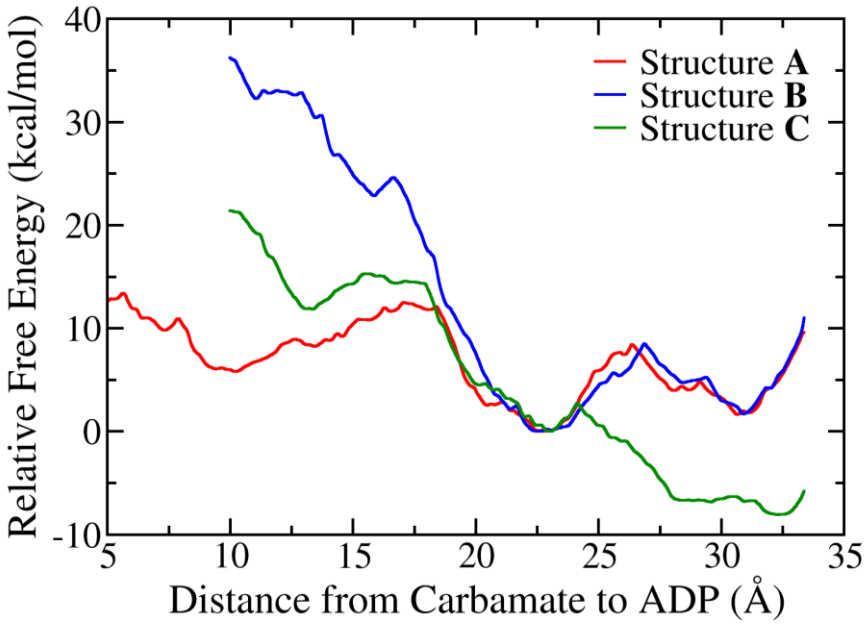

Figure 4.3. Potentials of mean force from the site for carbamate formation to the site for its utilization. The reaction coordinate is defined as the distance from the carbon atom of the carbamate to the phosphorus atom of the β-phosphate in ADP bound at the active site for carbamate formation.

In Case **C**, where ADP and P_i are bound at the carboxyphosphate active site and ADP is bound at the carbamoyl phosphate active site, the side chain of Arg-306 was manually rotated to interact with Glu-25, Glu-383 and Glu-604. During the energy minimization process for this structure, the side chain of Arg-848, at the carbamoyl phosphate active site, was observed rotating away from the bound ADP and interacting with Glu-577 and Glu-916. The high free energy at the entrance to the tunnel is indicative of the strong repulsion between carbamate and the bound P_i (green curve, **Figure 4.3**). As the distance between carbamate and the carboxyphosphate active site increases, the energy profile has a noticeably downward slope when compared to Cases

A and **B**. This is mainly due to the rotation of the side chain of Arg-848. The shielding of these negative charges allows for carbamate to easily enter the active site for the formation of carbamoyl phosphate.

Conformation Change of Arg-306. The free energy profiles calculated for the migration of carbamate through the tunnel revealed that the conformation of Arg-306 is critical for the delivery of carbamate into the tunnel. In order to gauge a better understanding of this behavior, a separate set of calculations was performed on the active site environment around Arg-306 for cases **A** and **B**. The distance between the guanidinium carbon of Arg-306 and the carboxylate carbon of Glu-604 was defined as the reaction coordinate.

The empty space left in the active site after the release of phosphate was quickly filled by the newly formed carbamate. This arrangement allows for the formation of hydrogen bonds between the carboxylate on carbamate and the side chain of Arg-306 (**Figure 4.4a**). While in this conformation, Arg-306 must overcome an 8 kcal/mol energy barrier in order to rotate to hydrogen bond with the glutamate triad (**Figure 4.4b**). After the rotation the free energy increases to 11 kcal/mol.

In the case where phosphate is bound (**Figure 4.4c**), the interaction between phosphate and Arg-306 is so strong that the rotation of Arg-306 is energetically unfavorable. When Arg-306 is manually rotated to interact with the glutamate triad in the presence of P_i (**Figure 4.4d**), the free energy is 22 kcal/mol higher than the *closed* conformation, in which P_i and Arg-306 hydrogen bond to each other.

It can be clearly seen, that the energy needed to go from a *closed* to an *open* conformation is lower in the presence of carbamate and in the absence of P_i. The energy barrier for the opening of the tunnel in the presence of phosphate is too high to be physiologically relevant. According to transition state theory, a 24 kcal/mol barrier corresponds to a reaction rate of one turnover every few hours. Since the rate for the synthesis of carbamoyl phosphate is 1.9 s^{-1}, these calculations clearly favor the need for phosphate release prior to the opening of the carbamate tunnel.

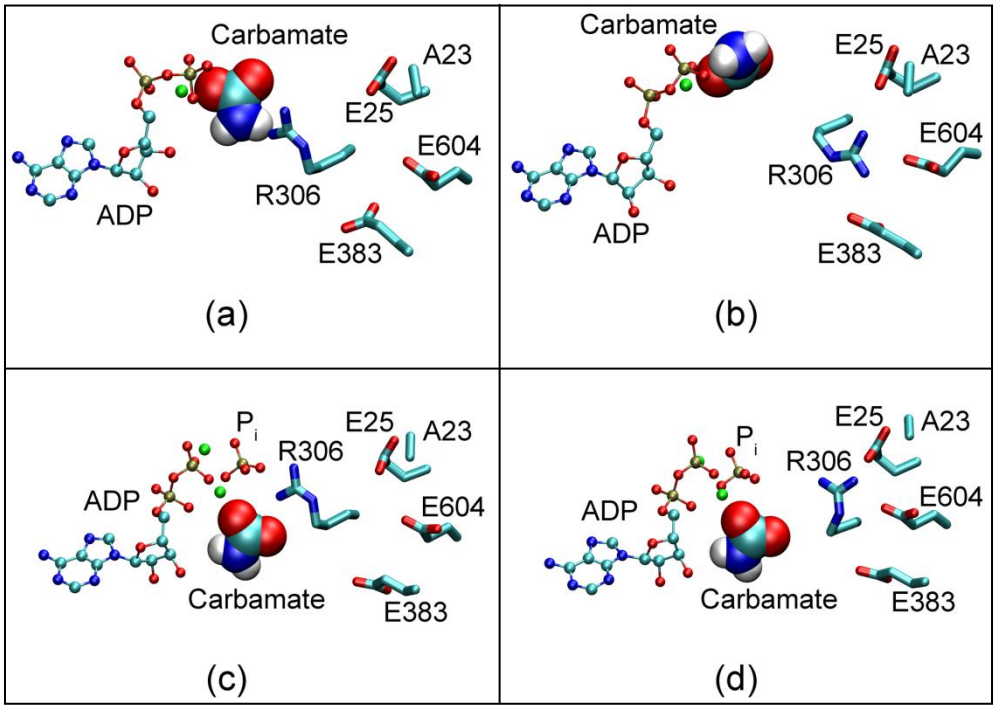

Figure 4.4. Conformational change of the Arg-306 side chain. In panels A and B, phosphate is released but in panels C and D it remains bound. The side chain of Arg-306 orients towards ADP (or phosphate) in panels A and C while it forms a salt bridge with Glu-25, Glu-383 and Glu-604 in panels B and D.

Selection of Mutation Sites. Amino acid residues within the carbamate tunnel were mutated in an attempt to engineer blockages that would impede the migration of carbamate from one active site to the next. A triple mutant, I18W/A23F/C24F, was initially constructed to fill the large water cluster in the middle pocket of the tunnel and impede the translocation of carbamate. Ala-23 was mutated previously to leucine and tryptophan to create a barrier inside the tunnel.[39] The kinetic constants of the A23W mutant indicated that a structural perturbation of the active site for the synthesis of carbamate had occurred. Since the original goal of this experiment was to hinder the migration of carbamate through the tunnel rather than disrupt the rate of carbamate formation, it was anticipated that an A23F mutation may be sufficient to accomplish this task without unwanted structural effects on the catalytic centers. The analogous mutant, G575F, was constructed at the opposite end of the carbamate tunnel. Previously, Gly-575 was mutated to alanine, serine, and leucine in an effort to probe the size of the tunnel in this region of the protein.[39,98] These substitutions to Gly-575 did not exhibit significant perturbations to the kinetic constants for the partial reactions. However, the G575L mutant had a 50-fold reduction in the rate of carbamoyl phosphate formation. This was attributed to the restricted passage of carbamate through the tunnel. The insertion of a larger phenylalanine side chain was anticipated to create a more efficient blockage of the tunnel. Two additional mutants, A23K and G575K, were made to affect the conformational orientation of Arg-306 and Arg-848 by competing for ionic interactions with Glu-25, Glu-383, Glu-577, Glu-604 and Glu-916.

Further attempts to disrupt putative interactions between the two special arginine residues (Arg-306 and Arg-848) and the five interior glutamate residues prompted the construction of mutants M174E, M378E, and M174E/M378E. Met-174 and Met-378 are reasonably close to Arg-306 and are on the opposite face of the tunnel wall near the first triad of glutamate residues. If Arg-306 were to interact with either of these new glutamate residues, the tunnel may remain in a more open conformation. The analogous pair of residues, Met-911 and Leu-720, were chosen at the other end of the carbamate tunnel near the active site for the synthesis of carbamoyl phosphate. Leu-648 was mutated to a glutamate to facilitate the formation of a salt bridge between this residue and Arg-845. The formation of salt bridges within the tunnel would block the exit of the carbamate tunnel, preventing carbamate from reaching the second molecule of ATP bound at the carbamoyl phosphate active site.

Kinetic Properties of Carbamate Tunnel Mutants. The triple mutant, I18W/A23F/C24F, was made to disrupt the water pocket that facilitates the passage of carbamate through the carbamate tunnel. While this mutant significantly hindered the overall rate of carbamoyl phosphate synthesis, it also diminished all of the other partial reactions. Therefore, substitution of three very large residues for three smaller residues may have caused unwanted conformational changes inside the protein, which may have perturbed the conformation of the two active sites. To diminish this problem, the A23F mutant was constructed and characterized. The methyl side chain of Ala-23 points directly into the interior of the carbamate tunnel and thus the substitution with phenylalanine may be sufficient to block this part of the tunnel. From the kinetic data

the only reaction significantly affected by this mutation was the overall synthesis of carbamoyl phosphate (**Tables 4.2** and **4.3**). A similar kinetic pattern was observed for the analogous mutation (G575F) near the active site for the synthesis of carbamoyl phosphate. This mutant has wild-type like activity in all of the partial reactions except for the carbamoyl phosphate synthesis reaction. Of the mutants made in the carbamate tunnel, G575F is the most efficacious at blocking the passage of carbamate without disrupting any of the active sites.

The substitution of Ala-23 with lysine decreased the glutamine-dependent ATPase activity by an order of magnitude. While there was a decrease in the rate of carbamoyl phosphate formation, the enzyme utilized two molecules of ATP for every molecule of carbamoyl phosphate synthesized. The analogous mutant, G575K, at the other end of the carbamate tunnel, had similar catalytic properties as the wild-type protein, suggesting that the conformational change of Arg-848 may not be crucial for the transport of carbamate.

Table 4.2. Kinetic Characterization of the Wild-Type CPS and Its Mutants.

Enzyme	Gln-dependent ATPase		HCO_3^--dependent ATPase[a]		ATP-dependent Glutaminase	
	k_{cat} (s^{-1})	K_m (mM ATP)	k_{cat} (s^{-1})	K_m (mM ATP)	k_{cat} (s^{-1})	K_m (mM Gln)
WT	3.60 ± 0.11	0.24 ± 0.04	0.170 ± 0.003	0.051 ± 0.008	2.20 ± 0.04	0.15 ± 0.01
I18W/A23F/C24F	0.06 ± 0.002	0.25 ± 0.05	0.039 ± 0.002	0.21 ± 0.05	0.13 ± 0.01	0.16 ± 0.04
A23F	1.30 ± 0.07	1.60 ± 0.25	0.097 ± 0.005	0.12 ± 0.04	1.08 ± 0.04	0.21 ± 0.03
A23K	0.28 ± 0.01	0.38 ± 0.08	0.17 ± 0.01	0.33 ± 0.06	0.21 ± 0.02	0.10 ± 0.04
G575F	3.30 ± 0.19	0.014 ± 0.030	0.19 ± 0.01	0.014 ± 0.003	3.00 ± 0.14	0.19 ± 0.03
G575K	3.3 ± 0.18	0.070 ± 0.01	0.18 ± 0.01	0.013 ± 0.002	3.10 ± 0.20	0.17 ± 0.04
M174E	0.11 ± 0.01	0.69 ± 0.17	0.053 ± 0.002	0.36 ± 0.05	0.15 ± 0.01	0.39 ± 0.06
M378E	0.035 ± 0.002	0.160 ± 0.04	0.013 ± 0.008	0.030 ± 0.008	0.13 ± 0.01	0.35 ± 0.07
M174E/M378E	0.043 ± 0.002	0.28 ± 0.07	0.028 ± 0.001	0.29 ± 0.07	0.10 ± 0.01	0.47 ± 0.11
L648E	3.2 ± 0.20	1.2 ± 0.22	0.59 ± 0.03	0.50 ± 0.09	1.3 ± 0.05	0.23 ± 0.03
L720E	2.0 ± 0.15	1.7 ± 0.36	0.39 ± 0.01	0.22 ± 0.03	0.84 ± 0.03	0.18 ± 0.02
M911E	0.50 ± 0.05	1.0 ± 0.31	0.33 ± 0.01	0.26 ± 0.04	0.14 ± 0.01	0.18 ± 0.05

[a] HCO_3^--dependent ATPase activity was measured in the absence of glutamine.

Table 4.3. Kinetic Characterization of the Synthesis of ATP and Carbamoyl Phosphate (CP) by CPS.

Enzyme	ATP-Synthesis[a]		CP Synthesis	ATP:CP
	k_{cat} (s^{-1})	K_m (mM ADP)	k_{cat} (s^{-1})	
WT	0.130 ± 0.005	0.13 ± 0.03	1.90 ± 0.01	1.9
I18W/A23F/C24F	0.086 ± 0.003	0.18 ± 0.03	<0.01	
A23F	0.230 ± 0.004	0.53 ± 0.007	0.033 ± 0.004	39
A23K	0.32 ± 0.01	0.022 ± 0.006	0.160 ± 0.002	1.8
G575F	0.058 ± 0.002	0.030 ± 0.005	0.072 ± 0.001	46
G575K	0.15 ± 0.007	0.054 ± 0.01	1.9 ± 0.01	1.8
M174E	0.10 ± 0.002	0.088 ± 0.01	1.90 ± 0.01	1.8
M378E	0.20 ± 0.004	0.13 ± 0.01	0.012 ± 0.002	2.9
M174E/M378E	0.22 ± 0.005	0.17 ± 0.02	<0.01	
L648E	0.024 ± 0.0004	0.34 ± 0.03	<0.01	
L720E	0.031 ± 0.001	0.42 ± 0.078	<0.01	
M911E	<0.01		0.015 ± 0.0004	33.3

[a] From ADP and carbamoyl phosphate.

The single mutants, M174E and M378E, which were created to form a salt bridge with Arg-306, were successful in disrupting the passage of carbamate through the tunnel. These mutants had significant reductions in the rates of the ATPase and carbamoyl phosphate synthesis reactions. Neither mutation affected the rate of the partial ATP synthesis reaction (**Tables 4.2** and **4.3**). The catalytic properties of the double mutant, M174E/M378E, are similar to the single mutants with regard to the various partial reactions. However, the double mutant was unable to synthesize carbamoyl phosphate.

The mutant L648E was successful at diminishing the synthesis of carbamoyl phosphate but the mechanism may be different from a simple blockage of the tunnel. The formation of a salt bridge between this glutamate and Arg-845 cannot block the exit of the tunnel but it can potentially interfere with the reaction between carbamate and ATP. There was no detectable rate of carbamoyl phosphate formation. Little effect on the rates of all partial reactions was observed (**Tables 4.2** and **4.3**). Thus the reactions at the small subunit and the carboxy phosphate active sites remained unperturbed.

The residues analogous to Met-174 and Met-378, Leu-720 and Met-911, respectively, were mutated to glutamate. The rates for both the glutamine- and HCO_3^{2-}-dependent ATPase reactions were largely unaffected by these mutations. The rate of the ATP-synthesis partial reaction was decreased 4-fold for the L720E mutant, and was undetectable for the M911E mutant. These perturbations may be due to an altered active site environment which diminishes the rate ADP phosphorylation by carbamoyl phosphate. No carbamoyl phosphate formation was detected with the L720E mutant

while only limited formation was detected with M911E (**Table 4.3**). Both mutants can structurally block the exit of the carbamate tunnel although the presence of these glutamates also weakens the assistance of Arg-848 during the synthesis of carbamoyl phosphate.

Discussion

The presence of an intramolecular tunnel for the transport of carbamate as been demonstrated by MD simulations. This tunnel appears to be tightly sealed because no leakage of carbamate at any point in this study was observed. It has been shown that the release of phosphate from the carboxyphosphate active site is critical for the opening of the carbamate tunnel. Once the phosphate is released, the side chain of Arg-306 has a small energy barrier to overcome in order to interact with the glutamate triad at the mouth of the tunnel. Once the negative charges on Glu-25, Glu-383 and Glu-604 are shielded, carbamate is free to enter to tunnel. The largely negatively charged environment of the tunnel allows carbamate to travel quickly through it.

The importance of the glutamate triad and Arg-306 was established previously by constructing R306A and E25Q/E383Q/E604Q mutants.[115] Neither of these mutants were capable of synthesizing carbamoyl phosphate. By replacing glutamate with glutamine the negative charge is removed and so is the possibility for the interaction between Arg-306 and the glutamate triad. By removing this interaction, Arg-306 is likely unable to rotate to create an open conformation at the entrance of the carbamate tunnel, thus trapping this intermediate in the active site. In addition, all the mutants

constructed for this study that disrupted the interaction between Arg-306 and the glutamate triad, M378E and M174E/M378E, significantly retarded the rate of carbamoyl phosphate synthesis. The mutants that were created to physically impede the progress of carbamate through the tunnel, A23F and G575F, were a success. The fact that each mutant retained less that 4% of its overall activity for the synthesis of carbamoyl phosphate relative to wild-type CPS confirms the presence of narrow portions of the tunnel that help to divide it into three distinct water pockets.

The side chains of Ala-23 and Gly-575 have also been previously mutated to several different residues. In an earlier study Ala-23 was mutated to a leucine and a tryptophan in order to create a blockage within the top portion of the carbamate tunnel.[39] Neither mutant showed significant deviations from the wild-type enzyme in the ATP synthesis reaction. However, the A23W had only 10% of the glutamine-dependent ATPase activity of the wild-type protein. Our data from the I18W/A23F/C24F triple mutant also confirms that bulky residues in the portion of the tunnel alter the integrity of the carboxyphosphate active site. Gly-575 was mutated to an alanine, serine, and a leucine in order to titrate the size of the C-terminal opening of the carbamate tunnel.[39] The G575L mutant was the most effective at blocking the tunnel. Our mutant G575F confirms the requirement for a large hydrophobic residue to block the tunnel exit. The lysine side chain used in the G575K mutant may have been too flexible and allowed carbamate to pass through, as was observed in the wild-type like kinetics for the synthesis of carbamoyl phosphate.

Overall, the transport of carbamate through the ~40 Å tunnel is rapid. It takes approximately 0.6 ms for carbamate to travel from the middle water pocket to the site for carbamoyl phosphate synthesis while overcoming the largest free energy barrier observed in the whole trajectory. This speed is approximately equivalent to a rate constant of 1600 s^{-1}, which is significantly faster that the overall reaction catalyzed by CPS. Therefore, our findings indicate that the migration of carbamate from the site of its formation to the site of its utilization is not the rate limiting step in the reaction mechanism.

CHAPTER V

UTILIZATION OF FORMATE AS A SUBSTRATE BY CARBAMOYL PHOSPHATE SYNTHETASE: EVIDENCE FOR CARBOXYPHOSPHATE AS A VALID INTERMEDIATE

Introduction

Carbamoyl phosphate synthetase (CPS) from *Escherichia coli* catalyzes the formation of carbamoyl phosphate, an intermediate in the biosynthesis of pyrimidine nucleotides and arginine, from glutamine, bicarbonate and two molecules of MgATP.[2,116-117] The enzyme contains three active sites that are separated in space by ~100 Å and are linked by an intramolecular tunnel (**Figure 5.1**). In the proposed reaction mechanism, the first molecule of ATP phosphorylates bicarbonate to form carboxyphosphate. Glutamine is hydrolyzed to glutamate and ammonia at a separate active site. Ammonia travels ~30 Å through the "ammonia tunnel" to react with carboxyphosphate to form carbamate. Carbamate then travels ~40 Å through a second tunnel to participate in the final step of the reaction where it is phosphorylated by a second molecule of ATP to produce the final product, carbamoyl phosphate. The reaction mechanism is summarized in **Scheme 5.1**.

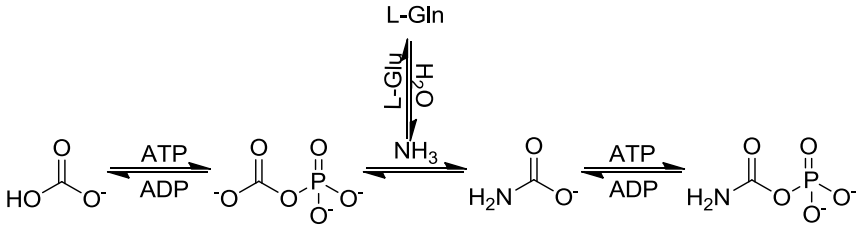

Scheme 5.1

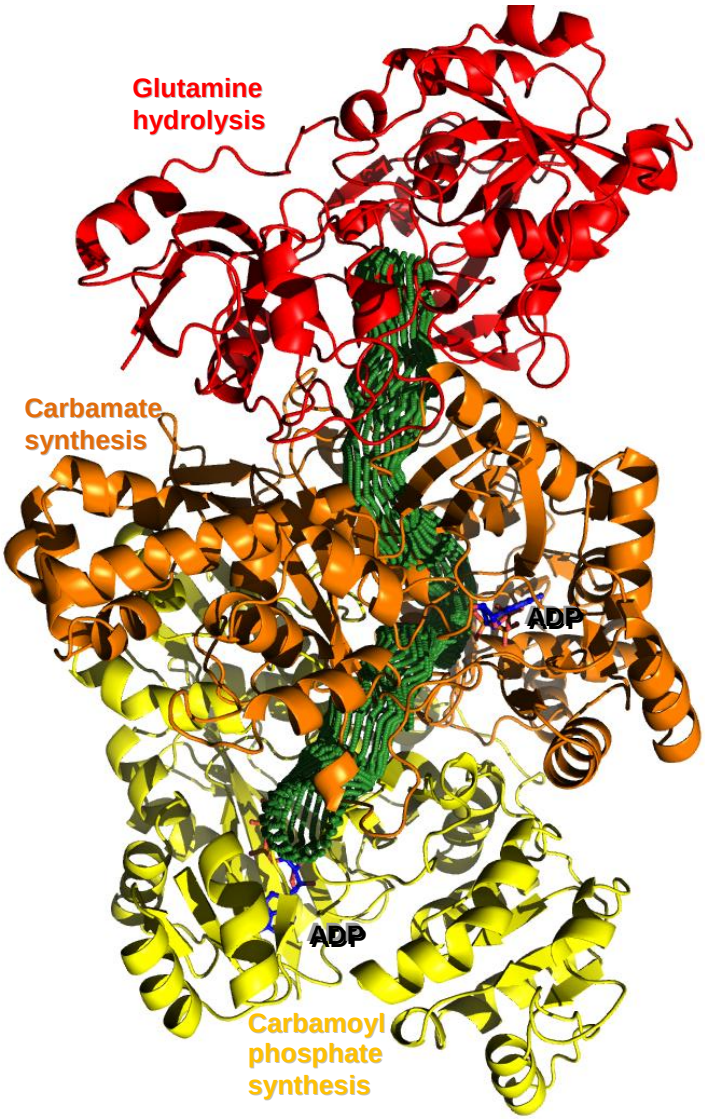

Figure 5.1. The crystallographic structure of carbamoyl phosphate synthetase. The small subunit containing the site for glutamine hydrolysis is shown in red. The large subunit is shown in orange and yellow. In orange is the N-terminal domain which is responsible for the synthesis of carboxyphosphate and carbamate. In yellow is the C-terminal domain which is responsible for the synthesis of carbamoyl phosphate. The two intramolecular tunnels for the transport of ammonia and carbamate are shown in green. The two bound ADP molecules are shown in blue. The image was constructed using the PDB file: 1BXR.

It has generally been accepted that the reaction for the synthesis of carbamoyl phosphate proceeds through carboxyphosphate and carbamate intermediates. In support of this mechanism, previous experiments have shown that CPS can catalyze bicarbonate-dependent ATPase reaction in the absence of an ammonia source as well as synthesize ATP from ADP and carbamoyl phosphate.[66] Further evidence for the presence of carboxyphosphate as a kinetically competent reaction intermediate was provided through positional isotope exchange (PIX) and chemical labeling experiments.[118-121] Evidence for the formation of carboxyphosphate was obtained by Powers and Meister by trapping this compound during the incubation of CPS with ATP and bicarbonate as a trimethyl ester with diazomethane. The presence of ^{14}C labeled formate was also observed after reducing carboxyphosphate with borohydride.[118] Those results, however, did not provide any kinetic information that can be related to the rates of the catalytic reactions. Wimmer *et al*. were able to use PIX to demonstrate that carboxyphosphate was indeed a kinetically competent reaction intermediate. Using $HC[^{18}O_3]^-$ they showed that one of the oxygens on P_i formed during the ATPase reaction came from bicarbonate. This led to the conclusion that HCO_3^- participates covalently in the reaction mechanism. In a subsequent set of PIX experiments done by Raushel and Villafranca the presence of carboxyphosphate was confirmed by monitoring the exchange of ^{18}O between βγ-bridge:β-nonbridge position in [γ-^{18}O]ATP. In addition, a rate constant, based on the exchange data, for the formation of this intermediate was determined to be 4.2 s^{-1}.[121] Since this rate constant is close to the k_{cat} for the overall reaction catalyzed by CPS, 3.6 ± 0.1 s^{-1}, it is probably the rate limiting step in the synthesis of carbamoyl phosphate.[121]

The role of carboxyphosphate in the reaction mechanism was further probed by Gibson *et al*. The interaction between carboxyphosphate and ammonia was elucidated through pH indicator assays coupled with NMR analysis. When H^+ release was monitored as a function of time for the HCO_3^- -dependent ATPase reaction the release of H^+ was linear with time without any detectable lag.[120] Moreover, the rate of proton release matched the rate of ADP formation. These results showed that carboxyphosphate does not dissociate unimolecularly to CO_2 and P_i, with CO_2 being the species that is nucleophilically attacked by ammonia. Instead, carboxyphosphate is the species that directly participates in the reaction which produces carbamate. The detection of $[^{18}O_3]PO^{2-}$ in the presence of [γ-$^{18}O_4$]ATP for the bicarbonate-dependent ATPase reaction by ^{31}P NMR coupled with the lack of a resonance corresponding to CO_2 in the ^{13}C NMR spectrum provided further evidence for the presence of carboxyphosphate as an intermediate.[120]

Carboxyphosphate has a very short half life in aqueous solutions (~70 msec) and decomposes at a rate of 10 s^{-1}.[8] This instability coupled with the fact that CPS sequesters this intermediate in the active site, makes it very difficult to directly observe the rate of its formation. Carboxyphosphate has also been proposed to be an intermediate in reactions catalyzed by the biotin enzyme family[122], *purK*-encoded N^5-carboxylaminoimidazole ribonucleotide synthetase (PurK)[123], phosphoenolpyruvate carboxylase[124], and pyruvate carboxylase.[125] This intermediate has never been detected directly for any of these enzymes.

Given the difficulty of directly detecting carboxyphosphate, in this study formate was used as a substitute for bicarbonate. The reaction of CPS with formate was predicted to yield formyl phosphate as an intermediate (**Scheme 5.2**). Formyl phosphate is more stable than carboxyphosphate ($t_{1/2}$=48 min, 20 ºC, pH 7.0)[126], and thus if released into solution should be present long enough to be observed directly. Two outcomes are possible after formyl phosphate is formed: it can be released from the active site into bulk solvent or it can react with ammonia and form formamide. Formyl phosphate has a hydrogen in place of a negatively charged oxygen on carboxyphosphate. It is possible that this chemical difference can lead to unfavorable interactions within the active site, thus enabling formyl phosphate to be released and detected in solution. However, if it remains in the active site and reacts with NH_3, from the glutaminase reaciton, it may be possible to detect formamide.

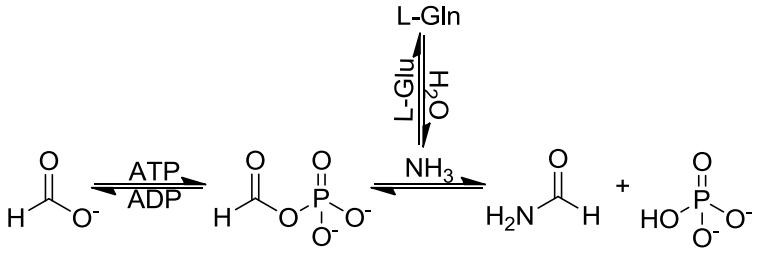

Scheme 5.2

Formyl phosphate has been detected as an intermediate in other reaction mechanisms. The *E. coli purT* encoded glycinamide ribonucleotide transformylase (GAR transformylase) has been shown to catalyze the formation of formyl glycinamide ribonucleotide (fGAR) from ATP, formate, and GAR via a formyl phosphate intermediate. This enzyme is a part of the purine biosynthetic pathway and belongs to

the ATPgrasp superfamily of proteins, of which CPS is a member of. Detection of formyl phosphate in the mechanism of this enzyme was accomplished through PIX experiments with [γ-^{18}O]ATP as well as with a site directed mutant which allowed seepage of formyl phosphate into solution.[127] Once released into bulk solvent it was possible to detect the hydroxamate derivate of this species using the trapping technique of Pechere and Capony.[128] Another enzyme proposed to have a reaction that proceeds through a formyl phosphate intermediate is N^{10}-formyltetrahydrofolate synthetase. This enzyme catalyzes the ATP-dependent formylation of tetrahydrofolate at the N^{10}-position.[66] The formyl phosphate produced in this case was also detected by trapping it in its hydroxamate form.[129]

In this study the direct detection of formyl phosphate by ^{31}P, ^{1}H, and ^{13}C NMR spectroscopies is reported. The three NMR techniques show a resonance corresponding to formyl phosphate at 2.15 ppm (^{31}P) , 162.4 ppm (^{13}C), and 7.87 and 8.27 ppm (^{1}H). The chemical shifts and the coupling constants are in good agreement with previously reported values.[126] The rate of formation of formyl phosphate was measured to be 0.025 ± 0.005 s^{-1}. Formamide was not detected in the presence of a nitrogen source.

Materials and Methods

Expression and Purification. The *Escherichia coli* strains used for this study were RC50 (*car*A50, *thi*-1, *mal*A1, *xyl*-7, *rsp*L135, *λ*r, *λ*-, and *tsx*-237) and XL1-Blue. The RC50 strain used for protein expression was a generous gift from Dr. Carol J. Lusty.

The RC50 cell line of *E. coli* was used for expression of wild-type CPS. CPS was purified as previously described.[59]

Bicarbonate Removal. Exogenous bicarbonate was removed using phosphoenolpyruvate carboxylase.[130] The reaction mixture contained 50 mM HEPES, pH 7.6, 10 mM $MgCl_2$, 4.0 mM phosphoenolpyruvate, 4.0 U phosphoenolpyruvate carboxylase (PEPC), 100 mM KCl, 10 mM ornithine, 10 mM glutamine, 30 μM wild-type CPS. The reactants were mixed in a glass vial with a rubber septum. Argon gas was used eliminate any remaining air in the head-space of the vial to prevent reintroduction of CO_2 into solutions. The reagents were incubated in a water bath at 35 ºC for 1 hour. Following the incubation, 10 mM ATP was added using a Hamilton gas-tight syringe and allowed to sit for 5 minutes. Finally, 20 mM HCO_2^- was added with a gas-tight syringe. In the reactions where 10 mM glutamine or 10 mM ornithine were present, these two components were added during the 1 hour incubation phase. When this reaction mixture was observed over time by ^{31}P NMR in the presence formate and in the absence of CPS, there was no production of formyl phosphate, ATP degradation, or phosphoenolpyruvate consumption (**Figure 5.2**). Based on these results, the bicarbonate-fixation system was considered useful for studying the glutamine-dependent ATPase activity of CPS in the presence of formate.

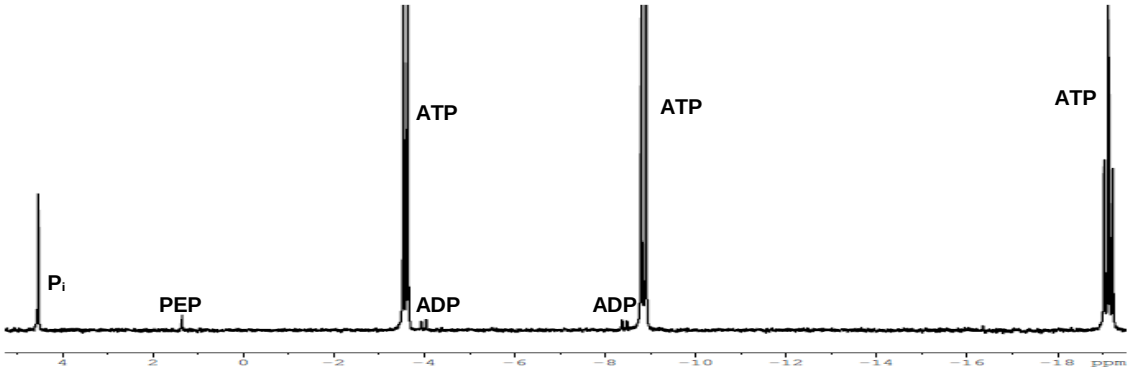

Figure 5.2. Proton decoupled ^{31}P NMR spectrum of the Gln-dependent ATPase reaction mixture in the absence of CPS. The resonance corresponding to P_i was used as a reference. Assay contains: 50 mM HEPES, pH 7.6, 100 mM KCl, 10 mM $MgCl_2$, 10 mM glutamine, 10 mM ornithine, 4 mM PEP, 4 U PEPC, 10 mM ATP, 20 mM $HC^{18}O_2^-$. Reaction was allowed to proceed for 20 min at 35 ºC after which it was quenched with 100 mM EDTA and the pH was brought up to 8.4 to increase resolution. PEP - phosphoenolpyruvate, ATP - adenosine triphosphate, ADP - adenosine diphosphate.

NMR Assays. The ATPase reactions in the presence and absence of glutamine, ornithine, bicarbonate, and formate were followed using ^{31}P, ^{13}C, and ^{1}H NMR spectroscopy. The reaction mixtures contained 50 mM HEPES, pH 7.6, 10 mM $MgCl_2$, 100 mM KCl, 4.0 mM PEP, 4.0 U PEPC, 10% D_2O, and 10 mM ATP. All reactions were initiated with the addition of 20 mM $H^{13}CO_2^-$. When the reaction was studied in the presence of an amine source the following compounds were added to the assay: 10 mM glutamine, 10 mM ornithine, 10 mM ^{15}N-glycine, 10 mM $^{15}N_\alpha$-lysine, 10 mM $^{15}N_\varepsilon$-lysine, and 10 mM $^{15}NH_4Cl$. All NMR time courses were monitored at 5 ºC in the absence of bicarbonate. All NMR tubes were sealed with a rubber septum.

Nuclear Magnetic Resonance Spectroscopy. All NMR spectra were acquired on Bruker ARX or Bruker Avance III 500 MHz spectrometers, operating at 202.5 MHz

for ^{31}P, 125.8 MHz for ^{13}C, and 500.1 MHz for ^{1}H. The ARX instrument was equipped with CH, HCN, and HBB 15 mm probes. The Avance III spectrometer was equipped with a triple resonance 5 mm cryoprobe.

^{31}P NMR. For ^{31}P NMR measurements the acquisition parameters were 6097.6 Hz sweep width, 0.6 sec acquisition time, and a 1.0 sec relaxation. Data acquisition size was 32768 and processed acquisition size was 65536 with waltz16 proton decoupling.

^{13}C NMR. ^{13}C NMR measurements were done using the following parameters: 29411 Hz sweep width, 0.6 sec acquisition time, 1.0 sec relaxation, and waltz16 proton decoupling. The data acquisition and the processed acquisition size was 32768.

^{1}H NMR. ^{1}H NMR measurements were performed using polarization transfer by a spin-echo difference method and water was suppressed by presaturation. The following acquisition parameters were used: 6009 Hz sweep width, 2.7 sec acquisition time, and a 1.0 sec relaxation. The data acquisition and the processed acquisition size was 32768.

Rate of P_i Release. The rate of P_i formation during the ATPase reaction in the presence and absence of HCO_3^- was determined using the EnzChek® Phosphate Assay Kit from Invitrogen. All of the kit components were prepared using degassed water and kept in airtight vials. All measurements using bicarbonate-free solutions were done in cuvettes covered with a rubber septum and purged with a gas. $MgCl_2$, HEPES, and KCl solutions were boiled and purged with a gas to remove bicarbonate. The ATP and formate solutions were made using degassed HEPES buffer and degassed water, respectively. The assay mixtures contained 50 mM HEPES, pH 7.6, 10 mM $MgCl_2$, and

100 mM KCl. ATP was varied for the reactions in which the rate of ATP hydrolysis was measured. Formate was varied in the reactions in which the rate of formate-dependent ATPase reaction was measured.

Results

NMR Studies. Historically, an hydoxamate trapping technique has been used to trap and detect acylated phosphates.[128] This method converts an acyl phosphate into its corresponding hydroxamate with the use of hydroxyl amine and $FeCl_3$. Formyl phosphate is not very stable at room temperature and physiological pH.[131] Moreover, CPS produces formyl phosphate in very small quantities that degrade quickly and are below the detection limit of the hydroxamate trapping assay. A more sensitive technique, such as NMR spectroscopy, was employed to elucidate the details of the reaction of CPS with formate. The ATPase partial reaction, in the presence and absence of glutamine and ornithine, was used to study formation of formyl phosphate by CPS. This reaction was monitored by ^{31}P, ^{13}C, and ^{1}H NMR. Different combinations of NMR spectroscopies and isotopically-labeled formate were employed to reveal the details of this reaction. Since this reaction intermediate is unstable at neutral pH at room temperature, all of the NMR measurements were taken at 5 ºC.

^{31}P NMR. Formation of formyl phosphate was studied by ^{31}P NMR spectroscopy. Previous studies have shown that formyl phosphate is able to formylate primary amines with 100% efficiency.[132] Thus, in order to prevent nonhydrolytic cleavage of formyl phosphate, glutamine and ornithine were excluded from the reaction.

Data collection began immediately after addition of formate to the reaction mixture. The reaction was observed for 1 day by continuously taking 2 hour scans of the sample. A resonance corresponding to formyl phosphate at 2.15 ppm (J_{CP} = 2-3 Hz) appeared in the spectrum after 4 hours (**Figure 5.3**). The chemical shift is consistent with previously reported data.[126] The amount of formyl phosphate produced increased in size for the first 8 hours, after which no net increase in the amount of formyl phosphate was observed. In the control experiment, in which formate was excluded from the reaction mixture, no peak in the region of 2.15 ppm was observed (data not shown).

In most of the ^{31}P NMR spectra, the amount of PEP present at the beginning of the ATPase reaction was always less than expected. Typically about 50% of the PEP added for the bicarbonate-fixation step was depleted. The amount of exogenous bicarbonate present in the assay solutions was quantitated using the PEPC/MDH coupled assay. The initial concentration of bicarbonate in the assay was determined to be approximately 0.21 ± 0.03 mM, which was lower than the amount of PEP being utilized. Using a PEPC/LDH coupled assay it was determined that excess PEP was being hydrolyzed by PEPC after all of the bicarbonate was depleted (data not shown). During the course of the regular PEPC-catalyzed reaction, pyruvate is not one of the products formed. However, when bicarbonate is absent, this enzyme is able to use water as a substitute to produce pyruvate and phosphate (**Scheme 5.3**). Formation of pyruvate was followed spectrophotometrically using LDH and NADH.

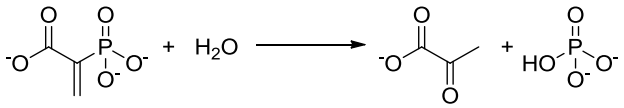

Scheme 5.3

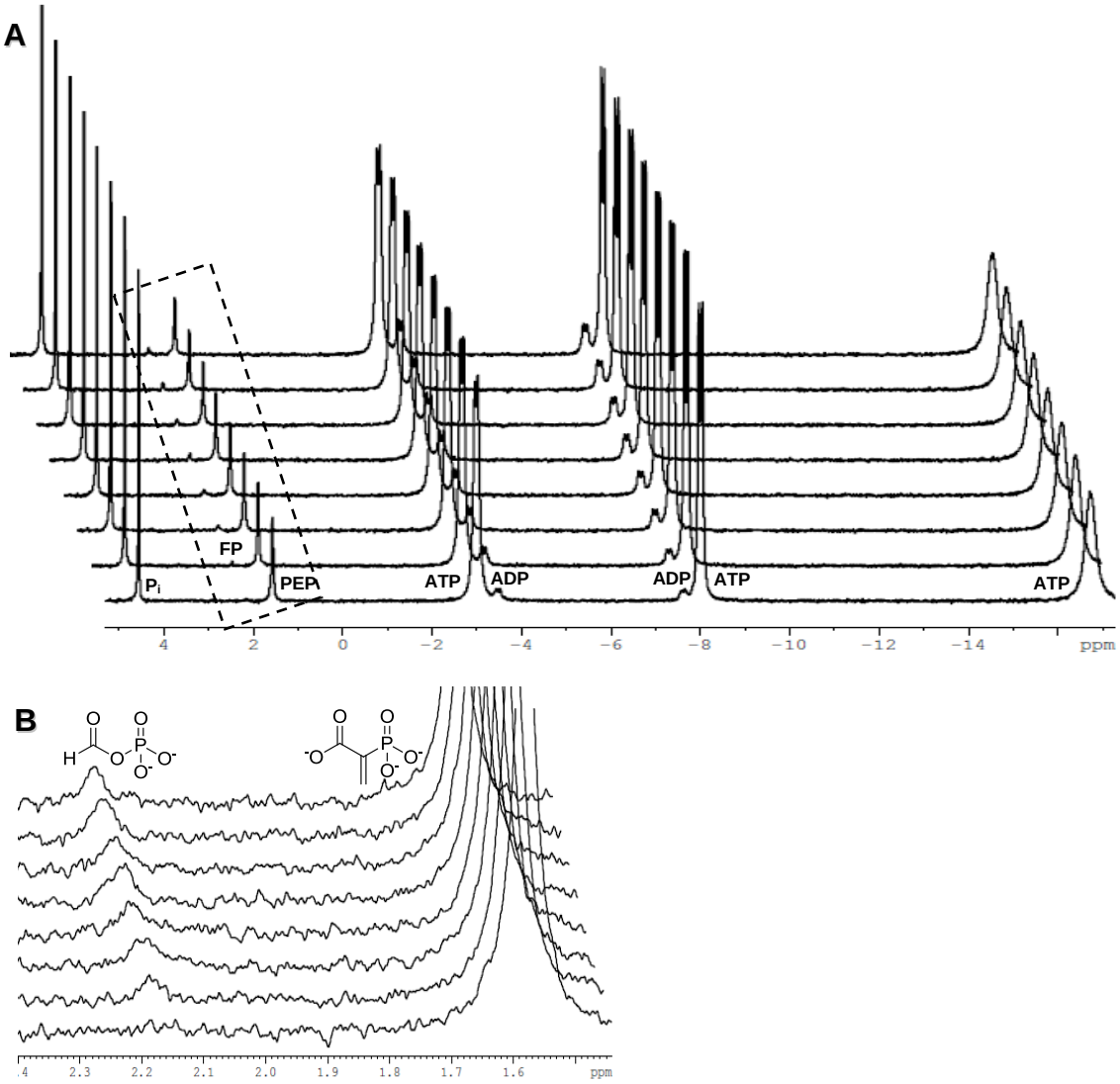

Figure 5.3. Proton decoupled ^{31}P NMR spectrum of the ATPase reaction time course. **A**) Two hour scans are shown. The resonance corresponding to P_i was used as a reference for all spectra. Assay contains: 50 mM HEPES, pH 7.6, 100 mM KCl, 10 mM $MgCl_2$, 4.0 mM PEP, 4.0 U PEPC, 10 mM ATP, 20 mM $H^{13}CO_2^-$. The reaction was mixed and immediately placed inside the NMR at 5 ºC. **B**) Zoomed in part of the spectrum showing formation of formyl phosphate. FP - formyl phosphate, PEP - phosphoenolpyruvate, ATP - adenosine triphosphate, ADP - adenosine diphophate.

^{13}C NMR. Formation of formyl phosphate over time was also observed using ^{13}C NMR using ^{13}C-labeled formate. In the initial reaction, both ornithine and glutamine were included in the assay mixture. The resulting spectrum contained a singlet resonance at 162.4 ppm ($J_{CP} = 3.0$ Hz) which increased in intensity for the first 6 hours (**Figure 5.4A, a**). This signal was identified as the ^{13}C of the formyl phosphate. The maximum amount of formyl phosphate observed under these conditions was 0.037 mM based on the ^{13}C resonance HEPES at 45.6 ppm as the reference. The amount of formyl phosphate produced after 6 hours began to decrease. A new signal, at 163.1 ppm, appeared in the spectrum after 4 hours and grew in intensity as the formyl phosphate signal strength decreased. The position of this resonance in the spectrum corresponded closely to a formyl amine. The only two sources of primary amines in the assay were ornithine and glutamine. When glutamine and ornithine were excluded from the assay, no signal at 163.1 ppm was observed (**Figure 5.4B**). Also, the amount of formyl phosphate produced in this case was nearly double the amount produced in the presence of an amine source (**Figure 5.4b, Table 5.1**).

Figure 5.4. Proton decoupled ^{13}C NMR spectra of the ATPase reaction time courses. The resonance from $H^{13}CO_2^-$ was used as a reference for all spectra. All reactions were mixed and immediately placed inside the NMR instrument at 5 ºC. The resonance corresponding to ^{13}C of formyl phosphate is shown at 162.4 ppm in the NMR spectra. The formylated primary amine species can be seen immediately down-field from the formyl phosphate signal. **A**) ATPase reaction in the presence of ornithine and glutamine. One hour scans are shown. Assay: 50 mM HEPES, pH 7.6, 100 mM KCl, 10 mM $MgCl_2$, 4 mM PEP, 4 U PEPC, 10 mM ATP, 10 mM glutamine, 10 mM ornithine, 20 mM $H^{13}CO_2^-$. **B**) ATPase reaction in the absence of an amine source. One hour scans are shown. Assay: 50 mM HEPES, pH 7.6, 100 mM KCl, 10 mM $MgCl_2$, 4 mM PEP, 4 U PEPC, 10 mM ATP, 20 mM $H^{13}CO_2^-$. **C**) ATPase reaction in the presence of NH_4Cl. One hour scans are shown. Assay: 50 mM HEPES, pH 7.6, 100 mM KCl, 10 mM $MgCl_2$, 4 mM PEP, 4 U PEPC, 10 mM ATP, 10 mM NH_4Cl, 20 mM $H^{13}CO_2^-$. **D**) ATPase reaction in the presence of $^{15}N_\alpha$-lysine. One hour scans are shown. Assay: 50 mM HEPES, pH 7.6, 100 mM KCl, 10 mM $MgCl_2$, 4 mM PEP, 4 U PEPC, 10 mM ATP, 10 mM $^{15}N_\alpha$-lysine, 20 mM $H^{13}CO_2^-$. **E**) ATPase reaction in the presence of $^{15}N_\varepsilon$-lysine. One hour scans are shown. Assay: 50 mM HEPES, pH 7.6, 100 mM KCl, 10 mM $MgCl_2$, 4 mM PEP, 4 U PEPC, 10 mM ATP, 10 mM $^{15}N_\varepsilon$-lysine, 20 mM $H^{13}CO_2$-. The corresponding plots show the change in concentrations of formyl phosphate (•) as well as formyl-ornithine (**a**), formamide (**c**), N_ε-formyl-lysine (**d**), and $^{15}N_\varepsilon$-formyl-lysine (**e**) (°).

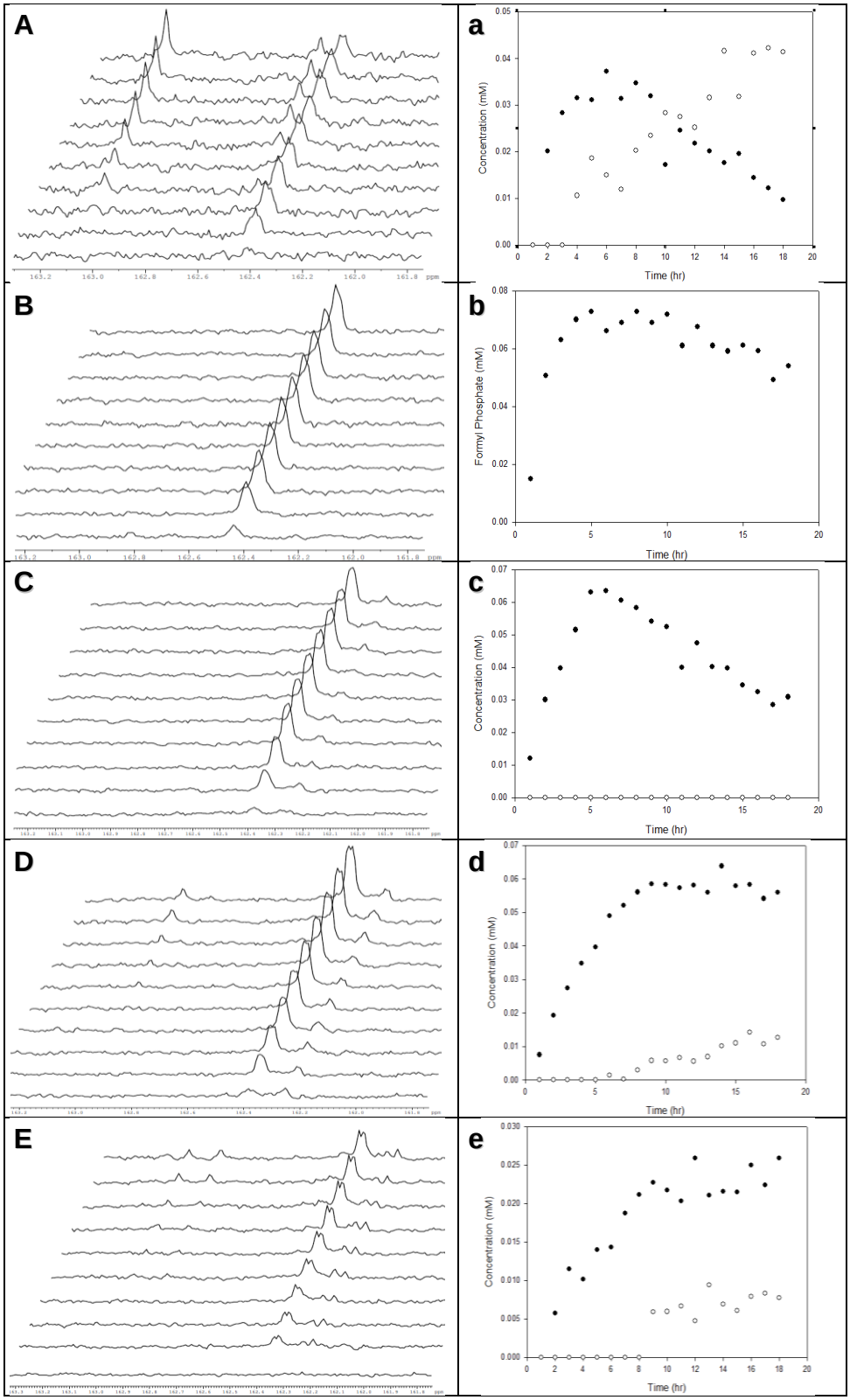
A
a
Concentration (mM)
Time (hr)
B
b
Formyl Phosphate (mM)
Time (hr)
C
c
Concentration (mM)
Time (hr)
D
d
Concentration (mM)
Time (hr)
E
e
Concentration (mM)
Time (hr)

Table 5.1. Concentrations of Formyl Phosphate and Various Formylated Amines as Observed by ^{13}C NMR.

Time (hr)	Full Assay		No amines	+ $^{15}NH_4Cl$	+ $^{15}N_\alpha$-lysine		+ $^{15}N_\varepsilon$-lysine	
	mM formyl phosphate	mM N_δ-formyl ornithine	mM formyl phosphate	mM formyl phosphate	mM formyl phosphate	mM N_ε-formyl lysine	mM formyl phosphate	mM $^{15}N_\varepsilon$-formyl lysine
1	0.00	0.00	0.015	0.0121	0.0075	0.00	0.00	0.00
2	0.020	0.00	0.051	0.030	0.019	0.00	0.0058	0.00
3	0.028	0.00	0.063	0.040	0.027	0.00	0.012	0.00
4	0.032	0.011	0.070	0.052	0.035	0.00	0.010	0.00
5	0.031	0.019	0.073	0.063	0.040	0.00	0.014	0.00
6	0.037	0.015	0.066	0.064	0.049	0.0014	0.014	0.00
7	0.031	0.012	0.069	0.061	0.052	0.00022	0.019	0.00
8	0.035	0.020	0.073	0.058	0.056	0.0029	0.021	0.00
9	0.032	0.023	0.069	0.054	0.059	0.0057	0.023	0.0059
10	0.017	0.028	0.072	0.053	0.058	0.0056	0.022	0.0060
11	0.025	0.028	0.061	0.040	0.057	0.0067	0.020	0.0067
12	0.022	0.025	0.068	0.048	0.058	0.0056	0.026	0.0048
13	0.020	0.032	0.061	0.040	0.056	0.0069	0.021	0.0094
14	0.018	0.042	0.059	0.040	0.064	0.010	0.022	0.0069
15	0.020	0.032	0.061	0.035	0.058	0.011	0.022	0.0061
16	0.014	0.041	0.059	0.033	0.058	0.014	0.025	0.0079
17	0.012	0.042	0.049	0.029	0.054	0.011	0.022	0.0083
18	0.0097	0.041	0.054	0.031	0.056	0.013	0.0259	0.0077

In order to assign identity to the resonance at 163.1 ppm, a series of experiments with various ^{15}N-labled species were performed. When the reaction was carried out in the presence of $^{15}NH_4Cl$ and no other amine sources, no signal at 163.1ppm was observed (**Figure 5.4C**). The resonance corresponding to ^{13}C of formyl phosphate was present and increased in intensity for 6 hours before beginning to diminish. The amount of formyl phosphate produced in this case was the same as the amount produced in the absence of an amine source (**Figure 5.4c, Table 5.1**). The lack of a resonance downfield from the formyl phosphate signal, in this case, ruled out the possibility that the resonance previously observed at 163.1 ppm was formamide.

It has been previously reported that formyl phosphate reacts with glycine to form formylglycine.[132] Therefore, formyl phosphate may also react with another primary amine to form an N-formyl species which resonates downfield from formyl phosphate. To test this hypothesis, ^{15}N-labled glycine was used in the absence of both ornithine and glutamine in the assay. As expected, a doublet at 163.0 and 162.8 ppm was observed with a J_{CN} = 14.9 Hz (**Figure 5.5**). Both the signal location and the coupling constant correspond well with literature values.[133] Since glycine only has a single amine group it was unclear whether formyl phosphate was reacting with the α-amino groups on glutamine and ornithine or if it was only reacting with the γ-amino group on ornithine.

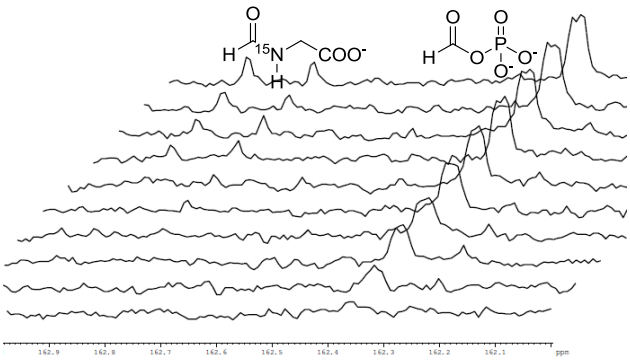

Figure 5.5. Proton decoupled ^{13}C NMR spectrum of the ATPase reaction time course in the presence of ^{15}N-gly. The resonance from $H^{13}CO_2^-$ was used as a reference for all spectra. The reaction was mixed and immediately placed inside the NMR at 5 ºC. The resonance corresponding to ^{13}C of formyl phosphate is at 162.4 ppm while the doublet corresponding to ^{15}N-formyl glycine appears at 163.0 and 162.8 ppm (J_{CN} = 14.9 Hz). One hour scans are shown. Assay: 50 mM HEPES, pH 7.6, 100 mM KCl, 10 mM $MgCl_2$, 4 mM PEP, 4 U PEPC, 10 mM ATP, 10 mM ^{15}N-gly, 20 mM $H^{13}CO_2^-$.

To determine the site and species with which formyl phosphate produced by CPS reacts, a close analog to ornithine, lysine, was used. In the absence of ornithine and glutamine, lysine labeled with ^{15}N at either the α- or ε-amino groups was used. The resulting spectra contained a peak corresponding to formyl phosphate at 162.4 ppm and a doublet directly downfield at 163.0 and 162.9 ppm (J_{CN}= 14.9 Hz) corresponding to the $^{15}N_{\varepsilon}$-formyl lysine (**Figure 5.4E**). A singlet, rather than a doublet, was observed at 162.97 ppm in the case of the $^{15}N_{\alpha}$-lysine (**Figure 5.4D**) . These data confirm that N_{α}-formyl-glutamine was not the source of the signal at 163.1 ppm. Formyl phosphate produced by CPS is released into solution where it reacts with ornithine at the γ-amino to produce a N_{γ}-formyl-ornithine which is the source of the signal at 163.1 ppm.

Kinetic Analysis of the NMR Data. The resulting data from ^{13}C NMR experiments was analyzed according to the models outlined in **Schemes 5.4** and **5.5**. In

the presence of a primary amine source the data was modeled according to **Scheme 5.4**, and in the absence of one **Scheme 5.5** was used. In the presence of amine source the formyl phosphate synthesized by CPS went on to react with a primary amine or hydrolyzed. Since for all cases studied the amount of formyl phosphate formed stopped increasing after 5-6 hours, it was necessary to add an enzyme inactivation step to the model. It may be possible that the inactivation of CPS occurs by formyl phosphate reacting with an arginine or a lysine residue in the active site where it is formed. In the absence of a primary amine formyl phosphate decayed by hydrolytic means only (**Scheme 5.5**).

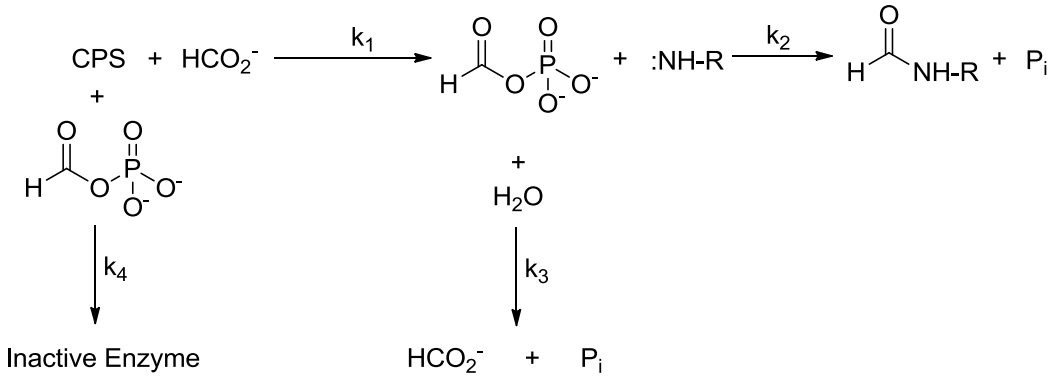

Scheme 5.4

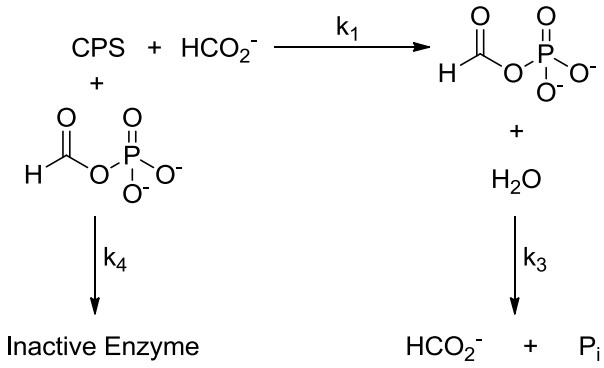

Scheme 5.5

The data from ^{13}C NMR spectra in the presence and absence of ornithine (**Figure 5.4a, b**) were analyzed globally to obtain a single set of kinetic parameters for each step in the reaction pathway. The traces showing changes in concentrations of products over time required a 4 and 3 parameter fits for the samples containing ornithine and ones without, respectively. The data were modeled with a mechanism that contained four irreversible steps. The resulting values are shown in **Table 5.2**. The enzymatic production of formyl phosphate was fit by a 0-order rate constant k_1=3.3x10^{-5} mM/s. The chemical reaction between formyl phosphate and ornithine occurred by a pseudo first order process with a rate constant k_2=3.1x10^{-5} s^{-1}. Non-enzymatic hydrolysis of formyl phosphate to formate and phosphate was fit to a first order process with k_3=6.7x10^{-5} s^{-1}. The fourth step in the model, which represented the deactivation of CPS by formyl phosphate, was a second order rate process with the kinetic constant k_4=1.4x10^{-4} mM^{-1} s^{-1}. The kinetic constants show that the reaction between CPS and formate is catalyzed at a slower rate than the inactivation reaction between CPS and formyl phosphate. The conversion of formyl phosphate to a formyl-ornithine occurs at approximately the same rate as the formation of this product.

Table 5.2. Rate Constants from Global Analysis of the ATPase Reaction in the Presence and Absence of Ornithine

Kinetic Paramter[a]	Value	Confidence Interval[b]
k_1, $mM \cdot s^{-1}$	3.3×10^{-5}	$(2.8\text{-}4.9) \times 10^{-5}$
k_2, s^{-1}	3.1×10^{-5}	$(2.5\text{-}3.5) \times 10^{-5}$
k_3, s^{-1}	6.7×10^{-5}	$(2.6\text{-}13) \times 10^{-5}$
k_4, $mM^{-1}\ s^{-1}$	1.4×10^{-4}	$(7.2 - 33) \times 10^{-5}$

[a]See **Schemes 5.4** and **5.5**. [b]Confidence intervals calculated using FitSpace option in KinTek Explorer [134-135]

^{1}H NMR. Formation of formyl phosphate was also studied by ^{1}H NMR. This technique provided additional evidence for the presence of formyl phosphate in the reaction solution. Since the signal corresponding to the proton on formyl phosphate appears directly underneath a peak originating from one of the protons on the purine ring of ATP, a subtraction technique was used to remove it. Polarization transfer was done by a spin-echo difference method. Water was suppressed by presaturation and globally optimized alternating phase rectangular pulse (GARP). This method allowed the observation of only the protons that were associated with ^{13}C while suppressing all other signals. The only species containing ^{13}C in the reaction was formate, therefore the only peaks observed in the spectrum would arise from the reaction with this molecule (**Figure 5.6**).

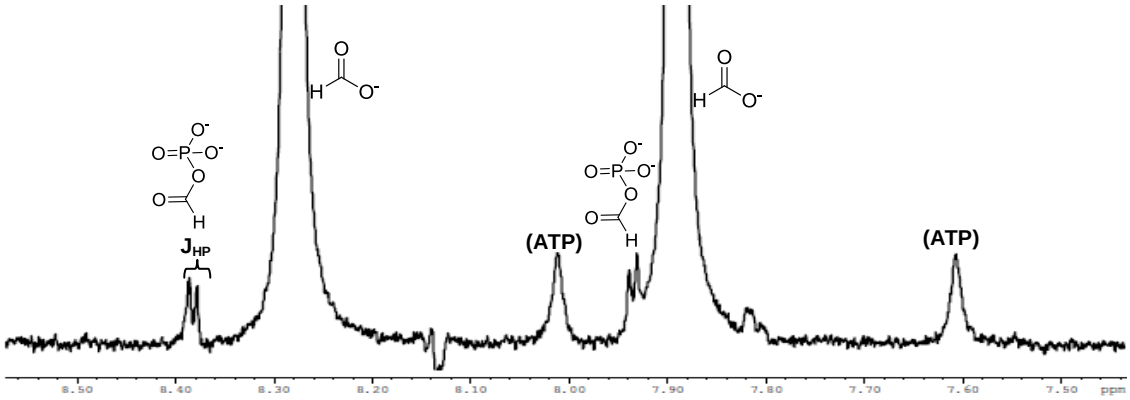

Figure 5.6. ^{1}H coupled NMR spectrum of the ATPase reaction. Only protons associated with ^{13}C are shown. Water signal was suppressed using Watergate. Formate signal is observed at 7.87 and 8.27 ppm. Formyl phosphate signal is observed at 7.94 and 8.39 ppm. The peaks at 7.61 and 8.03 ppm originate from 1% of ^{13}C ATP.

The major doublet in the spectrum at 8.27 and 7.87 ppm corresponds to ^{1}H on ^{13}C formate. The small doublet of doublets immediately downfield from it, at 8.39 and 7.94 ppm, corresponds to ^{1}H of ^{13}C-formyl phosphate. The coupling constants J_{HP} and J_{HC} are 4.0 Hz and 223.0 Hz, respectively. The peaks originating from formyl phosphate were not present in the starting material for the reaction. They also do not appear when CPS or formate is excluded from the reaction (data not shown). Both the chemical shifts and the coupling constants are in good agreement with the literature.[126] The other resonances in the spectrum, at 7.61 and 8.03 ppm correspond to the protons on the adenine ring of the ATP that are associated with the 1% of the naturally abundant ^{13}C.

Kinetic Studies. The rate of formyl phosphate formation was followed by monitoring the release of inorganic phosphate with a purine nucleoside phosphorylase (PNPase) coupled assay. The rate of the ATPase reaction with exogenous amounts of bicarbonate was determined (**Table 5.3**). Since HCO_3^- was not saturating, the k_{cat} is an

order of magnitude lower than when the assay contained saturating concentrations of bicarbonate. The rate of enzymatic rate of ATP hydrolysis was also determined in the absence of HCO_3^-, glutamine, and ornithine (**Figure 5.7**). This rate is 1.5 times slower than the same reaction in the presence of bicarbonate (**Table 5.3**). The K_M (ATP) for this reaction is three times higher than in the presence of bicarbonate. However, this K_M (ATP) value is comparable to the K_M (ATP) in the presence of saturating bicarbonate and glutamine.

Table 5.3. ATPase Partial Reaction Monitored by Release of P_i.

Reaction Conditions	k_{cat} **(s^{-1})**	K_M **(mM ATP)**
+ 40 mM HCO_3^-, 10 mM gln, 10 mM ornithine	3.60 ± 0.11[a]	0.24 ± 0.04[a]
+ 10 mM ornithine, 40 mM HCO_3^-	0.170 ± 0.003[a]	0.051 ± 0.008[a]
+ Exogenous HCO_3^-[b]	0.037 ± 0.002	0.092 ± 0.02
H_2O only[c]	0.024 ± 0.002	0.29 ± 0.07
+ 20 mM HCO_2^-[d]	0.029 ± 0.002	0.17 ± 0.04
HCO_2^-- dependent ATPase[e]	0.025 ± 0.005[f]	50.0 ± 20 (mM HCO_2^-)

Each reaction mixture contained 50 mM HEPES, pH 7.6, 10 mM $MgCl_2$, 100 mM KCl

[a] Kinetic constants were determined by following ADP production with an LDH/PK coupled assay.

[b] Solutions were not degassed.

[c] All solutions were degassed.

[d] All solutions were degassed, 20 mM HCO_2^- was added. ATP was varied.

[e] All solutions were degassed, 1 mM ATP. HCO_2^- was varied.

[f] Rate corrected for hydrolysis in the absence of formate and bicarbonate.

When 20 mM formate was added to the reaction mixture in the absence of bicarbonate and with varying ATP concentrations, the reaction rate remained largely unchanged (**Table 5.3**). The value for K_M (ATP), however, decreased slightly. The rate for this reaction is the apparent rate. It was not possible to determine whether or not formate displaced water in the active site 100% of the time. Thus, the rate is a combination of the hydrolysis and formate-dependent ATPase reactions. When ATP was held constant and formate was varied it was possible to determine the apparent rate of formyl phosphate formation (**Figure 5.7**). The rate determined for this reaction was corrected for the enzyme-catalyzed hydrolysis of ATP in the absence of bicarbonate by subtracting this rate from the formate-dependent ATPase reaction (**Table 5.3**). The apparent rate for the synthesis of formyl phosphate is 0.025 ± 0.005 s^{-1}, which is 6.5 times slower than when saturating amounts of bicarbonate are present. Since water is at a saturating concentration the fact that higher concentrations of formate are able to enhance the rate of this reaction indicates that formate is a better substrate than water (**Figure 5.7**). Even though formate is preferred by CPS over water the K_M for formate is very high, which supports that it is not the a good substrate overall. However, CPS is able to utilize it in the same manner as bicarbonate at a measurable rate.

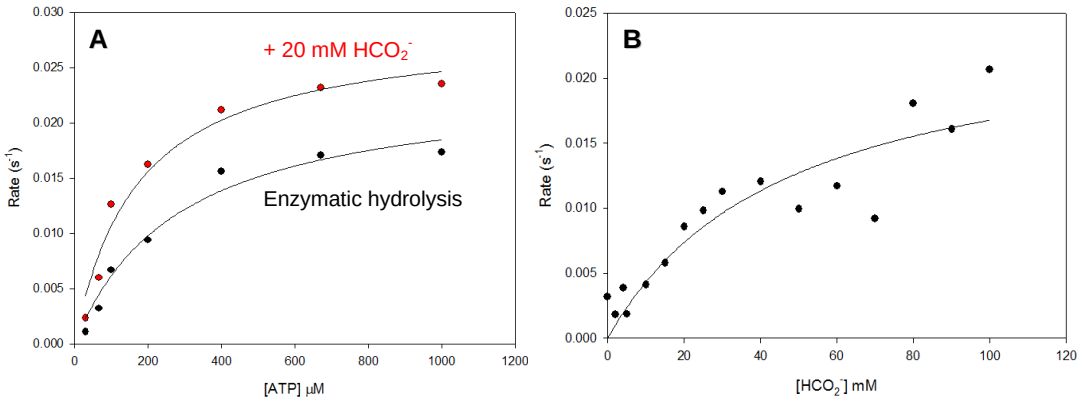

Figure 5.7. ATPase reaction catalyzed by CPS in the presence and absence of formate. **A**) Enzymatic hydrolysis of ATP in the absence of formate, bicarbonate, ornithine, and glutamine (•). Enzymatic hydrolysis of ATP in the presence of 20 mM HCO_2^- (•). **B**) Formate-dependent ATPase. ATP was kept constant while the concentration of formate was varied.

Discussion

Carboxyphosphate, a proposed intermediate in the synthesis of carbamoyl phosphate, has been a difficult intermediate to observe directly. It is rapidly hydrolyzed when it is released into solution, which is why it is sequestered within the active site during the course of the reaction. Previous efforts, including positional isotope exchange (PIX) and $NaBH_4$-trapping have provided evidence for this reaction intermediate.[118-119,136] However, all of the techniques employed thus far have looked at either a modified intermediate or indirect evidence pointing to the presence of carboxyphosphate. In this work we have shown that formyl phosphate, an intermediate in the CPS-catalyzed reaction between formate and ATP, can be detected directly. Formyl phosphate is analogous to carboxyphosphate in the steps leading up to the

synthesis of carbamoyl phosphate. The only difference being that it cannot go on to participate in the final phosphorylation step of the reaction mechanism (**Scheme 5.2**).

Formyl phosphate was detected using ^{31}P, ^{13}C, and ^{1}H NMR spectroscopies in the absence and presence of an amine source. In all cases a low intensity resonance corresponding to formyl phosphate appeared in the spectrum after one to two hours at 5 ºC. The coupling constants observed for this species, J_{CP} = 2-3 Hz and J_{HP} = 4.0 Hz, are in good agreement with the data reported in the literature.[126] The amount of formyl phosphate produced showed a steady increase in the first 5-6 hours of the reaction, however, the steady increase in production of formyl phosphate leveled off and began to decrease as the reaction progressed. This decrease in the amount of intermediate formed was accelerated in the presence of molecules containing a reactive primary amine, such as ornithine, glycine, and lysine. Since formamide was not detected under any conditions used in this study, it lead us to conclude that formyl phosphate is rapidly released from the active site into bulk solvent. The release of formyl phosphate from the active site must occur at a rate that is faster than the migration of ammonia from the glutaminase active site. It has been shown that the transport of ammonia from the site of its formation to the carboxyphosphate active site in approximately 100 μs at 300 K.[137] This means that the release of formyl phosphate from the active site must occur even faster than that.

Based on modeling of the kinetic data obtained by ^{13}C NMR spectroscopy it was possible to estimate the rates of various reaction steps involving formate and its products. It was shown that the ATPase reaction involving formate, instead of

bicarbonate, occurs at a similar rate regardless of the presence or absence of an amine source. Since the amount of primary amine added to the assay was much greater than the amount of formyl phosphate produced, the reaction between formyl phosphate and the amine was a pseudo first order reaction. The data also indicate that CPS becomes inactivated during the course of the reaction because there no net increase in the amount of formyl phosphate is observed after 5-6 hours. This inactivation step may be due to formyl phosphate reacting with a lysine or an arginine residue in the active site, thus rendering the enzyme dead.

Despite the fact that formate is not a good substrate for CPS, the enzyme can utilize it slowly to synthesize formyl phosphate. The apparent rate of formation of this intermediate is very close to the rate of enzymatic hydrolysis of ATP. The presence of formate does not significantly alter the K_M for ATP, which indicates that it does not interfere with the binding geometry of this molecule. Moreover, the increase in the rate of formate-dependent ATPase reaction with increasing concentrations of formate indicates that formate is preferred over water.

Formamide was not detected by NMR under any conditions used in this study. Formamide was not observed when $^{15}NH_4Cl$ was added to the assay. This may be due to the pKa of NH_4^+ being ~10.5 and the pH of the assay being 7.4. It may be possible that the ammonium ion was not in the preferred protonation state for the reaction with formyl phosphate. The fact that no formamide was observed in the presence of glutamine leads us to hypothesize that formyl phosphate is expelled from the active site faster than ammonia can travel through to tunnel to react with it.

Even though formyl phosphate is produced slowly and in small amounts it has been observed by both direct and indirect techniques. In order for this intermediate to form, the reaction at the carboxyphosphate active site must proceed by the same mechanism as in the presence of bicarbonate. This intermediate is only seen in the presence of CPS, ATP, and formate. The fact that it is not seen in the absence of formate or CPS confirms that it is an enzymatically produced species. Detection of formyl phosphate in the reaction catalyzed by CPS between formate and ATP confirms the presence of carboxyphosphate in the reaction catalyzed by CPS between bicarbonate and ATP.

CHAPTER VI

CONCLUSION

Carbamoyl phosphate synthetase from *E. coli* is a fascinating enzyme. It has intrigued researchers for decades with both the intricacy of its structure and the complexity of its reaction mechanism. Since the first crystal structure of CPS was solved in 1997, the conformation of the two B-domains located on the carboxyphosphate and the carbamoyl phosphate active sites has been of interest. The mechanism by which these domains close and open has not been completely elucidated, but great strides have been made in being able to develop a model for this. In a crystal structure solved by Thoden in the presence of the nonhydrolysable ATP analog AMPPNP both of the B-subdomains were found in the closed conformation. These findings are in line with the fact that both active sites must remain closed to bulk solvent in order to protect unstable intermediates. A different crystal structure solved in the presence of ADP and P_i revealed an open conformation at the carbamoyl phosphate active site and a bound molecule of ADP there. However, the N-terminal active site remained closed with both ADP and P_i bound. In all of the crystal structures of CPS solved to date, the N-terminal B-domain remains in the closed conformation.

We determined possible ways of studying the motions of both the N- and C-terminal B-domains. Fluorescence anisotropy is a sensitive technique that is able to report on the changes in the immediate environment of the fluorescent probe by measuring depolarization of its fluorescence emission. In order to employ this technique

it was necessary to introduce fluorescent reporters to CPS at appropriate sites on the mobile B-domains. The use of engineered tryptophans in a tryptophan-less CPS construct was not possible in our hands due to low expression levels and very poor solubility of the mutants. After a thorough examination of the solvent accessible cysteine residues, the most solvent exposed Cys-551 was mutated to an alanine, and two cysteines were engineered at positions 171 and 717 in the large subunit.

The anisotropy measurements made on the C551A/S171C and C551A/S717C mutants provided some insight into a possible mechanism of synchronization of the opening and closing of the N- and C-terminal B-domains. It was found that in the absence of all ligands the protein environment around both fluorophores was more rigid than in their presence. Upon addition of ornithine and K^+ to the reaction mixture the anisotropy of both mutants decreased. Based on crystallographic data, K^+ binds to regions of the protein near the carboxyphosphate and carbamoyl phosphate active sites termed the "K-loops" (**Figure 2.1**). Potassium ions do not have a role in catalysis, but rather help support the structure of the active sites. It has been previously reported that there is a requirement for potassium ions for the proper function of CPS. [66] The anisotropy data suggests that once potassium ions are bound that they alter the active site environment. It may be possible that the binding of K^+ makes the active site environment more conducive to ATP binding.

The biggest anisotropy change observed at the N-terminal domain was in the presence of AMPPNP and ATP. Even though these ligands were added at the same time as various other molecules, it was these two substrates that were responsible for the

change in the rotational response of the fluorophore at S171C. This is evident from no change in anisotropy being observed when P_i, Mg^{2+}, and glutamine were individually tested in the reaction mixture with CPS in the presence of ornithine and K^+ (**Figure 2.5**). From the X-ray crystallography data these domain adopts a closed conformation in the presence of AMPPNP. The change in anisotropy in the presence of this compound can be indicative of a conformational change that brings the domain from the open conformation to the closed. The presence and absence of ADP in the presence of ornithine and K^+ had no effect on either active site. The C-terminal B-domain remained unaffected in the presence of all ligands tested in this study.

While the anisotropy experiments were not conclusive, they provide a better insight into a possible connection between the N- and C-terminal active sites on the large subunit. Further experimentation is necessary to provide a clear picture of this relationship. A possible way of understanding these events is by using an in *trans* construct of CPS. It has been shown to be a kinetically competent species that presents many possibilities for manipulation.

The MD simulations demonstrate the functional existence of a molecular tunnel that traverses two non-covalently joined subunits in CPS. This tunnel serves as a means to transport ammonia from the site of its formation in the small subunit to the site of its utilization in the large subunit. The transfer of ammonia between the two active sites is spontaneous. The highest energy barrier in the small subunit is ~5.5 kcal/mol, which is due to the requirement for desolvation of NH_3 prior to entering the intersubunit space. The highest energy barrier in the large subunit is 7.2 kcal/mol and is also caused by the

need for ammonia to desolvate before passing through the narrow turning gate C232-A251-A314.

In the small subunit His-353, Ser-47, and Lys-202 function cooperatively by forming and breaking hydrogen bonds with ammonia in order to efficiently deliver it into the tunnel. Once inside the tunnel ammonia moves stepwise by forming and breaking hydrogen bonds with the backbone carbonyl groups of Gly-292, Pro-358 and Gly-293, and the side chains of Ser-35 and Thr-37. There is also a functional requirement for His-353 and Ser-35. The conformation of these side chains is what enables the delivery of NH_3 into the large water pocket between the small and large subunit. In this part of the trajectory the solvation energy is what drives the ammonia forward though the tunnel.

Most of the residues identified in the MD simulations as being important for function in the translocation of ammonia have been mutated and the effects on the kinetic constants for CPS have been determined. The most important of these residues appear to be Cys-269, His-353, and Ser-47. The mutation of Cys-269 to either serine or alanine results in a protein that is unable to hydrolyze glutamine.[20] However, the C269S mutant is able to bind glutamine and stimulate the hydrolysis of ATP in the large subunit.[20] The mutation of His-353 also results in a protein that is unable to hydrolyze glutamine.[57] However, an X-ray structure of the H353N mutant in the presence of glutamine showed that the thioester intermediate could form but not be hydrolyzed.[31] Thus, this residue seems to be more important for the hydrolysis of the thioester intermediate than for the formation. The hydroxyl group of Ser-47 functions as part of

the oxyanion hole during the formation and hydrolysis of the thioester intermediate. Mutation of this residue to alanine results in a protein that is unable to hydrolyze glutamine in the absence of ATP and HCO_3^-.[27] However, in the presence of ATP and HCO_3^-, the Michaelis constant for the glutamine is elevated by a factor of >10 but k_{cat} is largely unaffected.[27]

Perturbations to the kinetic constants have also been observed for mutations to Lys-202 and Glu-355.[27] When Lys-202 is mutated to methionine the k_{cat} values are unchanged but the K_M value for glutamine is elevated by a factor of ~10. When Glu-355 is mutated to alanine there is no change in k_{cat} but a significant increase in the K_M for glutamine.[27] However, when this residue is mutated to glutamine there is no detectable hydrolysis of glutamine and no carbamoyl phosphate formation.[27]

Once in the large subunit, ammonia has only one energy barrier to overcome. The magnitude of the energy barrier is 7.2 kcal/mol at the narrow turning gate formed by Cys-232, Ala-251, and Ala-314. Migration of ammonia in this part of the tunnel starts with a large drop in free energy once ammonia is injected into a large water pocket between Thr-37 and Tyr-291. From there ammonia travels through another water pocket and squeezes through the narrow turning gate by shedding all of its accompanying water molecules. The interaction between ammonia and Thr-249 is responsible for the delivery of NH_3 through this narrow gate.

The computational data suggest that the migration of ammonia through the C232-A251-A314 gate is the rate-limiting step in the transport process. A triple mutant C232V/A251V/A314V was designed to block the passage of ammonia through this

portion of the tunnel. The rate of ATP hydrolysis was decreased by a factor of 180 and there was no carbamoyl phosphate synthesis detected. However, the active site responsible for the final step in the synthesis of carbamoyl phosphate was fully functional as was observed by the wild-type like kinetics of the ATP-synthesis reaction. Also, the activity of the glutaminase active site was completely unaffected by this mutation.

The diffusion through the tunnel is fast, with an estimated rate constant on the order of 9.9 ms^{-1}. This rate is approximately 200 times faster than the rate constant for the overall synthesis of carbamoyl phosphate. Even though there are two energy barriers involved with the transport of ammonia to the carboxyphosphate active site, the transport of ammonia is not the rate limiting step in the reaction mechanism.

The presence of an intramolecular tunnel for the transport of carbamate has also been demonstrated by MD simulations. This tunnel appears to be tightly sealed because no leakage of carbamate at any point in this study was observed. It has been shown that the release of phosphate from the carboxyphosphate active site is critical for the opening of the carbamate tunnel. Once the phosphate is released, the side chain of Arg-306 has a small energy barrier to overcome in order to interact with the glutamate triad at the mouth of the tunnel. Once the negative charges on Glu-25, Glu-383 and Glu-604 are shielded, carbamate is free to enter to tunnel. The largely negatively charged environment of the tunnel allows carbamate to travel quickly through it.

The importance of the glutamate triad and Arg-306 was established previously by constructing R306A and E25Q/E383Q/E604Q mutants.[115] Neither of these mutants

were capable of synthesizing carbamoyl phosphate. By replacing glutamate with glutamine the negative charge is removed and so is the possibility for the interaction between Arg-306 and the glutamate triad. By removing this interaction, Arg-306 is likely unable to rotate to create an open conformation at the entrance of the carbamate tunnel, thus trapping this intermediate in the active site. In addition, all the mutants constructed for this study that disrupted the interaction between Arg-306 and the glutamate triad, M378E and M174E/M378E, significantly retarded the rate of carbamoyl phosphate synthesis. The mutants that were created to physically impede the progress of carbamate through the tunnel, A23F and G575F, were a success. The fact that each mutant retained less that 4% of its overall activity for the synthesis of carbamoyl phosphate relative to wild-type CPS confirms the presence of narrow portions of the tunnel that help to divide it into three distinct water pockets.

The side chains of Ala-23 and Gly-575 have also been previously mutated to several different residues. In an earlier study Ala-23 was mutated to a leucine and a tryptophan in order to create a blockage within the top portion of the carbamate tunnel.[39] Neither mutant showed significant deviations from the wild-type enzyme in the ATP synthesis reaction. However, the A23W had only 10% of the glutamine-dependent ATPase activity of the wild-type protein. Our data from the I18W/A23F/C24F triple mutant also confirms that bulky residues in the portion of the tunnel alter the integrity of the carboxyphosphate active site. Gly-575 was mutated to an alanine, serine, and a leucine in order to titrate the size of the C-terminal opening of the carbamate tunnel.[39] The G575L mutant was the most effective at blocking the tunnel. Our mutant G575F

confirms the requirement for a large hydrophobic residue to block the tunnel exit. The lysine side chain used in the G575K mutant may have been too flexible and allowed carbamate to pass through, as was observed in the wild-type like kinetics for the synthesis of carbamoyl phosphate.

Overall, the transport of carbamate through the ~40 Å tunnel is rapid. It takes approximately 0.6 ms for carbamate to travel from the middle water pocket to the site for carbamoyl phosphate synthesis while overcoming the largest free energy barrier observed in the whole trajectory. This speed is approximately equivalent to a rate constant of 1600 s^{-1}, which is significantly faster that the overall reaction catalyzed by CPS. Therefore, our findings indicate that the migration of carbamate from the site of its formation to the site of its utilization is not the rate limiting step in the reaction mechanism.

The reaction that takes place at the carboxyphosphate active site on the large subunit has been studied kinetically and by NMR spectroscopy. Carboxyphosphate, a proposed intermediate in the synthesis of carbamoyl phosphate, has been a difficult intermediate to observe directly. It is rapidly hydrolyzed when it is released into solution, which is why it is sequestered within the active site during the course of the reaction. Previous efforts, including positional isotope exchange (PIX) and $NaBH_4$-trapping have provided evidence for this reaction intermediate.[118-119,136] However, all of the techniques employed thus far have looked at either a modified intermediate or indirect evidence pointing to the presence of carboxyphosphate. In this work we have shown that formyl phosphate, an intermediate in the CPS-catalyzed reaction between

formate and ATP, can be detected directly. Formyl phosphate is analogous to carboxyphosphate in the steps leading up to the synthesis of carbamoyl phosphate. The only difference being that it cannot go on to participate in the final phosphorylation step of the reaction mechanism (**Scheme 5.2**).

Formyl phosphate was detected using ^{31}P, ^{13}C, and ^{1}H NMR spectroscopies in the absence and presence of an amine source. In all cases a low intensity resonance corresponding to formyl phosphate appeared in the spectrum after one to two hours at 5 ºC. The coupling constants observed for this species, J_{CP} = 2-3 Hz and J_{HP} = 4.0 Hz, are in good agreement with the data reported in the literature.[126] The amount of formyl phosphate produced showed a steady increase in the first 5-6 hours of the reaction, however, the steady increase in production of formyl phosphate leveled off and began to decrease as the reaction progressed. This decrease in the amount of intermediate formed was accelerated in the presence of molecules containing a reactive primary amine, such as ornithine, glycine, and lysine. Since formamide was not detected under any conditions used in this study it lead us to conclude that formyl phosphate is rapidly released from the active site into bulk solvent. The release of formyl phosphate from the active site must occur at a rate that is faster than the migration of ammonia from the glutaminase active site. It has been shown that the transport of ammonia from the site of its formation to the carboxyphosphate active site in approximately 100 μs at 300 K.[137] This means that the release of formyl phosphate from the active site must occur even faster than that.

Based on modeling of the kinetic data obtained by ^{13}C NMR spectroscopy it was possible to estimate the rates of various reaction steps involving formate and its products. It was shown that the ATPase reaction involving formate, instead of bicarbonate, occurs at a similar rate regardless of the presence or absence of an amine source. Since the amount of primary amine added to the assay was much greater than the amount of formyl phosphate produced, the reaction between formyl phosphate and the amine was a pseudo first order reaction. The data also indicate that CPS becomes inactivated during the course of the reaction because there no net increase in the amount of formyl phosphate is observed after 5-6 hours. This inactivation step may be due to formyl phosphate reacting with a lysine or an arginine residue in the active site, thus rendering the enzyme dead.

Despite the fact that formate is not a good substrate for CPS, the enzyme can utilize it slowly to synthesize formyl phosphate. The apparent rate of formation of this intermediate is very close to the rate of enzymatic hydrolysis of ATP. The presence of formate does not significantly alter the K_M for ATP, which indicates that it does not interfere with the binding geometry of this molecule. Moreover, the increase in the rate of formate-dependent ATPase reaction with increasing concentrations of formate indicates that formate is preferred over water.

Formamide was not detected by NMR under any conditions used in this study. Formamide was not observed when $^{15}NH_4Cl$ was added to the assay. This may be due to the pKa of NH_4^+ being ~10.5 and the pH of the assay being 7.4. It may be possible that the ammonium ion was not in the preferred protonation state for the reaction with

formyl phosphate. The fact that no formamide was observed in the presence of glutamine leads us to hypothesize that formyl phosphate is expelled from the active site faster than ammonia can travel through to tunnel to react with it.

Even though formyl phosphate is produced slowly and in small amounts it has been observed by both direct and indirect techniques. In order for this intermediate to form, the reaction at the carboxyphosphate active site must proceed by the same mechanism as in the presence of bicarbonate. This intermediate is only seen in the presence of CPS, ATP, and formate. The fact that it is not seen in the absence of formate or CPS confirms that it is an enzymatically produced species. Detection of formyl phosphate in the reaction catalyzed by CPS between formate and ATP confirms the presence of carboxyphosphate in the reaction catalyzed by CPS between bicarbonate and ATP.

Both the transport of ammonia and the transport of carbamate through the intramolecular tunnels of CPS have been elucidated. The transport of ammonia was the first instance of a molecule being able to spontaneously translocate from one active site to another without a requirement for input of external forces. I was also possible to demonstrate the same for carbamate. The presence of formyl phosphate as a reaction intermediate in a formate-dependent ATPase reaction catalyzed by CPS was also the first time that it has been shown that CPS is able to utilize formate as a substrate. The information that has been unveiled by these studies will facilitate further studies on enzymes with intramolecular tunnels. The elucidation of the reaction mechanism between CPS, ATP, and formate will also help solidify the reaction mechanism of CPS.

REFERENCES

(1) Anderson, P. M. *Biochemistry* **1977**, *16*, 587-593.

(2) Anderson, P. M.; Meister, A. *Biochemistry* **1966**, *5*, 3164-3169.

(3) Pierard, A.; Wiame, J. M. *Biochemical and biophysical research communications* **1964**, *15*, 76-81.

(4) Anderson, P. M., Meister, A. *Biochemistry* **1965**, *4*, 2803-2809.

(5) Raushel, F. M.; Anderson, P. M.; Villafranca, J. J. *Biochemistry* **1978**, *17*, 5587-5591.

(6) Raushel, F. M.; Villafranca, J. J. *Biochemistry* **1979**, *18*, 3424-3429.

(7) Raushel, F. M.; Mullins, L. S.; Gibson, G. E. *Biochemistry* **1998**, *37*, 10272-10278.

(8) Sauers, C. K., Jencks, W. P., Groh, S. *Journal of the American Chemical Society* **1975**, *97*, 5546-5553.

(9) Wang, T. T.; Bishop, S. H.; Himoe, A. *J Biol Chem* **1972**, *247*, 4437-4440.

(10) Jones, M. E. *Annu Rev Biochem* **1980**, *49*, 253-279.

(11) Coleman, P. F.; Suttle, D. P.; Stark, G. R. *J Biol Chem* **1977**, *252*, 6379-6385.

(12) Mergeay, M.; Gigot, D.; Beckmann, J.; Glansdorff, N.; Pierard, A. *Mol Gen Genet* **1974**, *133*, 299-316.

(13) Piette, J.; Nyunoya, H.; Lusty, C. J.; Cunin, R.; Weyens, G.; Crabeel, M.; Charlier, D.; Glansdorff, N.; Pierard, A. *Proc Natl Acad Sci U S A* **1984**, *81*, 4134-4138.

(14) Trotta, P. P.; Burt, M. E.; Haschemeyer, R. H.; Meister, A. *Proc Natl Acad Sci U S A* **1971**, *68*, 2599-2603.

(15) Nyunoya, H.; Lusty, C. J. *Proc Natl Acad Sci U S A* **1983**, *80*, 4629-4633.

(16) Post, L. E.; Post, D. J.; Raushel, F. M. *J Biol Chem* **1990**, *265*, 7742-7747.

(17) Miles, B. W.; Mareya, S. M.; Post, L. E.; Post, D. J.; Chang, S. H.; Raushel, F. M. *Biochemistry* **1993**, *32*, 232-240.

(18) Javid-Majd, F.; Stapleton, M. A.; Harmon, M. F.; Hanks, B. A.; Mullins, L. S.; Raushel, F. M. *Biochemistry* **1996**, *35*, 14362-14369.

(19) Stapleton, M. A.; Javid-Majd, F.; Harmon, M. F.; Hanks, B. A.; Grahmann, J. L.; Mullins, L. S.; Raushel, F. M. *Biochemistry* **1996**, *35*, 14352-14361.

(20) Rubino, S. D.; Nyunoya, H.; Lusty, C. J. *J Biol Chem* **1986**, *261*, 11320-11327.

(21) Thoden, J. B.; Raushel, F. M.; Benning, M. M.; Rayment, I.; Holden, H. M. *Acta Crystallogr D Biol Crystallogr* **1999**, *55*, 8-24.

(22) Trotta, P. P.; Estis, L. F.; Meister, A.; Haschemeyer, R. H. *J Biol Chem* **1974**, *249*, 482-489.

(23) Kim, J.; Raushel, F. M. *Biochemistry* **2001**, *40*, 11030-11036.

(24) Powers, S. G.; Meister, A.; Haschemeyer, R. H. *J Biol Chem* **1980**, *255*, 1554-1558.

(25) Braxton, B. L.; Mullins, L. S.; Raushel, F. M.; Reinhart, G. D. *Biochemistry* **1999**, *38*, 1394-1401.

(26) Braxton, B. L.; Mullins, L. S.; Raushel, F. M.; Reinhart, G. D. *Biochemistry* **1992**, *31*, 2309-2316.

(27) Huang, X.; Raushel, F. M. *Biochemistry* **1999**, *38*, 15909-15914.

(28) Miles, B. W.; Raushel, F. M. *Biochemistry* **2000**, *39*, 5051-5056.

(29) Thoden, J. B.; Wesenberg, G.; Raushel, F. M.; Holden, H. M. *Biochemistry* **1999**, *38*, 2347-2357.

(30) Thoden, J. B.; Holden, H. M.; Wesenberg, G.; Raushel, F. M.; Rayment, I. *Biochemistry* **1997**, *36*, 6305-6316.

(31) Thoden, J. B.; Miran, S. G.; Phillips, J. C.; Howard, A. J.; Raushel, F. M.; Holden, H. M. *Biochemistry* **1998**, *37*, 8825-8831.

(32) Kim, J.; Raushel, F. M. *Arch Biochem Biophys* **2004**, *425*, 33-41.

(33) Lund, L.; Fan, Y.; Shao, Q.; Gao, Y. Q.; Raushel, F. M. *J Am Chem Soc* **2010**, *132*, 3870-3878.

(34) Thoden, J. B.; Holden, H. M.; Wesenberg, G.; Raushel, F. M.; Rayment, I. *Biochemistry* **1997**, *36*, 6305-6316.

(35) Thoden, J. B.; Huang, X.; Raushel, F. M.; Holden, H. M. *J Biol Chem* **2002**, *277*, 39722-39727.

(36) Huang, X., Raushel, F. M. *Biochemistry* **2000**, *39*, 3240-3247.

(37) Huang, X., Raushel, F. M. *Journal of Biological Chemistry* **2000**, *275*, 26233-26240.

(38) Kim, J.; Raushel, F. M. *Biochemistry* **2004**, *43*, 5334-5340.

(39) Kim, J.; Howell, S.; Huang, X. Y.; Raushel, F. M. *Biochemistry* **2002**, *41*, 12575-12581.

(40) Weeks, A.; Lund, L.; Raushel, F. M. *Current Opinion in Chemical Biology* **2006**, *10*, 465-472.

(41) Zalkin, H. *Adv Enzymol Relat Areas Mol Biol* **1993**, *66*, 203-309.

(42) Larsen, T. M.; Boehlein, S. K.; Schuster, S. M.; Richards, N. G.; Thoden, J. B.; Holden, H. M.; Rayment, I. *Biochemistry* **1999**, *38*, 16146-16157.

(43) Binda, C.; Bossi, R. T.; Wakatsuki, S.; Arzt, S.; Coda, A.; Curti, B.; Vanoni, M. A.; Mattevi, A. *Structure* **2000**, *8*, 1299-1308.

(44) Chaudhuri, B. N.; Lange, S. C.; Myers, R. S.; Chittur, S. V.; Davisson, V. J.; Smith, J. L. *Structure* **2001**, *9*, 987-997.

(45) Teplyakov, A.; Obmolova, G.; Badet, B.; Badet-Denisot, M. A. *Journal of Molecular Biology* **2001**, *313*, 1093-1102.

(46) Schmitt, E.; Panvert, M.; Blanquet, S.; Mechulam, Y. *Structure* **2005**, *13*, 1421-1433.

(47) Endrizzi, J. A., Kim, H., Anderson, P.M., Baldwin, E.P. *Biochemistry* **2004**, *43*, 6447-6463.

(48) Hyde, C. C.; Ahmed, S. A.; Padlan, E. A.; Miles, E. W.; Davies, D. R. *J Biol Chem* **1988**, *263*, 17857-17871.

(49) Manjasetty, B. A.; Powlowski, J.; Vrielink, A. *Proceedings of the National Academy of Sciences of the United States of America* **2003**, *100*, 6992-6997.

(50) Maynard, E. L.; Lindahl, P. A. *Biochemistry* **2001**, *40*, 13262-13267.

(51) Wang, X. S.; Roitberg, A. E.; Richards, N. G. *Biochemistry* **2009**, *48*, 12272-12282.

(52) Krahn, J. M.; Kim, J. H.; Burns, M. R.; Parry, R. J.; Zalkin, H.; Smith, J. L. *Biochemistry* **1997**, *36*, 11061-11068.

(53) Medek, P., Beneš, P., Sochor J. *Journal of WSCG* **2007**, *8*, 107-114.

(54) Amaro, R. E.; Myers, R. S.; Davisson, V. J.; Luthey-Schulten, Z. A. *Biophys J* **2005**, *89*, 475-487.

(55) Klem, T. J.; Davisson, V. J. *Biochemistry* **1993**, *32*, 5177-5186.

(56) Mergeay, M.; Gigot, D.; Beckmann, J.; Glansdor.N; Pierard, A. *Molecular and General Genetics* **1974**, *133*, 299-316.

(57) Miran, S. G.; Chang, S. H.; Raushel, F. M. *Biochemistry* **1991**, *30*, 7901-7907.

(58) Rubio, V.; Llorente, P.; Britton, H. G. *European journal of biochemistry / FEBS* **1998**, *255*, 262-270.

(59) Mareya, S. M.; Raushel, F. M. *Biochemistry* **1994**, *33*, 2945-2950.

(60) Johnson, J. L.; West, J. K.; Nelson, A. D.; Reinhart, G. D. *Biochemistry* **2007**, *46*, 387-397.

(61) Potterton, E.; McNicholas, S.; Krissinel, E.; Cowtan, K.; Noble, M. *Acta Crystallogr D Biol Crystallogr* **2002**, *58*, 1955-1957.

(62) Potterton, L.; McNicholas, S.; Krissinel, E.; Gruber, J.; Cowtan, K.; Emsley, P.; Murshudov, G. N.; Cohen, S.; Perrakis, A.; Noble, M. *Acta Crystallogr D Biol Crystallogr* **2004**, *60*, 2288-2294.

(63) Huang, X.; Raushel, F. M. *Arch Biochem Biophys* **2000**, *380*, 174-180.

(64) Foley, R.; Poon, J.; Anderson, P. M. *Biochemistry* **1971**, *10*, 4562-4569.

(65) Lakowicz, J. R. *Principles of Fluorescence Spectroscopy*; 3rd ed.; Spring Science+Business Media, LLC: New York, NY, 2006.

(66) Anderson, P. M.; Meister, A. *Biochemistry* **1966**, *5*, 3157-3163.

(67) Quinlan, R. J.; Reinhart, G. D. *Biochemistry* **2006**, *45*, 11333-11341.

(68) Kimmel, J. L.; Reinhart, G. D. *Biochemistry* **2001**, *40*, 11623-11629.

(69) Piette, J.; Nyunoya, H.; Lusty, C. J.; Cunin, R.; Weyens, G.; Crabeel, M.; Charlier, D.; Glansdorff, N.; Pierard, A. *Proc. Natl. Acad. Sci. U. S. A.* **1984**, *81*, 4134-4138.

(70) Raushel, F. M.; Thoden, J. B.; Holden, H. M. *Acc. Chem. Res.* **2003**, *36*, 539-548.

(71) Mullins, L. S.; Raushel, F. M. *J. Am. Chem. Soc.* **1999**, *121*, 3803-3804.

(72) Thoden, J. B.; Huang, X.; Raushel, F. M.; Holden, H. M. *Biochemistry* **1999**, *38*, 16158-16166.

(73) Lin, Y. C., Cao, Z. X., Mo, Y. R. *Journal of the American Chemical Society* **2006**, *128*, 10876-10884.

(74) Arnold, K.; Bordoli, L.; Kopp, J.; Schwede, T. *Bioinformatics* **2006**, *22*, 195-201.

(75) Kopp, J.; Schwede, T. *Nucleic Acids Res* **2004**, *32*, D230-234.

(76) Schwede, T.; Kopp, J.; Guex, N.; Peitsch, M. C. *Nucleic Acids Res* **2003**, *31*, 3381-3385.

(77) Besler, B. H., Merz, K.M., Kollman, P.A. *Journal of Computational Chemistry* **1990**, *11*, 431-439.

(78) Singh, U. C., Kollman, P.A. *Journal of Computational Chemistry* **1984**, *5*, 129-145.

(79) Becke, A. D. *Phys Rev A* **1988**, *38*, 3098-3100.

(80) Becke, A. D. *Journal of Chemical Physics* **1993**, *98*, 1372-1377.

(81) Kendall, R. A., Dunning, T.H., Harrison, R. J. *Journal of Chemical Physics* **1992**, *96*, 6796-6806.

(82) Lee, C.; Yang, W.; Parr, R. G. *Phys Rev B Condens Matter* **1988**, *37*, 785-789.

(83) Cances, E., Mennucci, B., Tomasi, J. *Journal of Chemical Physics* **1997**, *107*, 3032-3041.

(84) Cossi, M., Barone, V., Mennucci, B., Tomasi, J. *Journal of Chemical Physics Letters* **1998**, *286*, 253-260.

(85) Mennucci, B., Tomasi, J. *Journal of Chemical Physics* **1997**, *106*, 5151-5158.

(86) Case, D. A., Darden T. A., Cheatham, III, T. E., Simmerling,C. L., Wang, J., Duke, R. E., Luo, R., Merz, K. M., Pearlman, D. A., Crowley, M., Walker, R. C., Zhang, W., Wang, B., Hayik, S., Roitberg, A., Seabra, G., Wong, K. F., Paesani, F., Wu, X., Brozell, S., Tsui, V., Gohlke, H., Yang, L., Tan, C., Mongan, J., Hornak, V., Cui, G., Beroza, P., Mathews, D. H., Schafmeister, C., Ross, W. S., and Kollman P. A. AMBER 9, University of California, San Francisco, 2006.

(87) Case, D. A.; Darden, T. E.; Cheatham, I., T. E.; Simmerling, C. L.; Wang, J.; Duke, R. E.; Luo, R.; Merz, K. M.; Wang, B.; Pearlman, D. A.; Crowley, M.; Brozell, S.; Tsui, V.; Gohlke, H.; Mongan, J.; Hornak, V.; Cui, G.; Beroza, P.; Schafmeister, C.; Caldwell, J. W.; Ross, W. S.; Kollman, P. A. AMBER 8, University of California, San Francisco, 2004.

(88) Meagher, K. L.; Redman, L. T.; Carlson, H. A. *J. Comput. Chem.* **2003**, *24*, 1016-1025.

(89) Bradbrook, G. M.; Gleichmann, T.; Harrop, S. J.; Habash, J.; Raftery, J.; Kalb, J.; Yariv, J.; Hillier, I. H.; Helliwell, J. R. *Journal of the Chemical Society, Faraday Transactions* **1998**, *94*, 1603-1611.

(90) van Gunsteren, W. F.; Berendsen, H. J. C. *Mol. Phys.* **1977**, *34*, 1311-1327.

(91) Darden, T.; York, D.; Pedersen, L. *Journal of Chemical Physics* **1993**, *98*, 10089-10092.

(92) Essmann, U.; Perera, L.; Berkowitz, M. L.; Darden, T.; Lee, H.; Pedersen, L. G. *J. Chem. Phys.* **1995**, *103*, 8577-8593.

(93) Kottalam, J.; Case, D. A. *Journal of the American Chemical Society* **1988**, *110*, 7690-7697.

(94) Kumar, S.; Bouzida, D.; Swendsen, R. H.; Kollman, P. A.; Rosenberg, J. M. *Journal of Computational Chemistry* **1992**, *13*, 1011-1021.

(95) Kumar, S.; Rosenberg, J. M.; Bouzida, D.; Swendsen, R. H.; Kollman, P. A. *Journal of Computational Chemistry* **1995**, *16*, 1339-1350.

(96) Roux, B. *Computer Physics Communications* **1995**, *91*, 275-282.

(97) Mareya, S. M.; Raushel, F. M. *Biochemistry* **1994**, *33*, 2945-2950.

(98) Matthews, S. L.; Anderson, P. M. *Biochemistry* **1972**, *11*, 1176-1183.

(99) Larsen, T. M.; Boehlein, S. K.; Schuster, S. M.; Richards, N. G. J.; Thoden, J. B.; Holden, H. M.; Rayment, I. *Biochemistry* **1999**, *38*, 16146-16157.

(100) van den Heuvel, R. H. H.; Ferrari, D.; Bossi, R. T.; Ravasio, S.; Curti, B.; Vanoni, M. A.; Florencio, F. J.; Mattevi, A. *J. Biol. Chem.* **2002**, *277*, 24579-24583.

(101) Douangamath, A.; Walker, M.; Beismann-Driemeyer, S.; Vega-Fernandez, M. C.; Sterner, R.; Wilmanns, M. *Structure* **2002**, *10*, 185-193.

(102) Mouilleron, S.; Badet-Denisot, M. A.; Golinelli-Pimpaneau, B. *J. Biol. Chem.* **2006**, *281*, 4404-4412.

(103) LaRonde-LeBlanc, N.; Resto, M.; Gerratana, B. *Nat. Struct. Mol. Biol.* **2009**, *16*, 421-429.

(104) Wojcik, M.; Seidle, H. F.; Bieganowski, P.; Brenner, C. *J. Biol. Chem.* **2006**, *281*, 33395-33402.

(105) Hyde, C. C.; Ahmed, S. A.; Padlan, E. A.; Miles, E. W.; Davies, D. R. *J. Biol. Chem.* **1988**, *263*, 17857-17871.

(106) Barends, T. R. M.; Dunn, M. F.; Schlichting, I. *Curr. Opin. Chem. Biol.* **2008**, *12*, 593-600.

(107) Dunn, M. F.; Niks, D.; Ngo, H.; Barends, T. R. M.; Schlichting, I. *Trends Biochem. Sci* **2008**, *33*, 254-264.

(108) Tan, X. S.; Volbeda, A.; Fontecilla-Camps, J. C.; Lindahl, P. A. *J. Biol. Inorg. Chem.* **2006**, *11*, 371-378.

(109) Tan, X. S.; Loke, H. K.; Fitch, S.; Lindahl, P. A. *J. Am. Chem. Soc.* **2005**, *127*, 5833-5839.

(110) Jorgensen, W. L.; Chandrasekhar, J.; Madura, J. D.; Impey, R. W.; Klein, M. L. *J. Chem. Phys.* **1983**, *79*, 926-935.

(111) Wang, J. M.; Cieplak, P.; Kollman, P. A. *Journal of Computational Chemistry* **2000**, *21*, 1049-1074.

(112) Wang, J. M.; Wolf, R. M.; Caldwell, J. W.; Kollman, P. A.; Case, D. A. *Journal of Computational Chemistry* **2004**, *25*, 1157-1174.

(113) Berne, B. J. Statistical Mechanics, Part A: Equilibrium Techniques; Plenum Press: New York, 1977.

(114) Snodgras, P. J.; Parry, D. J. *J. Lab. Clin. Med.* **1969**, *73*, 940-950.

(115) Kim, J.; Raushel, F. M. *Arch Biochem Biophys* **2004**, *425*, 33-41.

(116) Anderson, P. M. *Biochemistry* **1977**, *16*, 587-593.

(117) Pierard, A., Wiame, J. M. *Biochem Biophys Res Commun* **1964**, *15*, 76-81.

(118) Powers, S. G.; Meister, A. *J Biol Chem* **1978**, *253*, 1258-1265.

(119) Powers, S. G.; Meister, A. *Proc Natl Acad Sci U S A* **1976**, *73*, 3020-3024.

(120) Wimmer, M. J.; Rose, I. A.; Powers, S. G.; Meister, A. *J Biol Chem* **1979**, *254*, 1854-1859.

(121) Raushel, F. M.; Villafranca, J. J. *Biochemistry* **1980**, *19*, 3170-3174.

(122) Jitrapakdee, S.; Wallace, J. C. *Curr Protein Pept Sci* **2003**, *4*, 217-229.

(123) Thoden, J. B.; Kappock, T. J.; Stubbe, J.; Holden, H. M. *Biochemistry* **1999**, *38*, 15480-15492.

(124) Knowles, J. R. *Annu Rev Biochem* **1989**, *58*, 195-221.

(125) Phillips, N. F.; Snoswell, M. A.; Chapman-Smith, A.; Keech, D. B.; Wallace, J. C. *Biochemistry* **1992**, *31*, 9445-9450.

(126) Smithers, G. W.; Jahansouz, H.; Kofron, J. L.; Himes, R. H.; Reed, G. H. *Biochemistry* **1987**, *26*, 3943-3948.

(127) Marolewski, A. E.; Mattia, K. M.; Warren, M. S.; Benkovic, S. J. *Biochemistry* **1997**, *36*, 6709-6716.

(128) Pechere, J. F., Capony, J. P. *Analytical Biochemistry* **1968**, *22*, 536.

(129) Mejillano, M. R.; Jahansouz, H.; Matsunaga, T. O.; Kenyon, G. L.; Himes, R. H. *Biochemistry* **1989**, *28*, 5136-5145.

(130) Lane, D., Maruyama, H., Easterday, R. L. *Methods in Enzymology* **1969**, *13*, 277-283.

(131) Smithers, G. W., Johansouz, H., Kofron, J. L., Himes, R. H., Reed, G. H. *Biochemistry* **1987**, *26*, 3943-3948.

(132) Jahansouz, H., Mertes, K. B, Mertes, M. P., Himes, R. H. *Bioorganic Chemistry* **1989**, *17*, 207-216.

(133) Grehn, L., Ragnarsson, U., Welch, C.J. *Journal of Chemical Education* **1997**, *74*, 1477-1479.

(134) Johnson, K. A.; Simpson, Z. B.; Blom, T. *Anal Biochem* **2009**, *387*, 30-41.

(135) Johnson, K. A.; Simpson, Z. B.; Blom, T. *Anal Biochem* **2009**, *387*, 20-29.

(136) Gibson, G. W., Mullins, L.S., Raushel, F.M. *Bioorganic Chemistry* **1998**, *26*, 255-268.

(137) Fan, Y.; Lund, L.; Shao, Q.; Gao, Y. Q.; Raushel, F. M. *J Am Chem Soc* **2009**, *131*, 10211-10219.

VITA

Name: Liliya Lund

Address: Department of Chemistry
c/o Dr. Frank Raushel
Texas A&M University
P.O. Box 30012
College Station, TX 77843-3012

Email Address: Liliya.Lund@gmail.com

Education: B.S., Chemistry, Loyola University, Chicago, 2005
Ph.D., Chemistry, Texas A&M University, 2010